Universita' di Padova - Facolta' di Ingegneria

Dipartimento di Ingegneria dell'Informazione

Scuola di Dottorato di Ricerca in Ingegneria dell'Informazione
Indirizzo Scienza e Tecnologia dell'Informazione

Ciclo - XXIII

Estimation Techniques for OFDM with application to Digital Video Broadcasting Standards

Direttore della Scuola: Ch.mo Prof. M. Bertocco

Supervisore: Ch.mo Prof. L. Vangelista

Dottorando: Marco Rotoloni

To my family, Lisa, and in particular
to my beloved mother

Life is made of fleeting moments
stolen from the ordinary living
(Anonymous)

Contents

Acknowledgements

Innanzitutto, ringrazio sentitamente il *Prof. Lorenzo Vangelista* non solo per aver creduto in me e sostenuto fin dal primo giorno, ma sopprattuto per i caldi consigli e le opportunitá che mi ha presentato durante questi anni. Voglio ringraziarlo per essermi stato vicino sia nei momenti belli che in quelli meno felici. Vorrei ringraziare con lui tutti i componenti del gruppo di telecomunicazioni del dipartimento di Ingegneria dell'Informazione dell'Università di Padova, perchè grazie a loro, qualsiasi domanda mi ponessi trovava risposta. Un ricordo particolare va al *Dott. Stefano Tomasin* con il quale ho condiviso quasi tutti gli sforzi della mia attività di ricerca a Padova.

Per l'esperienza maturata e per l'opportunità che mi è stata concessa, vorrei anche ringraziare il *Prof. Merouane Debbah* e la *Chair Alcatel-Lucent* a *Supèlec*. Nei 4 mesi in Francia ho avuto la possibilità di conoscere un ambiente diverso di ricerca, e arricchire le mie competenze professionali.

Un sincero ringraziamento anche al *Dott. Roberto Padovani* e al *Prof. Gianfranco Cariolaro* per avermi permesso di intraprendere l'esperienza lavorativa più bella e formante che potessi desiderare, nell'ambito della *Cariolaro Scholarship*. Nella mia mente rimarrà sempre scolpito il livello di professionalità e di competenza che ho provato in *Qualcomm*. L'ambiente di collaborazione rimarrà sempre per me l'ideale da inseguire nella mia futura carriera professionale.

Ringrazio anche tutti i dottorandi e ricercatori che hanno condiviso con me non solo la sfida del Dottorato di Ricerca, ma soprattutto veri e propri momenti di vita. *Emiliano, Davide C., Riccardo, Francesco, Luca, Giorgio, Alfred, Alberto, Federico, Davide Z., Marco, Nicola, Paolo B., Paolo C., Antonio, Gio, Ermanna, Bea, Nicolò, Damiano*, e coloro che sicuramente mi sarò dimenticato. Non li chiamo colleghi, perchè prima di tutto sono Amici.

Ci sono stati momenti duri in questi anni, come tutti anch'io ogni tanto mi fermavo a chiedermi se la direzione su cui procedevo fosse quella giusta. In quei momenti ho avuto la fortuna di avere attorno persone che mi hanno fatto reagire e non mi hanno mai fatto mancare il loro sostegno. L'aiuto che ho ricevuto dai miei amici e dai miei familiari va oltre qualsiasi aiuto materiale. Voglio ringraziare mio padre *Pietro, Stefano, Ilaria*, il mio amore *Lisa*, e tutti gli amici e familiari che non ho lo spazio di elencare. Come ultimo pensiero, lascio a mia madre un posto particolare nei miei ricordi e nei ringraziamenti.

Marco Rotoloni

Abstract

This thesis deals with three among the major tasks of a receiver designed for Orthogonal Frequency Division Multiplex (OFDM): i) timing and frequency synchronization, ii) channel estimation and iii) data detection. These problems are very general, since OFDM is used in many different telecommunication environments, however the techniques involved are strongly dependent on the particular scenario. Here we focus on digital video broadcasting standards for terrestrial television.

Terrestrial Digital Video Broadcasting, also known as DVB-T, is a broadcasting standard from the European consortium DVB. It is the most widely deployed Digital Terrestrial Television (DTT) system worldwide. The system is based on a transmission of an audio/video stream from the MPEG-2 family, using an OFDM modulation. Besides, in March 2006, the desire to improve the service quality as well as to increase the number of services and the power of the digital television system, has stimulated the DVB group to study some new options for an improved DVB-T standard. A call for technology has been published in 2007, followed in 2009 by the release of the standard for the new generation DVB-T, called DVB-T2. Deployment tests have been studied, and field tests show that DVB-T2, still based on OFDM, can guarantee a 30% increase of the system capacity with respect to its predecessor.

As already stated, in both DVB-T standards the elected modulation scheme is OFDM. In fact, OFDM is widely used thanks to its low complexity structure allowing for simple demodulation and modulation by means of Fast Fourier Transform (FFT) and inverse FFT, respectively. The FFT algorithm is well optimized for computing blocks of samples with power of two sizes, i.e. 2048, 8096, etc. However, to allow simple equalization procedures and avoid interblock interference, a guard interval (GI) has to be appended to the OFDM block. GI reduces the efficiency of the transmission, because it is discarded at the receiver. The first part of this thesis proposes a receiver structure which takes advantage of the GI to improve data detection exploiting the redundancy of the signal. The performance of this structure is then analyzed comparing it with other two structures in a simulation scenario arisen from DVB-T2 reception configurations. The impact of low-density parity check codes (LDPC) which are part of the standard is also outlined.

The second part of the thesis focuses on the channel estimation which is the basis for most of the signal processing techniques involved in the reception of an OFDM signal. In particular we focus on channel estimation using known pilot symbols. Transmission of pilot symbols on a sub-set of subcarriers in an orthogonal frequency division multiplexing system allows for an efficient channel estimation at the receiver by means of the Least-Square (LS) method. Usually, for these systems channel estimation is performed on pilots and then interpolated over the time and the frequency axis. We propose to

improve the LS estimate on pilots by filtering the estimated channel both across the subcarriers and across different OFDM blocks, with adaptive filters in order to exploit the inter-carrier correlation and reduce the noise on the estimate. We consider various adaptive techniques to let the filter track the time-varying channel conditions: least mean square and Kalman filter theory are applied to design the finite impulse response filters. Besides, also infinite impulse response filters have been designed. Aim of the design is to obtain simple structures suitable for large OFDM blocks and receivers with limited computational/memory resources, while still being adaptive to time-varying channel conditions. However, while most approaches consider a single smoothing filter over time-interpolated estimates, i.e. after time interpolation, we propose the innovative use of multiple adaptive filters that take into account the different correlation among pilot estimates and interpolated estimates. In other words, we propose to design multiple adaptive frequency filters to perform frequency filtering in order to decrease the degree of noisiness of the time-interpolated samples. The idea is to leverage the fact that time-interpolated estimates have different reliability with respect to pilot LS estimates, and thus weighting accordingly the estimates during filtering, performance can be improved. Moreover, as a simpler approach we consider also the use of a single adaptive filter updated taking into account the reliability of the various estimates. Performance results are reported with reference to the DVB-T and DVB-T2 standards showing that the proposed *multiple filters* technique performs similar or better than existing approaches at a much lower complexity. Although these techniques have been developed considering the DVB-T/T2 pilot patterns, they can be applied to whatever system using pilot-patterned OFDM symbols.

The last part of the thesis deals with the initial signal synchronization for DVB-T2. In fact, the new standard for DTT provides a specific symbol, called P1 symbol, to ease initial signal acquisition and synchronization. We revise a synchronization technique based on the correlation of parts of the received signal showing that it fails to synchronize in practical channel conditions, e.g. single-frequency network (SFN) channels. Hence, we first propose a modified version of the existing technique to better exploit the correlation signal, then we analytically derive the maximum likelihood (ML) time and carrier frequency offset synchronization function. Unfortunately, the maximization of the likelihood function requires numerical methods, therefore we decided to simplify the scheme by considering a ML time (MLT) synchronization scheme, while resorting to a suboptimal estimator for carrier frequency offset (CFO). The proposed schemes are compared with existing solutions on both flat and frequency selective channels typically encountered in DVB-T2 transmissions, showing that both ML and MLT approaches are able to achieve synchronization with probability higher than 99%.

The last chapter collects all the simulation results supporting the topics covered in the previous chapters.

Sommario

La tesi discute tre tra le principali operazioni svolte da un ricevitore per segnali OFDM: i) sincronizzazione di simbolo e di frequenza, ii) stima di canale e iii) demodulazione del segnale. Dal momento che la modulazione OFDM è adottata in molti sistemi diversi, ognuno dei quali fa fronte agli stessi problemi con tecniche caratteristiche, gli argomenti proposti assumono un carattere molto generale. In questo lavoro, perciò, si tratteranno alcune tecniche OFDM applicate agli standard di diffusione terrestre della televisione digitale.

La radiodiffusione terrestre della TV digitale ha come standard più diffuso in ambito mondiale il DVB-T. Il sistema è basato sulla trasmissione di un flusso audio/video della famiglia MPEG-2, mediante modulazione OFDM. Recentemente, nel Marzo 2006, il desiderio di migliorare la qualità del servizio, e migliorare la potenza del sistema televisivo hanno stimolato il gruppo DVB a studiare delle nuove opzioni per il miglioramento dello standard DVB-T. Nel 2007 è iniziata l'opera di standardizzazione del nuovo sistema. Dopo due anni, nel 2009, è stato pubblicato lo standard del sistema DVB-T di nuova generazione, che ha preso il nome di DVB-T2. Test sul campo hanno dimostrato che la nuova tecnologia, ancora basata su OFDM, può garantire un incremento di capacità del 30% in più rispetto al sistema precedente. I primi a trasmettere secondo la modalità DVB-T2 sono state alcune reti inglesi. Tuttavia, benché BBC, ITV1 e Channel 4, trasmettessero già in DVB-T2 su uno o due canali, nell'Ottobre 2010, l'emittente televisiva italiana Europa 7 ha lanciato il suo bouquet di 12 canali che trasmettono con tecnologia DVB-T2, divenendo di fatto il primo broadcaster al mondo a trasmettere esclusivamente in DVB-T2. Nel Novembre 2010, i 14 paesi componenti la comunità dei paesi Sud-Africani ha selezionato DVB-T2 come standard di diffusione televisivo della regione. La comunità prevede di operare lo switch-over digitale indicativamente nel Dicembre 2013.

Come già abbiamo detto, entrambi gli standard DVB-T hanno scelto OFDM come schema di modulazione. Infatti, il largo utilizzo dell'OFDM si deve alla sua praticità di utilizzo, dovuta alla possibilità di realizzare modulatori e demodulatori a ridotta complessità. Le operazioni di demodulazione e modulazione sono realizzate rispettivamente tramite Trasformata di Fourier (FFT) e la sua operazione inversa (IFFT). FFT e IFFT sono entrambe realizzate mediante lo stesso algoritmo che è ottimizzato per operare su blocchi di campioni di lunghezza pari alle potenze di due, per esempio 2048 e 8096. Comunque, per permettere la realizzazione di procedure semplici di equalizzazione e quindi evitare l'interferenza tra simboli successivi, un Intervallo di Guardia (GI) deve essere trasmesso prima del blocco OFDM. Il GI riduce l'efficienza di trasmissione, in quanto è subito scartato dal ricevitore. La prima parte di questa tesi propone una struttura per il ricevitore che permetta di usare il GI per migliorare la decodifica dei

dati. Le prestazioni di questa struttura sono analizzate confrontandola con altre due strutture in uno dei possibili scenari per il DVB-T2. Successivamente, è anche valutato l'impatto dei codici LDPC sulle prestazioni della struttura proposta.

La seconda parte della tesi si concentra sulla stima di canale, che in molti casi rappresenta la base per le tecniche di elaborazione di segnale utilizzate nella ricezione di un segnale OFDM generico. In particolare noi consideriamo la stima di canale per sistemi OFDM che utilizzano delle portanti note al ricevitore. La trasmissione di simboli pilota in un sottoinsieme di portanti in un sistema OFDM permette di ottenere una efficiente stima di canale Least Square (LS) al ricevitore. Per questi sistemi la stima di canale è realizzata prima sulle portanti pilota, e successivamente interpolata nel tempo e in frequenza. In questo lavoro si propone di migliorare la stima LS sulle portanti filtrando la stima di canale con dei filtri adattativi. L'operazione di filtraggio è realizzata prima tra simboli OFDM successivi e poi tra portanti di un medesimo simbolo, in modo da sfruttare le correlazioni tra i diversi campioni stimati e ridurre così il livello di rumore. Si sono considerati diverse tecniche adattative per permettere ai filtri di seguire le condizioni di tempo-varianza del canale. Sono state applicate le teorie sui filtri least mean square e Kalman, per progettare filtri a risposta impulsiva limitata o infinita. Lo scopo degli algoritmi adattativi sviluppati è di ottenere delle strutture semplici, in grado di operare su simboli OFDM di grandi dimensioni, e con ricevitori con limitate risorse in termini di potenza di calcolo e memoria. Comunque, mentre molte tecniche considerano un singolo filtro per operare nel dominio della frequenza, cioé dopo l'interpolazione temporale, questa tesi propone l'utilizzo innovativo di più filtri che tengano in considerazione le diverse statistiche di correlazione tra le stime ottenute sulle portanti pilota e quelle ottenute tramite interpolazione temporale. In altre parole, si è proposto di progettare in parallelo più filtri adattativi, ognuno che operi su un sottoinsieme indipendente di portanti. L'idea è quella di sfruttare il fatto che le stime ottenute per interpolazione temporale hanno un'affidabilità diversa rispetto alle stime ottenute con il metodo LS, e quindi pesando le correlazioni in modo appropriato, al momento della procedura di filtraggio adattativo, è possibile un miglioramento delle prestazioni di stima. I risultati sono riportati con riferimento agli standard DVB-T e DVB-T2, dimostrando che la tecnica proposta è competitiva, o addirittura migliore, rispetto alle tecniche utilizzate in precedenza, permettendo una riduzione sostanziale della complessità di calcolo. Sebbene i risultati siano presentati con riferimento agli standard televisivi, queste tecniche possono essere applicate a qualsiasi sitema che utilizzi una modulazione OFDM con portanti pilota note al ricevitore.

L'ultima parte della tesi si occupa di sincronizzazione del segnale DVB-T2. Lo standard DVB-T2 definisce un simbolo specifico, detto simbolo P1, per facilitare l'acqusizione iniziale del segnale e la sincronizzazione. In questa parte della tesi si rivisita la tecnica di sincronizzazione basata su correlazione delle parti ridondanti del segnale ricevuto, definita nelle linee guida dello standard. Dopodiché si mostra che essa fallisce quando certe configurazioni reali di canale si presentano, per esempio nel caso di canale caratteristico di una single-frequency network (SFN). Perciò, prima si propone una versione modificata della tecnica base che sfrutti meglio la correlazione del segnale, successivamente si ricava l'espressione analitica della funzione di massima verosimiglianza (ML) per la sincronizzazione di tempo e frequenza. Sfortunatamente non è possibile trovare una forma analitica dello stimatore ML che massimizza la funzione di massima verosimiglianza, perciò è stato introdotto uno schema semplificato che considera la stima ML solo del tempo (MLT), lasciando la stima dell'offset di frequenza ad uno

stimatore sub-ottimo. Gli schemi proposti sono confrontati con soluzioni pre-esistenti sia con canali selettivi in frequenza che non. I risultati mostrano che sia la tecnica ML, che la tecnica MLT, sono in grado di raggiungere una corretta sincronizzazione con una probabilità maggiore del 99%.

Infine, l'ultimo capitolo raccoglie i risultati di tutte le simulazioni delle tecniche trattate nei capitoli precedenti.

List of Acronyms

ACE Active Constellation Extension

AWGN Additive White Gaussian Noise

BCH Bose-Chaudhuri-Hocquenghem coding

BER Bit Error Rate

BPSK Binary PSK

CBS Correlation-Based Synchronization scheme

CD3 Coded Decision Directed Demodulation

CDS Carrier Distribution Sequence

CFO Carrier Frequency Offset

COFDM Coded OFDM

CP Continual Pilots

CS Complementary Sequence

CSS Complementary Set of Sequences

DAB Digital Audio Broadcast

DBPSK Differential BPSK

DFT Discrete Fourier Transform

DRM Digital Radio Mondiale

DVB Digital Video Broadcast

DVB-T/T2 Terrestrial DVB first/second generation

DVB-S/S2 Satellite DVB first/second generation

EIT Event Info Table

ETSI European Telecommunications Standards Institute

FC Frame Closing symbol

FEC Forward Error Correction

FEF Future Extension Frame

FF Frequency Filtering

FF-MF Frequency Filtering with Multiple Filters

FF-SF Frequency Filtering with Single Filter

FFT Fast Fourier Transform

FIR Finite Impulse Response

GI Guard Interval

GSE Generic Stream Encapsulation

HDTV High Definition TV

IBI Inter-Block Interference

IDFT Inverse Discrete Fourier Transform

IIR Infinite Impulse Response

IFFT Inverse Fast Fourier Transform

ISDB-T Terrestrial Integrated Services Digital Broadcasting

ISI Inter-Symbol Interference

LDPC Low-Density Parity Check

LLF Log-Likelihood Function

LMS Least-Mean-Square

LS Least-Square

LSE LS Estimator

LTE Long Term Evolution

mac Multiplier Accumulator Chip operations

MIMO Multiple-Input-Multiple-Output

MISO Multiple-Input-Single-Output

MF Multiple Filters

MFN Multi-Frequency Network

ML Maximum Likelihood

MLT ML Time estimator

MMSE Minimum Mean-Square Error

MPEG Moving Picture Experts Group

MSE Mean-Square Error

OFDM Orthogonal Frequency Division Multiplex

PAPR Peak to Average Power Ratio

PDF Power Density Function

PLP Physical Layer Pipe

PRBS Pseudo Random Bit Sequence

PSK Phase Shift Keying modulation

QAM Quadrature-Amplitude Modulation

SBS Slope-Based Synchronization scheme

SC Single Carrier

SF Single Filter

SFN Single-Frequency Network

SF-R SF with Reliability

SISO Single-Input-Single-Output

SNR Signal to Noise Ratio

SoAC Sum of Auto-Correlations

SP Scattered Pilots

ST Subspace Tracking

TI Time Interpolation

TFS Time-Frequency Slicing

TS Transport Stream

TU6 Typical Urban 6

TV Television

WLAN Wireless Local Area Network

Introduction

Orthogonal Frequency Division Multiplexing (OFDM) is a well known modulation scheme for wideband digital communications. In the last few decades OFDM has become the most adopted modulation scheme of modern digital communications scenarios, such as digital television and audio broadcasting, wireless networking and broadband Internet access. Since the first OFDM-based standard in 1995, *ETSI Digital Audio Broadcasting standard EUreka* by ETSI, the number of systems adopting OFDM has increased incredibly fast. This speed is due to OFDM's ability to cope with severe channel conditions, in particular frequency selectivity, Doppler shifts, and presence of severe multipath caused by Single-Frequency Networks (SFNs). In addition to this, OFDM has the advantage to achieve good demodulation performance, while retaining both low complexity hardware and spectral efficiency. Besides, channel equalization, as well as demodulation, is simplified because OFDM may be viewed as using many slowly-modulated narrowband signals. The low symbol rate allows the use of a Guard Interval (GI) between symbols, making it possible to eliminate Inter-Symbol interference (ISI). Although the benefits of OFDM have been known since 1960s, OFDM is popular for wideband communications today by way of low-cost digital signal processing components that efficiently calculate the Fast Fourier Transform (FFT). In fact, low complexity receivers are based on the FFT algorithm which performs the discrete Fourier transform on powers-of-two-sized block of complex valued symbols. In this way the signal transmitted between the antennas is conceptually considered as a time-domain signal, while the demodulated signal is considered as in frequency domain.

Lots of literature has been produced about OFDM. The topics span from synchronization of clock, symbol and frequency, to channel estimation, from reducing the Peak-to-Average Noise Ratio (PAPR), to optimizing the transmitter beamforming in order to decrease the interference between transmissions, or optimize the power consumption. This thesis aims at discussing some general results obtained for a class of OFDM systems. We focused on terrestrial Digital Video Broadcasting (DVB-T), where channel estimation is performed on non-fixed pilot carriers, i.e. known carrier symbols which change position symbol by symbol, and where signal detection is performed with a unique preamble (just for DVB-T2).

This thesis is organized as follows. The first chapter is dedicated to the next generation digital TV standard (DVB-T2). The aim of this chapter is to review the main features of the standard, as in the following we will discuss particular OFDM techniques which fit the characteristics of DVB-T2, or when appropriated the features in common between DVB standards. The analysis of DVB-T2 standard of the first chapter is based on paper [1], where the main features of DVB-T2 have been firstly outlined. The second chapter deals with a technique designed for broadcasting systems on OFDM

making use of GI. GI is inserted to reduce inter-symbol interference (ISI) and provide protection against multipath. However, it decreases the transmission efficiency, since GI is the repetition of part of the transmitted signal. Usually, the receiver discards the GI because it is corrupted and does not carry additional information. The proposed technique aims at recovering the GI and use the signal redundancy to provide a better decoding quality. The third chapter introduce the problem of channel estimation on DVB-T/T2 standard, where OFDM modulation with pilot carriers is adopted. Although these standards provide for both, fixed and non-fixed pilot carriers, Fixed, or Continual Pilots (CP), are not enough to achieve good channel estimation performance, hence non-fixed, or Scattered Pilots (SP), are used along with CP to get a better estimation. In literature, many papers deals with channel estimation using known pilots; the general way to cope with it is to interpolate Least Square estimates, obtained in the frequency domain, both on the time and the frequency axis. However, the most part of these papers assume the pilots have fixed position, hence in the frequency domain, after Time Interpolation (TI), all the TI estimated channel frequency response are assumed to have carriers with the same reliability. This assumption does not hold any longer when pilot patterns are cyclic, as in the DVB-T and DVB-T2 cases. Each TI estimate from a single OFDM symbol has a different reliability with respect to adjacent estimates. Hence Frequency refinement, usually referred as Frequency Filtering (FF), which is a component of the frequency interpolation, must take this fact into account. The third chapter covers the TI and FF problems applying the adaptive filtering theory of Kalman, the Least-Mean Square (LMS) and an IIR algorithm. The last part of the thesis focus on the synchronization procedure of the DVB-T2 standard. The next generation DVB-T introduces a novel preamble to ease the receiver initialization tasks. The preamble is composed by one OFDM-like symbol, called P1, and one or more P2 symbols. The fourth chapter deals with the former symbol, P1, its detection, timing, and frequency synchronization. P1 symbol is devoted to DVB-T2 signal discovery, and to provide coarse timing and carrier frequency offset (CFO) estimation, as well as to carry few information bits. This symbol is built as a 1K OFDM symbol, i.e. 1024 complex values, to which two guard interval=like portions are added. This portions are repetitions of part of the 1K OFDM symbol, frequency shifted by a fixed amount. The redundancy and the uniqueness of these portions, make it easy for the receiver to look for DVB-T2 signal over the air. Moreover, techniques borrowed from well known OFDM estimation schemes can be used with few modifications to perform time and CFO estimation with P1 symbol. Two appendices are included before bibliography to support chapter 4. The first appendix describes the complete demodulation chain of P1 symbol, while the second reports the analytical derivation of the Log-likelihhod function (LLF) for the time and CFO estimation. Finally, the simulation results for the techniques explained in the previous chapters are all collected in chapter 5.

Chapter 1

A Digital TV Overview

Terrestrial digital TV broadcasting (DVB-T) is the most popular way to distribute TV in Europe and many other parts in the world. However, its success has been under pressure after the introduction of the MPEG4 compression standard and the new digital video broadcasting standard for satellite transmissions, DVB-S2 [2], which are driving the first adoption of high definition television (HDTV) on satellite and cable networks. Therefore, in 2006, the terrestrial TV broadcasting community felt the need for an improved system. DVB-T2 [3] is a second-generation terrestrial transmission system for digital television broadcasting. It builds on the technologies used as part of the first-generation system, DVB-T [4], developed over a decade ago. DVB-T2 extends the range of most of the parameters of DVB-T and significantly reduces overhead to build a system with a throughput close to theoretical channel capacity, with the best possible ruggedness of transmission. The key motivation behind this new standard was the desire in several European countries to offer HDTV services as efficiently and effectively as possible. The move to HDTV inevitably brings with it a change of source coding, necessitating the introduction of new domestic reception equipments (set-top boxes and TV sets), and therefore offers an ideal opportunity to upgrade the transmission system simultaneously.

This chapter gives a brief overview of the transmission system described by the standard [3]. As we will show in the following, DVB-T2 adopts orthogonal frequency division multiplexing (OFDM) with pilot carriers for channel estimation and synchronization purposes. Even if OFDM makes possible to arrange low complexity communication devices, it is a modulation scheme which greatly suffers symbol timing mismatches and carrier frequency offsets (CFO) between the transmitting and the receiving oscillators. A CFO on the received signal drastically decreases the performance of the system [5], since the orthogonality of the modulated symbols is no longer guaranteed. DVB-T2 preamble introduces a particular structure which reduces the time spent for signal tracking, and simplifies the synchronization process. Also channel estimation is very important in digital television broadcasting, because wideband systems as DVB-T2 experience severe frequency selective channels. To achieve good demodulation performance, synchronization is important as well as signal equalization. For these reasons we choose to insert this chapter before dive into detailed discussions about our solutions for the underlined problems, which however constitute the main topic of this thesis. In particular, chapter 3 shows a robust method to perform channel estimation using OFDM signals with pilots, as in DVB-T/T2 case, while chapter 4 focus on the initialization step

of the synchronization process, i.e the process carried out by P1 symbol. The review of the standard, and the simulation results, will make clear that the approaches of the following chapters can be integrated within a DVB-T2 receiver. Moreover, performance results will be reported with reference to DVB-T/DVB-T2 standard.

1.1 DVB Terrestrial Second Generation

Finishing in a record time by March 2007, a detailed set of commercial requirements was written for the system.

The DVB-T2 system specification, recently standardized by ETSI [3], includes the following key features:

- the same basic modulation technique as DVB-T: OFDM with guard interval (GI), which provides a fundamentally resilient transmission system for the terrestrial channel;
- extended range of fast Fourier transform (FFT) sizes of OFDM, to increase the single frequency network (SFN) performance and, together with an increased range of GIs, to provide significantly improved bandwidth efficiency;
- the same baseband framing and forward-error-correction (FEC) mechanisms included in DVB-S2 [2], adding the 256-QAM constellation, to take full advantage of the efficiency of the error-correction technique, and introducing a concept called rotated constellation, which can significantly improve the system performance in frequency selective terrestrial channels;
- a method of transporting individual data services in separate logical channels, known as physical-layer pipes (PLPs) within the physical layer, where the error-correction coding and interleaving are applied separately to each PLP; this allows for the implementation of service-specific robustness;
- a time interleaver, which provides at least 70 ms of time interleaving for the high data rate service, with options to extend this without increasing the memory required in the receiver; this will provide substantially increased immunity to impulsive interference, and could provide improved reception in high-speed mobile conditions;
- a very flexible frame structure, where the data can either be spread evenly across a whole frame for maximum time diversity, or concentrated into bursts, to allow power-saving techniques to be used in the receiver; the frame structure includes an efficient physical-layer signaling mechanism, called layer 1 (L1) signaling, which signals all of the parameters of the transmission system to the receiver;
- extended range of reference signals — scattered pilots (SP) and continual pilots (CP) — to allow an optimum choice to be selected for any given channel;
- an optional mechanism for transmit diversity, based upon the Alamouti scheme, to improve reception in areas where the coverage from two transmitters overlaps;
- two separate mechanisms for reducing the peak-to-average power ratio (PAPR) of the transmitted signal;

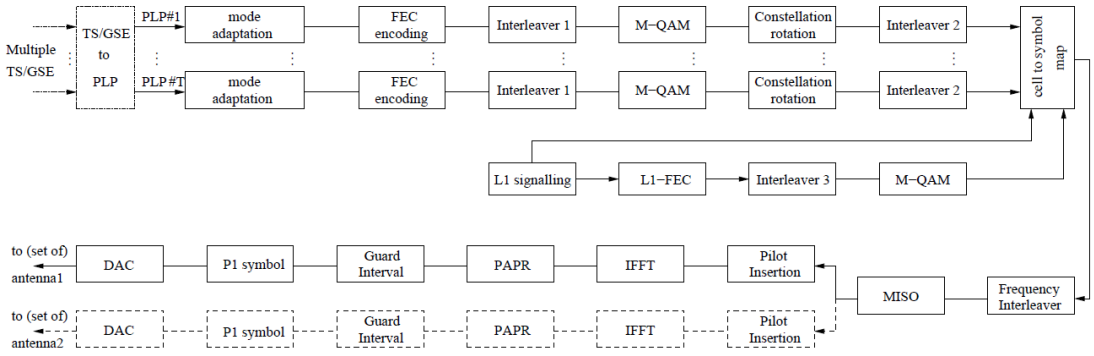

Figure 1.1: DVB-T2 block diagram.

- extra *hooks* to allow future extensions of the system in a backwards-compatible way: time-frequency slicing (TFS) and future-extension-frame (FEF) parts.

Fig. 1.1 shows the block diagram of a DVB-T2 transmitter. A DVB-T2 transmitter has the capability of handling multiple PLPs, to provide multiple services, while the DVB-T2 receiver is only required to decode a single data PLP together with its associated common PLP (if any).

DVB-T2 allows each PLP to carry its own independent service transport stream (TS) or generic stream encapsulation (GSE) stream. However, the DVB-T2 standard also defines a possible method to avoid transmitting many times the same information when handling multiple TSs (see Annex D of [4]). If multiple TSs share common packets, e.g. the event information table (EIT), these can be removed from the TSs and mapped into the common PLP. The receiver will then merge the content of the common PLP and the user-selected data PLP to reconstruct the valid TS.

The *TS/GSE to PLP* block of Fig. 1.1 realizes the splitting and merging function, which ensures synchronization among the user-selected data PLPs and the common PLP, and provides a full end-to-end transport stream transparency with improved bandwidth efficiency.

1.1.1 Error protection coding

Following the philosophy of the DVB standard family, forward error correction of DVB-T2 includes the BCH and low density parity check (LDPC) codes of DVB-S2, which proved to have an excellent error-rate performance also in the terrestrial channels. The concatenated shortened BCH outer codes avoid possible error floors of LDPC codes at low error rates.

In order to reduce the encoding complexity, the LDPC parity check matrices are of the form $\mathbf{H} = [\mathbf{A}\,\mathbf{B}]$, where $\mathbf{A}$ which is applied to the information part, is a sparse cyclic matrix and $\mathbf{B}$, which is applied to the parity part, has a staircase shape, with only its main and first lower diagonal containing ones. The cyclic nature of $\mathbf{A}$ reduces the storage requirements.

Two block lengths are available: 64800 bits or 16200 bits. The performance of the short codes is some tenths of dB worse than normal codes, but allows for low-bit-rate applications with shorter latency. LDPC code rates available in DVB-T2 are a selection

of the code rates of the DVB-S2 code[1]: 1/2, 3/5, 2/3, 3/4, 4/5 and 5/6 are used for PLP protection, 1/4, for short code length only, is used in L1 signaling protection.

The LDPC codes in DVB-T2 are irregular and the error protection level of each code bit is not uniform, but depends on the column weight of the parity check matrix. The performance of a LDPC code with QAM multi-level constellation is characterized by a non-uniform protection among bits. In order to optimize the correspondence between code bits and constellation bits, a bit interleaver and demultiplexer (interleaver 1 in Fig. 1.1) are inserted between the FEC encoder and the mapper in DVB-T2.

1.1.2 Scheduling

In order to offer service-specific robustness and optimize time-interleaving memory requirements, the DVB-T2 system can be described as a set of fully transparent PLPs, each one performing independent mode adaptation, FEC encoding, bit-mapping onto constellations points (cells) and time interleaving. The scheduler/frame builder is a functional element which maps the data cells at the output of the time interleavers into OFDM symbols, adding also signaling information in order to construct DVB-T2 frames and super-frames (see Fig. 1.2). The cell-mapping strategy in time and frequency may be selected in a very flexible way.

At the top level, the frame structure consists of super-frames (maximum duration of 64 s when FEFs are not used), which are divided into DVB-T2 frames and these are further divided into OFDM symbols. The frame starts with one reference symbol called P1 and one or more reference symbols called P2 (discussed in more detail in the following), followed by a configurable number of data symbols. The frame duration is of the order of 100 to 250 ms. A data PLP does not have to be into a single DVB-T2-frame, but it may span multiple frames.

The main purpose of the P2 symbols is to carry signaling data. Since the PLP throughput is time-variant, the position in time and frequency of the cells associated with a PLP changes frame-by-frame. Hence, the receiver must be able to extract at least the user-selected data PLP and the common PLP (when present) and so, it must be able to track the data-cells' positions. Therefore cell position signaling (the so called *dynamic L1* information) is transmitted in each frame within the P2 symbol, even if this information may also be embedded in the PLP data.

1.1.3 Modulation techniques

DVB-T2 uses coded orthogonal frequency division multiplex (COFDM) [6]), as used by the DVB-T, digital audio broadcasting (DAB), terrestrial integrated services digital broadcasting (ISDB-T) and digital radio mondiale (DRM) broadcast standards and by other radio systems such as IEEE 802.11a/n and the long term evolution (LTE) of 3GPP. A wider range of OFDM parameters is offered than for DVB-T, while coding is also changed. There are 1K, 2K, 4K, 8K, 16K and 32K FFT sizes, and each subcarrier, in each symbol, is modulated using QAM constellations. A range of options is available for payload data: 4-, 16-, 64- and 256-QAM. The combination of 256-QAM with the new LDPC error correction offers increased throughput with performance roughly comparable with 64-QAM in DVB-T.

[1]Nominal code rate. The effective LDPC code rate is in some cases of short codes slightly lower.

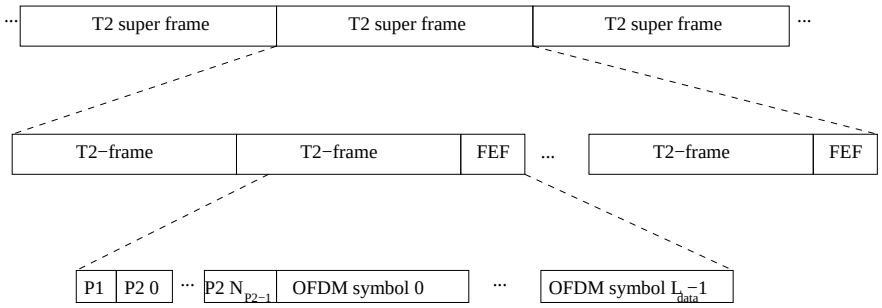

Figure 1.2: DVB-T2 frame structure.

Rotated constellations

The LDPC codes of DVB-T2 offer adequate performance in non-selective channels using a higher code rate than DVB-T. However, frequency selective channels need extra redundancy previously given by a lower-rate code. DVB-T2 includes the option of another kind of redundancy, *rotated constellations*, making the throughput advantage of high-rate LDPC available even for frequency selective channels.

In regular QAM, different information is mapped onto the I and Q axes, with no correlation between the axes. Rotating the constellation by a suitable angle means that every constellation point maps onto a different point on each of the I and Q axes. So a 16-QAM constellation has 16 different values for both of I and Q.

PAPR reduction

OFDM has the disadvantage that the transmitted signal increasingly resembles Gaussian noise as the number of sub-carriers increases, with the consequence that the peak-to-average-power-ratio is high. This places demands on the transmitter's power amplifier. DVB-T2 includes two optional features which can reduce PAPR.

Active constellation extension (ACE) modifies some of the transmitted constellations by selectively moving their outer points to positions having greater amplitude. ACE reduces PAPR without throughput loss, but is not used together with rotated constellation.

Reserved-carrier PAPR reduction sacrifices a small amount of throughput by reserving some sub-carriers, which do not carry data. They are used instead to carry arbitrary values, which permit the synthesis of a peak-canceling waveform.

1.1.4 Synchronization and channel estimation

The DVB-T2 standard includes particular design solutions to ease the time and frequency synchronization of the receiver. The most apparent one is the use of a frame made of a preamble and a payload, as schematically depicted in Fig. 1.2.

The preamble consists of a P1 symbol and a number of P2 symbols with the number depending on the chosen FFT size. For the 32K and the 16K sizes, there is only a single P2 symbol. For the 8K, 4K, 2K, and 1K sizes there are 2, 4, 8 and 16 P2 symbols, respectively. The payload follows the P2 symbols, although some of the data might already be carried within the P2 symbols, and consists of OFDM symbols of which sub-carriers can be modulated by data symbols or by known pilot symbols.

The use of the preamble significantly improves some synchronization steps and it further allows for a much wider choice of transmitter parameters without increasing the overall synchronization time.

P1 symbol

Denoting as T_s the sampling period of the transmitted signal, P1 symbol is a 1K OFDM symbol (called 'A') with two portions added, one before ('C') and one after ('B') (see Fig. 4.1). The total symbol is composed by 2K samples, which in 8 MHz system (T_s =7/64 μs) lasts 224 μs, comprising the useful part A, and the two modified guard-interval like sections of 542 and 482 samples, respectively. The two added components are obtained from A; C block is obtained repeating the first 542 samples of A, whereas B is obtained from the last 482 samples of A. The structure of the training symbol is similar to the one proposed by Schmidl and Cox [7]. The main innovation is that in order to avoid the false detection problem and improve the robustness against continuous waves superimposed to the signal, B and C parts are frequency shifted by f_{SH} before transmission. Hence, the actual transmitted 2K symbol is presented in Fig. 4.1, where $f_{\mathrm{SH}} = 1/KT_s$, or in other words f_{SH} is equal to the frequency spacing between adjacent subcarriers.

The subcarriers of a 1K OFDM symbol are 853, for a nominal bandwidth of 7.61 MHz in 8 MHz systems, however P1 symbol exploits only 384 subcarriers as defined in Table 62 of [3]. This allows better correlation properties and besides, allows the extension of the CFO estimation range. In fact the used carriers occupy roughly 6.83 MHz band from the middle of the nominal 7.61 MHz signal bandwidth. Even a frequency offset up to 500 kHz can be estimated since most of the used subcarriers are still within the 7.61 MHz nominal bandwidth window. The active subcarriers of the part A are differentially BPSK (DBPSK) modulated by a signaling sequence denoted as MSS_SCR. Detailed description of P1 symbol is reported in Appendix A where complete demodulation of P1 symbol signaling is investigated.

The particular $C - A - B$ structure is designed to improve the robustness of P1 detection in the presence of the most challenging channels such as a zero dB echo with opposite phase, typical of SFNs. The fixed P1 structure, together with the limited and highly protected signaling part, enables a fast scanning of the broadcast frequencies. The receiver can recognize the presence of a DVB-T2 transmission and store the key parameters, e.g. the FFT size or the presence of a FEF frame. The detection of the P1 symbol is also used to derive an initial time and frequency reference.

P2 symbols

The main role of the P2 symbol is carrying the L1 signaling, which can be quite large mainly because each PLP has its own transmission parameters. The L1 signaling is organized in an L1 pre-signaling part (where e.g. the GI size is signaled) and an L1 post-signaling part. The protection of the bits of the L1 pre-signaling is based on a BCH code followed by a punctured LDPC code. The choice of the LDPC code might seem odd given the short length of the codeword. Nevertheless it ensures no loss compared to a convolutional code with the same rate and does not require a Viterbi decoder, which would only be used to decode the L1 signaling.

Another important role of the P2 symbol is to initiate the channel estimation process and to provide synchronization refinements.

Scattered and continual pilots

A DVB-T2 receiver needs to estimate the channel experienced by the transmitted waveform to properly retrieve the transmitted information. To this end, the DVB-T2 standard defines conventional scattered pilot sequences which modulate a set of equally spaced sub-carriers. The main novelty introduced by DVB-T2 is that it supports eight different scattered pilots (SP) patterns for data symbols (eleven considering also the special SP patterns for P1, P2, and frame closing (FC) symbols). The guiding principle in the design has been to match the pilot distance to the inverse of the GI length. Whilst the SP are mainly designed to provide a reliable channel estimate, the continual pilots (CP), which are matched to the FFT size, provide a means for fine frequency synchronization and common phase error correction.

The pilots in the P2 symbol are fixed and are made to support the largest possible GI size, which is assumed to be acquired through conventional correlation-based methods. The pilot and data sub-carriers' position in the P2 symbol are independent of other transmission parameters such as the bandwidth extension and the PAPR methods, thus allowing detection just knowing the FFT size and whether the transmission mode is SISO or MISO.

Some of the SP patterns require a channel estimate to be formed from several symbols, and the P2 or P1 pilots help to initiate this process. This is particularly the case with a very efficient mode mainly meant for fixed roof-top reception. The DVB-T2 standard defines an option where very few pilots are transmitted in the payload (see PP8 in Table 1.1) and the channel estimation is based on the initial estimate offered by the P2 symbol followed by a data-aided channel estimation in which the decoded bits are fed back and used to refine the channel estimate [8]. This approach is only possible if an initial complete estimate is available.

The different pilot distances also require adaptation of the pilot boosting factors, i.e. how much power is allocated to the pilots compared with the data. The DVB-T2 standard defines three boosting factors for SP and three for the CP.

Pilot reference sequence

The pilot values depend on the sub-carrier index in the same way as for DVB-T. However, in DVB-T2, all the pilots (CP, SP and P2), in each OFDM symbol are multiplied by plus or minus one according to a frame-level PN sequence, and thus also depend on the OFDM symbol index. This provides an alternative and more robust frame-synchronization approach that can indicate the current OFDM position within the frame, if the preamble was lost, for instance, in the event of strong impulsive noise. Moreover, synchronization algorithms can exploit this frame level sequence to estimate and track the clock, symbol, frequency and frame synchronization. This is achieved with no influence on the quality of the channel estimation.

Table 1.1: Achievable data rate (in Mbit/s) for some DVB-T2 configurations.

	LDPC Code Rate	16-QAM	64-QAM	256-QAM
16K	3/5	18.07	27.11	36.14
1/128 GI	2/3	20.11	30.17	40.21
PP7	3/4	22.62	33.93	45.24
32K	3/5	17.05	25.63	34.23
1/16 GI	2/3	18.97	28.52	38.09
PP8	3/4	21.34	32.08	42.85
32K	3/5	18.07	27.02	36.14
1/128 GI	2/3	20.11	30.06	40.21
PP7	3/4	22.62	33.82	45.24

1.1.5 Multiple antennas techniques

The DVB-T standard allows the simultaneous transmission on the same frequency of the same signal by multiple transmitters, in order to implement a single-frequency network (SFN). By ensuring strict synchronization constraints, an SFN allows a simple network deployment where receivers see an equivalent channel obtained by the superposition of the channels relating to the multiple transmitters. However, when a receiver receives similar power levels from two transmitters, the channel frequency response will contain deep nulls, due to destructive interference. The new DVB-T2 standard provides an efficient means to exploit the presence of multiple transmit antennas even when the receiver is equipped with a single-antenna (i.e., a multiple-input-single-output, MISO, system) by using a modified form of Alamouti [9] encoding. In this configuration the data on the two transmitters are not identical but closely related, avoiding the destructive interference. As a result, the SFN coverage is improved.

In the case of 2x1 MISO, the pilots have to provide two independent channel estimations. Therefore, the number of pilots needs to be doubled.

1.1.6 Performance and mode comparison

The DVB-T2 standard provides a large set of transmitter configurations. The choice of some parameters is dictated also by the network deployment, an example being the GI duration and SP pattern configuration, which are related to the maximum tolerable delay channel spread, including possible SFN transmissions. For other parameters, such as the code rate and the constellation size, the choice is guided by noise level and channel statistics. For each configuration, different throughputs are achieved, as shown in Table 1.1, under different channel conditions.

We provide here an idea of possible throughput gains achieved with the deployment of DVB-T2 on existing networks, by considering two relevant cases. A typical SFN deployment of the DVB-T standard (adopted e.g. in Italy) includes 8K FFT, 1/4 GI, 64-QAM constellation and 2/3 convolutional code rate, yielding a data rate of 19.91 Mbit/s on a fixed channel at a SNR of 17 dB. In the same channel conditions, DVB-T2 transmission with extended bandwidth and parameters 32K FFT, 1/16 GI, PP8, 256 QAM and LDPC code rate 3/5, provides a data rate of 34.23 Mbit/s, which is 72% higher. Another typical multi frequency network (MFN) DVB-T configuration (adopted in UK) includes 2K FFT, 1/32 GI, 64-QAM and 2/3 code rate. Correspondingly, a DVB-T2 configuration with extended bandwidth, 32K FFT, 1/128 GI, PP8, 256 QAM and a LDPC code rate of 3/5 provides a data rate of 36.14 Mbit/s, which is about 50% higher. In both cases we observe that DVB-T2 allows HDTV MPEG-4 transmissions.

Chapter 2

Data Detection Improvement for OFDM Signals

Modulation techniques based on Orthogonal Frequency Division Multiplexing (OFDM) have been widely applied into nowadays wireless broadcasting standards such as Digital Audio Broadcasting (DAB) [10] and Digital Video Broadcasting (DVB) [4]. Even in the next generation DVB-T (DVB-T2) [11], OFDM has been elected as modulation scheme thanks to its low complexity structure which allow simple modulation and demodulation making use of an inverse Fourier Transform (IFFT) at the transmitter and a Fourier Transform (FFT) at the receiver.

Improvement of data detection exploiting the guard interval (GI) has already been considered in [12]. However, due to Inter-Block Interference (IBI) caused by channel multipath, only part of the GI is exploited. In fact, the received GI symbols, which are corrupted by the previous transmitted OFDM block, are discarded. In [13] IBI is taken into account, but [13] deals with a single-carrier system (SC) and is not of practical use in nowadays scenarios. The system proposed in [13] introduces an additional latency in the OFDM block detection, as it needs the next OFDM block to perform the demodulation.

In this chapter we propose a major improvement with respect to the current architecture, showing how to exploit the *complete* GI for data detection without additional latency w.r.t. conventional receivers. Furthermore, we apply this architecture to a timely application scenario, i.e. the improvement of DVB-T system. Finally, in the results chapter (Chap. 5) we provide simulation results for a receiver using the CD3 channel estimation technique [14], considering both the uncoded and coded scenarios. We allow ourselves in the proposed receiver a reasonable complexity increase, having as a priority the performance gain with respect to the conventional receiver structures. As a matter of fact this is in line with the commercial requirements for DVB-T2 [11] where the focus is on the increase of performances.

The following sections are organized as follows. Section 2.1 describes the system model adopted. In section 2.2 we derive our reduced complexity Least-Square solution, generalizing the one in [12]. Simulation results are presented in section 5.1 of the simulation results chapter (Chap. 5), both for uncoded and LDPC coded case.

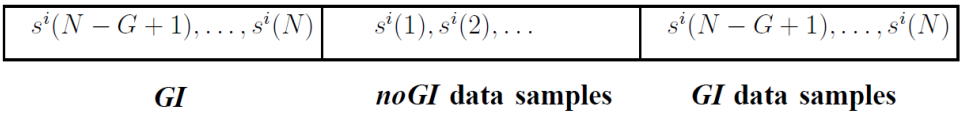

Figure 2.1: i-th time domain OFDM block transmitted.

2.1 System model

Let $\mathbf{s}^i = [s^i(N), s^i(N-1), \ldots, s^i(1)]^T$ be the modulated complex values of the i-th OFDM block transmitted over the channel. Applying the IFFT we obtain

$$\overline{\mathbf{s}}^i = \mathbf{F}^H \mathbf{s}^i \tag{2.1}$$

where $\overline{\mathbf{s}}^i$ represents the i-th OFDM block in the time domain transmitted over the channel, and $\mathbf{F}$ is the unitary Discrete Fourier Transform (DFT) matrix. $(\cdot)^H$ denotes the transpose conjugate of the argument. A GI of length G is appended to $\overline{\mathbf{s}}^i$ repeating the last G values of IFFT. Then the OFDM block, as in Fig. 2.1, is transmitted through the channel which is modeled as a Finite Impulse Response (FIR) filter with $L+1$ taps: $\mathbf{h}^i = [h_0^i, \ldots, h_L^i]^T$. In Fig. 2.1 we have divided the information symbols of the OFDM block in two groups: the ***noGI*** data samples which do not fall inside the GI portion of the signal, and the ***GI*** data samples which are repeated in the GI. In the following we suppose that the GI length is at least equal to the channel length, i.e. $L \leq G$, so the previous OFDM block leaks only into the i-th block's GI, which normally is discarded. As in [12], the received GI samples are not discarded, but usefully exploited to improve the detection performance. According to Fig. 2.1, we can express the relation between the transmitted signal $\overline{\mathbf{s}}^i$ and the received time domain samples $\overline{\mathbf{r}}^i = [\overline{r}^i(N+G), \overline{r}^i(N+G-1), \ldots, \overline{r}^i(1)]^T$ as

$$\overline{\mathbf{r}}^i = \mathbf{H} \begin{bmatrix} \overline{s}^i(N) \\ \overline{s}^i(N-1) \\ \vdots \\ \overline{s}^i(1) \\ \overline{s}^i(N) \\ \vdots \\ \overline{s}^i(N-G+1) \\ \overline{s}^i(N) \\ \vdots \\ \overline{s}^i(N-L+1) \end{bmatrix} + \overline{\mathbf{n}}^i \tag{2.2}$$

where $\overline{\mathbf{n}}^i$ is the complex vector of the zero-mean Gaussian noise, and $\mathbf{H}$ is a $(N+G)\times(N+G+L)$ Toeplitz matrix given by

$$\mathbf{H} = \begin{bmatrix} h_0 & h_1 & \dots & h_L & 0 & \dots & 0 \\ 0 & h_0 & h_1 & \dots & h_L & \ddots & \vdots \\ \vdots & \ddots & \ddots & & \dots & \ddots & 0 \\ 0 & \dots & 0 & h_0 & h_1 & \dots & h_L \end{bmatrix} \tag{2.3}$$

The matrix operation in (2.2) is the counterpart of the convolution of the transmitted signal and the channel impulse response. The samples $[\overline{r}^i(G),\dots,\overline{r}^i(1)]^T$ represent the receiving of the i-th OFDM block guard interval. Those samples are corrupted by the leakage of the last transmitted OFDM block, i.e. by the convolution of $[\overline{s}^{i-1}(N+G),\dots,\overline{s}^{i-1}(N-L+1)]^T$ (which are the last L samples of the GI of the previous OFDM block) with the channel impulse response. Based on the decisions at the $(i-1)$-th block, i.e. the previous decoded symbols and the estimation of the $(i-1)$-th channel impulse response, we are able to remove the contribution of $\overline{\mathbf{s}}^{i-1}$ to the received GI. Unfortunately this procedure is not enough to let exploit the redundancy introduced by GI. In fact, due to channel multipath, the ***GI*** data samples have contributes given by the last L ***noGI*** data samples, $[\overline{s}^i(N-G),\dots,\overline{s}^i(N-G-L+1)]^T$. For this reason, after the IBI removal we add to the received GI a useful component of Inter-Symbol Interference (ISI). This contribute is given by the convolution between the last L samples of the ***noGI*** portion of data and the current channel impulse response $\mathbf{h}^i$. To obtain this contribution, we first decode the i-th OFDM block with the conventional receiver, that is discarding the GI and performing the Fourier Transform (FFT), then we compute the impulse channel response estimation $\mathbf{h}^i$, and finally we compute the convolution between the last L samples of ***noGI*** data and $\mathbf{h}^i$. Supposing perfect interference cancellation and ISI recovering, we can rewrite (2.2) as

$$\overline{\mathbf{y}}^i = \mathbf{H}\begin{bmatrix} \overline{s}^i(N) \\ \overline{s}^i(N-1) \\ \vdots \\ \overline{s}^i(1) \\ \overline{s}^i(N) \\ \vdots \\ \overline{s}^i(N-G+1) \\ \overline{s}^i(N-G) \\ \vdots \\ \overline{s}^i(N-G-L+1) \end{bmatrix} + \overline{\mathbf{n}}^i \tag{2.4}$$

where we have indicated with $\overline{\mathbf{y}}^i$ the received signal modified by the above procedure. As in [12] we can simplify (2.4) as

$$\overline{\mathbf{y}}^i = \mathbf{H}_c\overline{\mathbf{s}}^i + \overline{\mathbf{n}}^i \tag{2.5}$$

defining $\mathbf{H}_c$ as the following $(N+G)\times N$ circulant matrix

$$\mathbf{H}_c = \left[\begin{array}{cccccccc} h_0^i & h_1^i & \dots & & h_L^i & 0 & \dots & 0 \\ 0 & h_0^i & h_1^i & \dots & & h_L^i & \ddots & \vdots \\ \vdots & \ddots & \ddots & & & & \ddots & 0 \\ 0 & & 0 & h_0^i & h_1^i & \dots & & h_L^i \\ h_L^i & 0 & & 0 & \ddots & & & \vdots \\ \vdots & \ddots & \ddots & & \ddots & \ddots & & \vdots \\ h_2^i & \dots & h_L^i & 0 & & 0 & h_0^i & h_1^i \\ h_1^i & \dots & & h_L^i & 0 & \dots & 0 & h_0^i \\ \hline h_0^i & h_1^i & \dots & & h_L^i & 0 & \dots & 0 \\ 0 & \ddots & \ddots & & & \ddots & \ddots & \vdots \\ \ddots & 0 & h_0^i & h_1^i & \dots & & h_L^i & 0 \end{array}\right] \tag{2.6}$$

In (2.6) we have split matrix $\mathbf{H}_c$ by a line to show that the matrix is equal to the product of a square circulant matrix $\mathbf{H_0}$, obtained selecting the first N rows of $\mathbf{H}_c$, by a $(N+G)\times N$ matrix as follows

$$\begin{aligned} & & \mathbf{H}_c &= \mathbf{K}\mathbf{H}_0 \\ \text{where} & & \mathbf{K} &= \left[\begin{array}{c|c} \multicolumn{2}{c}{\mathbf{I}_N} \\ \hline \mathbf{I}_G & \mathbf{0}_{N-G} \end{array}\right] \end{aligned} \tag{2.7}$$

where $\mathbf{I}_n$ and $\mathbf{0}_n$ are respectively the identity and zeros $n\times n$ matrix. Since $\mathbf{H_0}$ is a square circulant matrix, it can be decomposed by the well known relation between the circulant matrices and the DFT matrix $\mathbf{F}$. Assuming to use the unitary DFT and IDFT matrix, we can express $\mathbf{H_0}$ as

$$\begin{aligned} & & \mathbf{H}_0 &= \mathbf{F}^H\mathbf{\Lambda}\mathbf{F} \\ \text{where} & & \mathbf{\Lambda} &= \operatorname{diag}\left(\mathbf{F}^H\left[\begin{array}{c} \mathbf{h}^i \\ \mathbf{0}_{(N-(L+1))\times 1} \end{array}\right]\right) \end{aligned} \tag{2.8}$$

$\mathbf{\Lambda}$ is the diagonal matrix which contains the eigenvectors of $\mathbf{H}_0$. Since all the terms considered refer to the current i-th OFDM block, we drop the block index i for simplicity and rewrite the system relations

$$\overline{\mathbf{y}} = \mathbf{K}\mathbf{H}_0\mathbf{F}^H\mathbf{s} + \overline{\mathbf{n}} \tag{2.9}$$

We remark that (2.9) is similar to the relation (9) of [12] but for a different number of 1s in the rows below the horizontal line in $\mathbf{K}$ (2.7), i.e. $\mathbf{K}$ considers the last L symbols of GI, which in [12] are discarded.

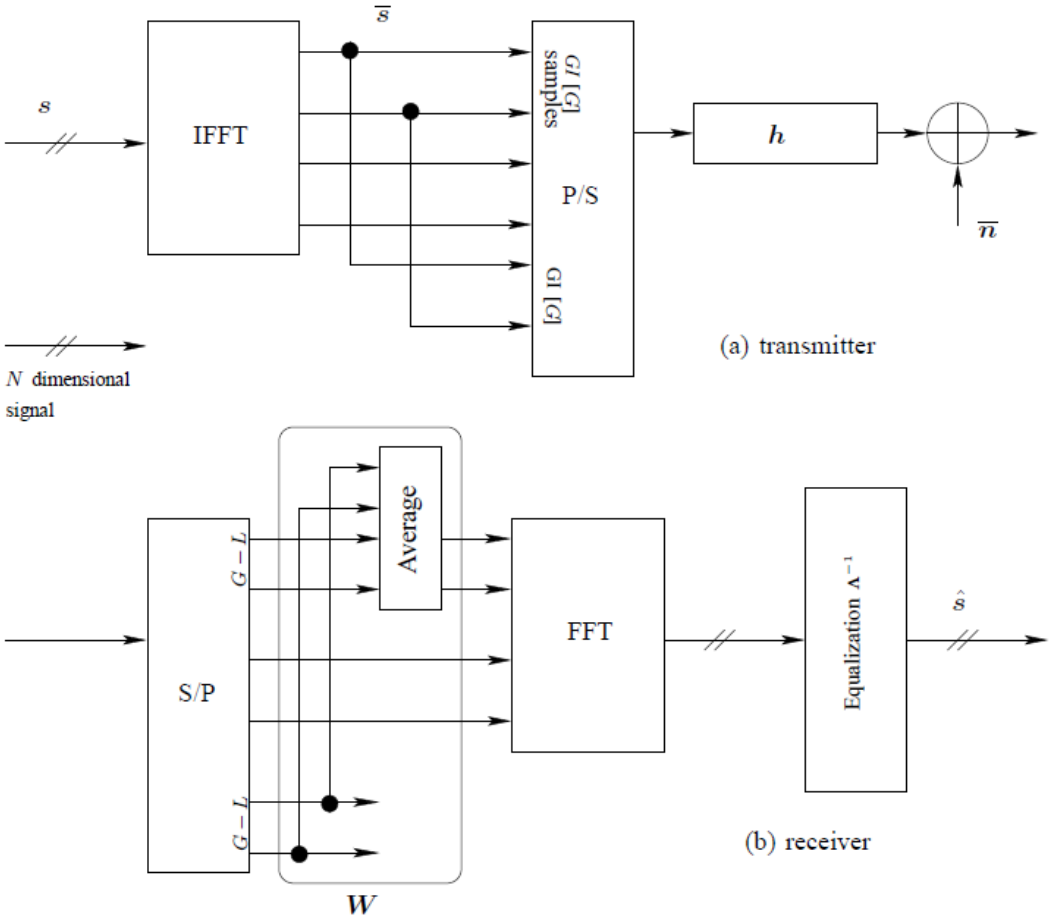

Figure 2.2: a) The conventional OFDM transmitter and b) the proposed OFDM receiver in [12], exploiting only $G - L$ free from interference GI symbols. The block $\mathbf{W}$ is what distinguishes this structure from a conventional receiver and the one in [12] from our proposed receiver.

2.2 Least-Square Solution

Let the form $\mathbf{y} = \mathbf{X}\boldsymbol{\theta} + \mathbf{w}$ be a linear model where $\mathbf{y}$ is a known vector denoting the output signal of the system, $\boldsymbol{\theta}$ and $\mathbf{w}$ are unknown random uncorrelated vectors, where $\mathbf{w}$ is zero-mean, denoting respectively the input signal and the noise of the system, while $\mathbf{X}$ is a known deterministic matrix denoting the transformation of the system. The linear Least-Square Estimator (LSE) of $\boldsymbol{\theta}$ given $\mathbf{y}$ is [15]

$$\hat{\boldsymbol{\theta}} = (\mathbf{X}^H\mathbf{X})^{-1}\mathbf{X}^H\mathbf{y} \tag{2.10}$$

Although LSE solution is suboptimal with respect to Minimum Mean Square Error (MMSE) solution, we propose (2.10) as the solution of our problem because, differently from MMSE, it is implementable in a receiver with reduced complexity. Besides, [12] shows that LSE solution closely achieves MMSE optimal performance.

Applying (2.10) to (2.9) we obtain the LSE of $\mathbf{s}$

$$\hat{\mathbf{s}} = (\mathbf{\Lambda}^H \mathbf{F}\mathbf{K}^H \mathbf{K}\mathbf{F}^H \mathbf{\Lambda})^{-1} \mathbf{\Lambda}^H \mathbf{F}\mathbf{K}^H \overline{\mathbf{y}}. \tag{2.11}$$

Defining the matrix $\mathbf{E}$ as

$$\mathbf{E} \triangleq \begin{bmatrix} \mathbf{I}_G & \\ & \mathbf{0}_{N-G} \end{bmatrix} \tag{2.12}$$

and noting that $\mathbf{K}^H\mathbf{K} = \mathbf{I}_N + \mathbf{E}$, (2.11) yields

$$\hat{\mathbf{s}} = (\mathbf{\Lambda}^H \mathbf{\Lambda} + \mathbf{\Lambda}^H \mathbf{F}\mathbf{E}\mathbf{F}^H \mathbf{\Lambda})^{-1} \mathbf{\Lambda}^H \mathbf{F}\mathbf{K}^H \overline{\mathbf{y}}. \tag{2.13}$$

Applying the matrix inversion lemma[1] to (2.13), we get

$$\hat{\mathbf{s}} = \mathbf{\Lambda}^{-1}\mathbf{F} \left(\mathbf{I}_N - (\mathbf{I}_N + \mathbf{E})^{-1} \mathbf{E} \right) \mathbf{K}^H \overline{\mathbf{y}} \tag{2.14}$$

and since $\left(\mathbf{I}_N - (\mathbf{I}_N + \mathbf{E})^{-1} \mathbf{E} \right) = (\mathbf{I}_N + \mathbf{E})^{-1}$, (2.14) is equivalent to

$$\hat{\mathbf{s}} = \mathbf{\Lambda}^{-1}\mathbf{F} (\mathbf{I}_N + \mathbf{E})^{-1} \mathbf{K}^H \overline{\mathbf{y}} \tag{2.15}$$

where

$$(\mathbf{I}_N + \mathbf{E})^{-1} = \begin{bmatrix} \frac{1}{2}\mathbf{I}_G & \\ & \mathbf{I}_{N-G} \end{bmatrix}. \tag{2.16}$$

Finally, defining $\mathbf{W}$ as $\mathbf{W} = (\mathbf{I}_N + \mathbf{E})^{-1}\mathbf{K}^H$, we get

$$\begin{aligned} \hat{\mathbf{s}} &= \mathbf{\Lambda}^{-1}\mathbf{F}\mathbf{W}\overline{\mathbf{y}} \\ \mathbf{W} &= \left[\begin{array}{c|c} \frac{1}{2}\mathbf{I}_G & \frac{1}{2}\mathbf{I}_G \\ \hline & \mathbf{I}_{N-G} \end{array}\right] \end{aligned} \tag{2.17}$$

If we compare (2.17) with the equivalent LSE solution given in [12], we note that after the transformation of the received OFDM block, removing IBI and adding an opportune ISI contribution, the structure of the receiver remains the same; we simply extend the average computed by the structure of Fig. 2.2, to the last G samples of the signal $\overline{\mathbf{y}}$. Since the structure of Fig. 2.2 does not increase the complexity of the system, we note that the additional complexity resides only in the interference recovering procedure. In fact, the algorithm to perform interference recovering requires to compute a temporary conventional detection on data and channel estimation. Then the performance is increased computing an improved data detection using a structure similar to the one depicted in Fig. 2.2. Thus, for our receiver structure, equalization and demodulation steps are doubled with respect to the conventional OFDM receiver.

[1] $(A + BCD)^{-1} = A^{-1} - A^{-1}B(C^{-1} + DA^{-1}B)^{-1}DA^{-1}$

Chapter 3

Adaptive Channel Estimation for DVB-T

The equalization of signals transmitted over multipath fading channels can be easily accomplished by using orthogonal frequency division multiplexing (OFDM) as transmission technology. Indeed, OFDM has been adopted in a variety of wireless standards, including digital audio (DAB) and video broadcasting (DVB-T) [10], [4] and wireless local (WLAN) and metropolitan area (WiMax) networks [16], [17].

Unless differential transmission schemes are used, which however decrease the spectral efficiency, channel estimation is needed for equalization and decoding of error protection codes. Various schemes for the channel estimation of OFDM systems have been proposed, which can be divided into two main categories: pilot-based techniques and training-based techniques. The pilot-based techniques provide that specific positions of the OFDM block (pilot subcarriers) are used to transmit symbols known at the receiver: the channel is first estimated at pilot positions and then interpolated on all subcarriers. When pilots are in different positions at each OFDM block, time interpolation (TI) is first performed to exploit the correlation among channels at different OFDM blocks and then frequency interpolation allows to recover the channel response on all subcarriers. On the other hand, training based techniques reserve one, or more, entire OFDM blocks for the transmission of symbols known at the receiver, usually at the beginning of the data block. For fading channel, tracking is performed by refining the channel estimate by decision-directed techniques [8], [18], which can be extended also to systems using multiple antennas [19].

Both with pilot and training signals, the estimated frequency response is affected by noise that can be reduced by exploiting the correlation among channel estimates both in time and frequency. Although correlation is optimally exploited by a two dimensional filter, it has been shown [20] that two consecutive filters in time and frequency, respectively, provide almost optimal performance. For the exploitation of the frequency correlation, matrix operations on the channel estimate are usually based on the singular value decomposition of the channel correlation matrix [21], [22], which requires additional discrete Fourier transforms (DFT). In [23] a *sub-space tracking* (ST) method is proposed requiring matrix operations that are infeasible for large OFDM blocks (such as in the DVB-T standard). A lower-complexity technique can be obtained by a filter in the frequency domain designed according to the *Wiener filter theory* [24], [20]. However,

as the channel statistics are changing in time, the use of fixed filters is suboptimal. In this respect, in [25] an adaptive Wiener filter is proposed, where the correlation matrix is estimated adaptively from the pilot subcarriers and conventional Wiener filter design (including matrix inversion) is used. In [26] the filter is reduced to a low-pass filter implemented in the time domain, where the adaptation is limited to the estimate of the effective duration of the channel impulse response. A fully adaptive time-domain Wiener filter is considered in [27]. However, this choice is both complex, as it requires additional DFTs, and suboptimal, as it does not take into account the power profile of the channel, but only its duration. For fast fading channels an estimator based on *oversampling basis expansion* model is derived in [28], still having a high complexity. The channel estimate refinement can be included in the interpolation process to obtain a channel estimate for all subcarriers, e.g. by fixed filters [29]. For the exploitation of the time correlation, interpolators have been proposed [30]. In [31], [32] two-dimensional adaptive channel estimators are proposed, where a least mean square (LMS) algorithm is used to predict channel estimation of future OFDM blocks. When the Doppler effect is relevant, inter-carrier interference is present and special channel estimation structures must be devised [33], [34].

In this chapter we consider a pilot-based OFDM system and propose various adaptive filters to exploit the time and frequency correlation among pilot estimates. We investigate adaptive filters both for TI and for filtering pilots in the frequency domain. In particular, the frequency filtering (FF) can be seen as a predictor that estimates the frequency response of the channel in correspondence of a pilot subcarrier by using surrounding pilots. The predicted estimate is then linearly combined with the Least-Square (LS) or TI estimate of the central pilot to reduce noise. For both TI and FF, we implement and design both finite impulse response (FIR) and infinite impulse response (IIR) filters, and the adaptation is performed by LMS or Kalman technique. Our objective for the filter design is twofold. On one hand we aim at obtaining simple structures that are suitable for large OFDM blocks and receivers with limited computational/memory resources. On the other hand, we look for adaptive structures that can easily match time-varying channel conditions.

The chapter is organized as follows. We first describe the system model of the OFDM system with pilot assisted channel estimation in section 3.1, in particular revising the LS method yielding channel estimates on pilots. Then, we describe the proposed techniques for the channel estimation refinement both in time (section 3.2) and frequency (section 3.3), based on adaptive filters. Various adaptation techniques are analyzed and applied to the channel refinement problem in section 3.4. Section 3.5 draws some comparisons between the computational complexity of the algorithms presented. Lastly, section 5.2 in the simulation results chapter (Chap. 5) provides numerical results comparing the various proposed techniques as applied to a DVB-T system.

3.1 System model

Let us consider an OFDM system with N subcarriers using a guard interval (GI) [35] of G taps, where just K_{tot} subcarriers are used, and where the symbol transmitted on subcarrier k of OFDM block n is $S_k(n)$, $k = 0,\ 1, \ldots,\ K_{tot} - 1$. Transmission is performed over a frequency selective fading channel. We assume that the nth OFDM block comprises L_{init} pilot symbols located at subcarriers $p \in \mathcal{P}(n)$ carrying symbols

$X_p(n)$, i.e. $S_p(n) = X_p(n)$. The position and content of pilots is known at the receiver and will be used for channel estimate purposes. The duration of an OFDM block including GI is T_S.

3.1.1 DVB-T pilot arrangement

The DVB-T and DVB-T2 standards [4], [3] define two types of pilots: continual and scattered pilots. Although the continual pilots are transmitted on each OFDM block at fixed locations, for channel estimation we consider the scattered pilots, whose position is changing at each OFDM block. Let $\mathcal{P}(n)$ be the set of scattered pilots indices for OFDM block n. Let also Δ_B be the number of OFDM blocks between two OFDM blocks having the same pilot subcarriers

$$\mathcal{P}(n) = \mathcal{P}(n + \Delta_B) \tag{3.1}$$

We also indicate with Δ'_F the spacing of adjacent pilots on the same OFDM symbol. Hence, we can write

$$\mathcal{P}(n) = \left\{ p \ : \ p = p^{(0)}_{n \bmod \Delta_B} - \Delta'_F \ell, \ \ell \geq 0 \text{ and } p \leq K_{\max} \right\}, \tag{3.2}$$

where $K_{\max}$ is a fixed value for the chosen OFDM block size and $p^{(0)}_{n \bmod \Delta_B}$ is a fixed offset. After time interpolation (TI) the interpolated channel estimates are equally spaced by $\Delta_F = \Delta'_F / \Delta_B$ subcarriers in all OFDM blocks and the set of subcarrier indices for which we have an estimate after TI can be written as

$$\mathcal{Z} = \{ z \ : \ (z \bmod \Delta_F) = 0 \}. \tag{3.3}$$

The total number of estimates per OFDM block after TI is $L_T = \|\mathcal{Z}\|$. For DVB-T a list of positions of continual pilot positions is reported in Table 7 of [4], while scattered pilots for OFDM block n are placed according to 3.2 with $\Delta_F = 3$, $\Delta_B = 4$ and the following offset rule

$$p^{(0)}_{n \bmod \Delta_B} = 3 \cdot (n \bmod 4). \tag{3.4}$$

3.1.2 Channel model

Although we assume that the channel is not varying during each OFDM block, our model includes fading across OFDM blocks (i.e. block fading model). In particular, tap m of the channel impulse response at time t is modeled as

$$h_m(t) = \sum_{q=1}^{N_J} e^{2\pi j f_q(m) t} \tilde{h}_q(m), \quad m = 0, 1, \ldots, N_h - 1, \tag{3.5}$$

where N_J is the number of random Doppler frequencies $f_q(m)$, and $\tilde{h}_q(m)$ are independent random variables accounting for multipath. The frequency response of the channel at subcarrier k and at time t can be written as

$$\bar{H}_k(t) = \sum_{m=0}^{N_h - 1} e^{-2\pi j \frac{km}{N}} h_m(t). \tag{3.6}$$

Let v be the relative speed between the transmitter and the receiver, c the speed of light and f_0 the central frequency of transmission providing the maximum Doppler frequency

$$f_d = \frac{v f_0}{c}\,. \tag{3.7}$$

According to the Jakes model [36], the Doppler frequencies $f_q(m)$ are generated as

$$f_q(m) = \cos(\phi_q(m)) f_d\,, \tag{3.8}$$

where $\phi_q(m)$ is a uniform random variable in the range $[-\pi, \pi)$.

Assuming quasi-static conditions, i.e., slow variations of the channel with respect to the duration of one OFDM block, the nth OFDM block at the receiver after OFDM demodulation can be written as [35]

$$R_k(n) = H_k(n) S_k(n) + w_k(n)\,, \quad k = 0, 1, \ldots, K_{tot} - 1\,, \tag{3.9}$$

where $w_k(n)$ is an additive white Gaussian noise term, with zero mean and variance σ_w^2 and $H_k(n)$ is the frequency response of the channel at subcarrier k of the nth OFDM block, i.e.

$$H_k(n) = \frac{1}{T_S} \int_{nT_S}^{(n+1)T_S} \bar{H}_k(t) \mathrm{d}t\,. \tag{3.10}$$

For pilot symbols we have

$$R_p(n) = H_p(n) X_p(n) + w_p(n)\,, \quad p \in \mathcal{P}(n). \tag{3.11}$$

In a coherent OFDM communication system, symbol detection at the receiver is performed with the aid of channel estimate. Let $\tilde{H}_k(n)$ be an estimate of $H_k(n)$. Hard detection for subcarrier k of OFDM block n is implemented on the zero-forced equalized sample

$$\tilde{d}_k(n) = \frac{R_k(n)}{\tilde{H}_k(n)}\,. \tag{3.12}$$

Soft detection integrated with decoding of error correction codes still requires channel estimate to compute the log likelihood ratios of data bits.

3.1.3 Least-Square channel estimate

By the Least-Square (LS) estimate of the channel, the received samples on pilot carriers are divided by the transmitted pilot symbols to obtain, from (3.11),

$$\tilde{H}_p^{(LS)}(n) = \frac{R_p(n)}{X_p(n)} = H_p(n) + w'_p(n)\,, \quad p \in \mathcal{P}(n), \tag{3.13}$$

where $w'_p(n)$ is a zero mean noise term. In a conventional receiver, the LS estimate on pilots is then interpolated on the other carriers with linear or higher order interpolation techniques [30] to obtain a channel estimate for all subcarriers.

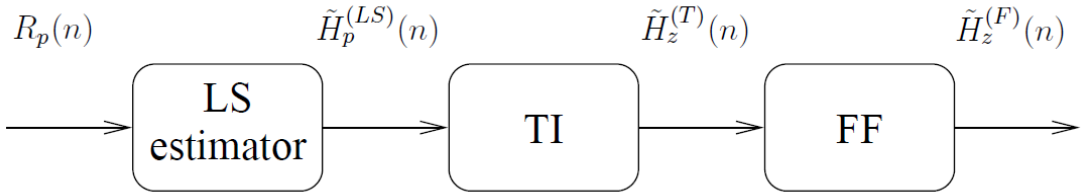

Figure 3.1: Proposed channel estimation scheme.

3.1.4 Channel estimation refinement by adaptive filtering

The LS estimate can be refined by exploiting the correlation of the channel frequency response both among subcarriers of the same OFDM block and among blocks on the same subcarrier. To this end we consider time interpolation (TI) and frequency filtering (FF) to improve the channel estimate, as shown in Fig. 3.1. With reference to OFDM block n of the DVB-T signal, we first obtain the LS estimate on pilots subcarriers, $\tilde{H}_p^{(LS)}(n)$ from (3.13).

Subsequently, TI provides an estimate for subcarriers z', $z' \in \mathcal{Z}/\mathcal{P}(n)$, where no pilot is present by interpolating pilots of nearby OFDM blocks, while keep the LS estimation for $z' = p$, $p \in \mathcal{P}(n)$. With reference to the DVB-T standard, $\mathcal{Z}$ is the set of all scattered pilots, spaced by 3 symbols. After TI the position of the pilots are fixed for each OFDM block, index n is not used for $\mathcal{Z}$. The estimate after TI is denoted as $\tilde{H}_z^{(T)}(n)$.

A further improvement of channel estimate is obtained by FF, which applies an adaptive filter on the TI estimate in order to exploit the frequency correlation of the channel, which provides $\tilde{H}_z^{(F)}(n)$.

The proposed channel estimation chain is illustrated in Fig. 3.1. An adaptive technique for TI is proposed in section 3.2, while in section 3.3 we propose an adaptive technique for FF.

3.2 Adaptive Time Interpolation

Adaptive TI aims at estimating the channel in correspondence of a position where no pilot is present in the current OFDM block, but pilots are present on the same subcarrier in surrounding OFDM blocks.

Let $\tilde{H}_p^{(LS)}(n_0 + m\Delta_B)$, $p \in \mathcal{P}(n_0)$ be the LS estimate for a given pilot subcarrier at different OFDM block $n_0 + m\Delta_B$, where n_0 denotes an OFDM block offset. TI is performed by a filter with N_F pilots in forthcoming OFDM blocks, and N_B pilots in previous OFDM blocks providing estimates for all blocks, i.e. $\tilde{H}_z^T(n)$, $z \in \mathcal{Z}$. This can be achieved by introducing a delay of N_F OFDM blocks in the decoding and storing N_F entire OFDM blocks and the pilots of N_B OFDM blocks.

We consider two options for TI: FIR interpolation and IIR interpolation. With FIR interpolation, TI is performed by a linear FIR using surrounding pilot estimates. We have $\Delta_B - 1$ filters with coefficients $c_\ell^{(T)}(\delta_n)$, $\delta_n \in \{1, 2, \ldots, \Delta_B - 1\}$, $\ell = -N_B, -N_B + 1, \ldots, N_F - 2, N_F - 1$ in correspondence of each shift with respect to the previous nearest

pilot at the same frequency. Let define

$$\psi(n) = \frac{n - n_0}{\Delta_B} \tag{3.14}$$

such that $\lceil \psi(n) \rceil$ can be the shift in terms of OFDM blocks with respect to the nearest pilot at the same frequency for OFDM block n at a given carrier. In this way one can compute δ_n as

$$\delta_n = n - n_0 - \lfloor \psi(n) \rfloor \Delta_B, \qquad \forall n \neq m\Delta_B,\ m \in \mathbb{N} \tag{3.15}$$

The TI estimate is then

$$\tilde{H}^{(T)}_{z'}(n) = \sum_{m=-N_B}^{N_F-1} c^{(T)}_m(\delta_n) \tilde{H}^{(LS)}_{z'}(n_0 + \lceil \psi(n) \rceil \Delta_B + m\Delta_B)\,, \tag{3.16}$$

where $z' \in \mathcal{Z}/\mathcal{P}(n)$.

For the IIR filter, let $b^{(T)}_\ell(\delta_n)$, $\ell = -N_B, -N_B+1, \ldots, N_F-2, N_F-1$ and $a^{(T)}_\ell(\delta_n)$, $\ell = 1, 2, \ldots, R$, be the direct and recursive filter coefficients, respectively, where $\delta_n \in \{1, 2, \ldots, \Delta_B - 1\}$ (3.15). The TI estimate is then

$$\begin{aligned} \tilde{H}^{(T)}_{z'}(n) = \sum_{m=-N_B}^{N_F-1} b^{(T)}_m(\delta_n) \tilde{H}^{(LS)}_{z'}(n_0 + \lceil \psi(n) \rceil \Delta_B + m\Delta_B) + \\ + \sum_{m=1}^{R} a^{(T)}_m(\delta_n) \tilde{H}^{(T)}_{z'}(n - m\Delta_B)\,. \end{aligned} \tag{3.17}$$

In both cases, filter coefficients are adapted for each OFDM block, as described in section 3.4. Note that in the following $\tilde{H}^{(T)}_z(n)$ represents the estimate on both TI and scattered pilots of OFDM block n

$$\tilde{H}^{(T)}_z(n) = \begin{cases} \tilde{H}^{(LS)}_p(n) & z = p, \quad p \in \mathcal{P}(n) \\ \tilde{H}^{(T)}_{z'}(n) & z = z', \quad z' \in \mathcal{Z}/\mathcal{P}(n) \end{cases} \tag{3.18}$$

For ideal TI, $\tilde{H}^{(T)}_{z'}(n)$, $z' \in \mathcal{Z}/\mathcal{P}(n)$ are affected only by the filtered version of w'. In practice, TI estimates will also be affected by imperfect interpolation and by the variations of the channels. Therefore, in general TI and pilot estimates have a different mean square error (MSE). For example, assuming a time-invariant channel and by denoting expectation with $\mathrm{E}[\cdot]$ we have

$$MSE_{\text{pilot}} = \mathrm{E}_{p \in \mathcal{P}(n)} \left[|\tilde{H}^{(LS)}_p(n) - \tilde{H}_p(n)|^2 \right] = \sigma^2_w, \tag{3.19}$$

$$MSE_{\text{TI}} = \mathrm{E}_{z' \in \mathcal{Z}/\mathcal{P}(n)} \left[|\tilde{H}^{(T)}_{z'}(n) - \tilde{H}_{z'}(n)|^2 \right] = \frac{\sigma^2_w}{M} \sum_{\ell=N_B}^{N_F} \sum_{m=1}^{\Delta_B - 1} |c^{(T)}_\ell(m)|^2, \tag{3.20}$$

where average for TI is taken with respect to both the OFDM block index and the subcarrier index (i.e. across the interpolating filters).

Note that for high Doppler frequencies we need to interpolate on more pilots in order to adequately track channel variations.

3.3 Adaptive Frequency Filtering

Correlation among carriers of the same OFDM block is exploited designing one or more adaptive filters in order to decrease the level of noise on the time interpolated (TI) channel estimates. We propose to refine the TI estimate $\tilde{H}_z^{(T)}(n)$ by a two-step procedure: a) predict the channel frequency response at each TI subcarrier by combining (filtering) surrounding received pilots on the same OFDM block and b) combine the predicted estimate with the TI estimate.

The reliability of the TI estimates is different with respect to pilot estimates, hence optimal frequency filter taps should take into account the different reliabilities. This leads to the design of multiple filters (MF), according to the reliability of each input. The number of different patterns to consider depends on the number of TI estimates between two scattered pilots at the same frequency, $\Delta_B - 1$. We can show this solution does not increase the computational complexity of the single filter solution, however it is much more memory consuming.

In this section we propose three techniques to implement the refinement. In the optimal approach TI estimates of each OFDM block are filtered with a *frequency filter* (FF) that takes into account the different MSEs between TI and pilot estimates. The second solution is simpler, since the idea is to design a single FF for all the carriers irrespective of the different reliabilities among the estimates. This solution, even if performs worse, is provided as a performance benchmark for more elaborated solutions. The last solution is based on the design of a single FF which takes into account the different MSEs, combining the benefits of the optimal solution with the simplified architecture of the single-filter. Anyway, all the techniques are based on adaptive filters, either Infinite Impulse Response (IIR), or linear Finite Impulse Response (FIR) filters which rely upon the LMS or Kalman algorithms to derive the coefficients.

3.3.1 Frequency Filtering with Multiple Filters

When we design more than one filter, each of the FF operates on a different input pattern defined as a different sequence of TI and pilot estimates. The number of prediction filters is thus fixed by Δ_B. According to (3.2) for DVB-T we consider $\Delta_B = 4$. An example of positions of pilot and TI estimates is reported in Fig. 3.2, where we also can easily derive the number of FF required by this method, i.e. Δ_B. Note that the prediction filters are applied and updated $1/\Delta_B$ of the times a single-filter solution would require thus yielding the same complexity. However, memory is increased by a factor Δ_B to store the coefficients of the multiple filters (MF). Let $\nu(z) \in \{1, 2, \ldots, \Delta_B\}$ be the index of the filter to be used to obtain the filtered version of subcarrier z. Later we will show how the filter index $\nu(z)$ is related to the reliability of the subcarrier considered.

The filtered estimate at position $z \in \mathcal{Z}$ is the combination of a) the TI or pilot estimate $\tilde{H}_z^{(T)}(n)$ and b) a *predicted estimate* obtained combining (FIR filtering) surrounding TI pilots on the same OFDM block denoted as $\tilde{H}_z^{(P)}(n)$. In formulas the predicted estimate is obtained as

$$\tilde{H}_z^{(P)}(n) = \sum_{q=-Q, q\neq 0}^{+Q} c_{q,\nu(z)}^{(F)} \tilde{H}_{z+q\Delta_F}^{(T)}(n)\,, \quad z \in \mathcal{Z}\,, \tag{3.21}$$

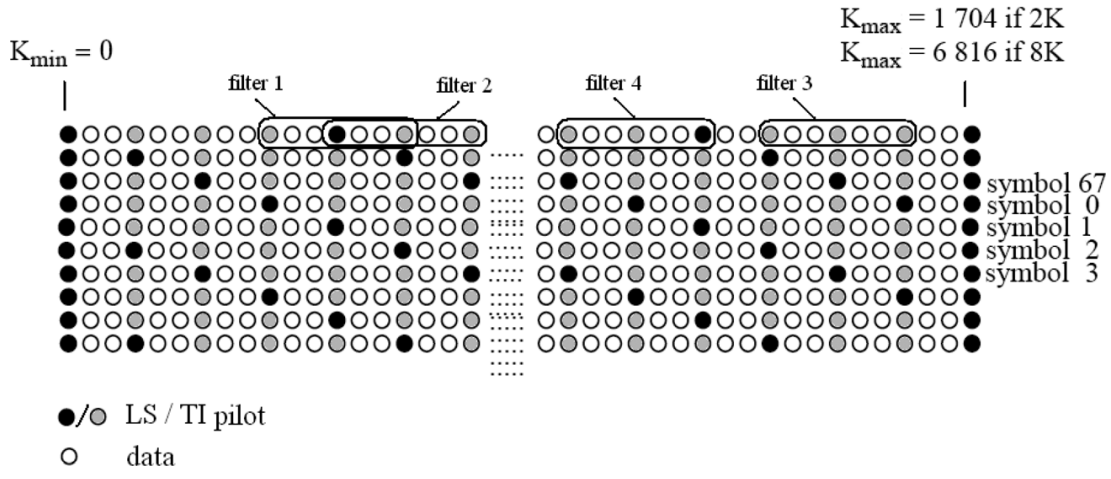

Figure 3.2: Position of estimates after TI and use of multiple frequency filters. Number of filter coefficients $2Q + 1 = 3$.

where $2Q$ is the filter order, and $\{c^{(F)}_{q,\nu(z)}\}$ are filter coefficients to be adapted as described in section 3.4. Note that, as $\tilde{H}^{(P)}_z(n)$ provides a prediction of the channel estimate at z, the filter does not include the TI estimate $\tilde{H}^{(T)}_z(n)$. Considering that predicted estimates and TI estimates have a different MSE we combine them with suitable coefficients to obtain the FF estimate

$$\tilde{H}^{(F)}_z(n) = \alpha_{\nu(z)}\tilde{H}^{(P)}_z(n) + \beta_{\nu(z)}\tilde{H}^{(T)}_z(n)\,, \tag{3.22}$$

where $\alpha_{\nu(z)}$ and $\beta_{\nu(z)}$ are combining coefficients which are derived later in section 3.3.3 depending on the filtering approach.

Each frequency filter is adapted independently using the corresponding available pattern of TI and pilot estimates. For example, with reference to Fig. 3.2 filter 1 is adapted whenever in the OFDM block we have a sequence TI/pilot/TI estimates, i.e. the reference signal is a pilot while the filtered signals are both TI estimate, whereas filter 2 is adapted whenever we have a sequence of pilot/TI/TI estimates.

In this way, the number of pilots over which to perform interpolation is depending on the frequency selectivity of the channel. The more the channel is selective, the more pilots we need to interpolate to have an accurate channel estimate.

3.3.2 Frequency Filtering with Single Filter

As we will show later, $\alpha_{\nu(z)} = 1$ for all practical implementations, hence, in case of FF Single Filter (FF-SF) we have just one combining coefficient, i.e. $\beta_{\nu(z)} = \beta$ which is independent by the filter index. Moreover, we need to consider just one set of filter coefficients, since $\nu(z)$ is a constant. Thus (3.22) can be rewritten to get the single-filter FF estimate

$$\tilde{H}^{(F)}_z(n) = \tilde{H}^{(P)}_z(n) + \beta\tilde{H}^{(T)}_z(n)\,, \tag{3.23}$$

where β will be determined according to the channel conditions, as detailed in section 3.3.3. For the channel estimate prediction we consider two approaches: a) FIR filter prediction and b) IIR filter prediction.

For the FIR prediction filter we have the same as in (3.21), but with only one set of filter coefficients, i.e. $\{c^{(F)}_{q,\nu(z)}\} = \{c^{(F)}_q\}$

$$\tilde{H}^{(P)}_z(n) = \sum_{q=-Q,q\neq 0}^{+Q} c^{(F)}_q \tilde{H}^{(T)}_{z+q\Delta_F}(n)\,, \quad z \in \mathcal{Z}, \tag{3.24}$$

where $2Q$ is the filter order. $\{c^{(F)}_q\}$ are the filter coefficients to be adapted as described in section 3.4. The last equation shows that with FF-SF, differently from FF Multiple Filters (FF-MF), the adaptation makes use of all available estimates, irrespective of the reliability.

For the IIR prediction filter we have

$$\tilde{H}^{(P)}_z(n) = \sum_{q=-Q,q\neq 0}^{+Q} b^{(F)}_q \tilde{H}^{(T)}_{z+q\Delta_F}(n) + \sum_{q=1}^{Q_2} a^{(F)}_q \tilde{H}^{(P)}_{z-q\Delta_F}(n)\,, \quad z \in \mathcal{Z}\,, \tag{3.25}$$

where $\{a^{(F)}_q\}$ and $\{b^{(F)}_q\}$ are adapted as described in section 3.4. In this case the predicted signal is obtained by combining both TI estimates at surrounding pilots and previous estimates. Note that for the IIR filter, only the direct part is fed with pilots having both a lower and a higher subcarrier index, while the recursive part can only be fed with one of the two. In (3.25) the recursive component is fed with lower subcarriers but an equivalent solution would have been

$$\tilde{H}^{(P)}_z(n) = \sum_{q=-Q,q\neq 0}^{+Q} b^{(F)'}_q \tilde{H}^{(T)}_{z+q\Delta_F}(n) + \sum_{q=-Q_2}^{-1} a^{(F)'}_q \tilde{H}^{(P)}_{z-q\Delta_F}\,, \quad z \in \mathcal{Z}\,. \tag{3.26}$$

3.3.3 Adaptation of combining coefficients

For the combining of the predicted and TI estimates (3.22) we aim at minimizing the mean square error (MSE) of the combined estimate with respect to the actual channel frequency response, i.e., by denoting expectation with E[·],

$$\min_{\alpha_{\nu(z)},\beta_{\nu(z)}} \{\mathrm{E}[|\tilde{H}^{(F)}_z(n) - H_z(n)|^2]\}, \quad z \in \mathcal{Z}. \tag{3.27}$$

In particular, indicating respectively, the power of the prediction error and of the noise as

$$\sigma^2_{\mathrm{P}}(\nu(z)) = \mathrm{E}[|\tilde{H}^{(P)}_z(n) - H_z(n)|^2], \tag{3.28a}$$

$$\sigma^2_w = \mathrm{E}[|\tilde{H}^{(F)}_z(n) - H_z(n)|^2], \tag{3.28b}$$

the minimum MSE solution provides

$$\alpha_{\nu(z)} = \frac{\sigma^2_w}{\sigma^2_w + \sigma^2_{\mathrm{P}}(\nu(z))}\,, \quad \beta_{\nu(z)} = \frac{\sigma^2_{\mathrm{P}}}{\sigma^2_w + \sigma^2_{\mathrm{P}}(\nu(z))}\,. \tag{3.29}$$

Minimum MSE combining requires the estimation of the powers of both, noise and prediction error. These estimates can only rely on the received pilot estimates which are affected by both noise and channel response (both unknown), making it difficult

to compute (3.29). Instead, we resort to a different approach by setting $\alpha_{\nu(z)} = 1$ and minimizing the MSE of the combined estimate with respect to the TI estimate

$$\beta_{\nu(z)} = \arg\min_{\beta_{\nu(z)}} \left\{ \mathrm{E}\left[|\tilde{H}_z^{(F)}(n) - H_z^{(T)}(n)|^2 \right] \right\} . \tag{3.30}$$

By replacing the expectation with an average, we obtain the *average power* combining coefficient

$$\beta_{\nu(z)} = 1 - \frac{\sum_{(k,n)\in\mathcal{K}(q)} \Re\left\{ \tilde{H}_z^{(P)}(n) \tilde{H}_z^{(T)*}(n) \right\}}{\sum_{(k,n)\in\mathcal{K}(\nu(z))} |\tilde{H}_z^{(F)}(n)|^2} \tag{3.31}$$

where $\Re\{x\}$ is the real part of x and set $\mathcal{K}(\nu(z))$ collects subcarrier and OFDM block couples where filter $\nu(z)$ is used. In case of FF-SF, $\mathcal{K}(\nu(z)) = \mathcal{Z}$, since there is just one set collecting all available subcarriers.

3.4 Adaptation of prediction filters

The filter coefficients must be adapted in order to track variations of the statistical properties of the channel and we consider adaptive techniques for both FIR and IIR filters, namely the least mean square (LMS) and the Kalman filter method. The filter coefficients are adapted with each new frequency response LS estimate on pilots. In particular, at each received OFDM block, a new block of patterned pilot samples is available and the filter is first adapted using the new pilots and then used to refine the channel estimate. Note that, while in [25] a complex technique requiring the direct estimation of the correlation matrix among channel estimates has been used, here we propose simpler methods based either on the least mean square (LMS) approach, or the Kalman filter, or an Infinite Impulse Response filter theory presented in [37]. In the following we first focus on the single coefficient set implementation, while the generalization to implement FF by means of MF is shown later.

Let us consider a generic filter with U taps obtained at adaptation step $i-1$, $\{c_\ell(i)\}$, $\ell = 1, 2, \ldots, U$, and let $\boldsymbol{c}(i) = [c_1(i), c_2(i), \ldots, c_U(i)]^T$ be the column vector containing the filter coefficients, where $[\cdot]^T$ is the transpose operator. For an input signal $\{x_i\}$ define the column vector

$$\boldsymbol{X}(i) = [x_{\ell_1(i)}, x_{\ell_2(i)}, \ldots, x_{\ell_U(i)}]^T . \tag{3.32}$$

where $\ell_j(i)$ is a function of i and j. The filter output can be written as

$$y_i = \boldsymbol{X}(i)^T \boldsymbol{c}(i-1) , \quad i \in \mathcal{I} , \tag{3.33}$$

and $\mathcal{I}$ is the set of indices over which the filter is computed.

3.4.1 LMS FIR adaptive filtering

The LMS algorithm is derived from the Wiener filter [35] with the aim of minimizing the MSE of the filter output with respect to a desired signal $\{d_i\}$, i.e.

$$\boldsymbol{c}^{(opt)}(i) = \arg\min_{\boldsymbol{c}(i)} \mathrm{E}[|y_i - d_i|^2] . \tag{3.34}$$

At adaptation step i, $i \in \mathcal{I}$, of the LMS algorithm, we first compute the error of the filter output

$$\epsilon(i) = d_i - \boldsymbol{X}(i)^T \boldsymbol{c}(i-1) \tag{3.35}$$

and then update the filter coefficients as

$$\boldsymbol{c}(i) = \boldsymbol{c}(i-1) + \mu(i)\epsilon(i)\boldsymbol{X}(i)^H \,, \tag{3.36}$$

where $[\cdot]^H$ is the Hermitian operator and $\mu(i)$ is the adaptation step. A variety of choices for $\mu(i)$ have been considered and we selected

$$\mu(i+1) = \frac{\alpha_1}{\alpha_2 + M_X(i)} \,, \tag{3.37}$$

where α_1 and α_2 are suitable constants and $M_X(i) = \|\boldsymbol{X}(i)\|^2$, as it gives the best convergence performance. The resulting LMS algorithm is reported in Table 3.1, where $\xi_{\mu(i)} = 1$ is a constant value, which is defined later to account for MF.The LMS algorithm operates by updating the filters coefficients at steps $i \in \mathcal{I}$.

TI adaptation

For TI, we apply the adaptation of the filter coefficients on the continual pilots, so that the LS estimate is available on all OFDM blocks and we have a reference value for all interpolated positions. However, the adaptation filters are then used to filter the scattered pilots, whose the continual are a subset. In particular, we adapt simultaneously $\Delta_B - 1$ filters, with impulse responses $c_j = c^{(T)}_{j-N_B-1}(\delta_n)$, $\delta_n \in \{1, 2, \ldots, \Delta_B - 1\}$ and length $U = N_F + N_B$. In this case, the output signal is ignored. The input signal is $x_{\ell_j(i)} = \tilde{H}_p^{(LS)}(\ell_j(i))$, $p \in \mathcal{P}'(n) \subset \mathcal{P}(n)$, where $\mathcal{P}'(n)$ is the set collecting the continual pilots. The input indices are given by this rule

$$\ell_j(i) = n_0 + \lceil \psi(n) \rceil \, \Delta_B + \Delta_B(j - N_B - 1) \,, \tag{3.38}$$

and $\mathcal{I} = \{i_0, i_0 + 1, \ldots\}$, where i_0 is such that $\psi(i_0) > N_B - n_0/\Delta_B$. The desired signal is $d_i = \tilde{H}_i^{(LS)}(n)$, which is available for all $i \in \mathcal{I}$ as we are considering continual pilots.

FF adaptation

For FF the filter coefficients are adapted with each new frequency response estimate at pilots z, $z \in \mathcal{Z}$. Considering that all carriers have the same statistics and that the correlation among channel gains at different carriers is depending only on their mutual position in the spectrum, we conclude that the correlation matrix is Hermitian and the vector of the frequency domain adaptive filter coefficients $\boldsymbol{c}$ is Hermitian symmetric. Therefore, we can limit the estimation to half of the filter, i.e. $\{c_q\}$, $q = -Q, -Q + 1, \ldots, -1$ while for the remaining taps we have

$$c_q = c^*_{-q} \,, \quad q = 1, 2, \ldots, Q \,, \tag{3.39}$$

where $[\cdot]^*$ denotes complex conjugate. For MF technique, at each step a different coefficient set has to be considered. The LMS algorithm operates by updating the

filter coefficients at steps $\mathcal{I} = \mathcal{Z}$. With reference to the algorithm of Table 3.1, the input signal is $x_{\ell_j(i)} = \tilde{H}^{(T)}_{\ell_j(i)}(n)$, with indices

$$\{\ell_j(i)\} = \{i-Q, i-Q+1, \ldots, i-1\}, \quad \text{such that} \begin{cases} i-Q > K_{\min} \\ i-1 < K_{\max} \end{cases} \tag{3.40}$$

The desired signal is $d_i = \tilde{H}^{(T)}_i(n)$, the output signal is $y_i = \tilde{H}^{(P)}_i(n)$ and the filter is $\{c^{(F)}_j\}$ with length $U = Q$, where we used (3.39).

3.4.2 FIR adaptive filtering by Kalman filter

The LMS algorithm is slow in convergence and a faster adaptation technique is provided by the Kalman filter. The Kalman filter pertains a dynamic system where we observe the noisy output associated to an unknown state of a process and we aim at estimating the state. In our problem of channel estimate the unknown state is the set of filter coefficients $\{c_\ell\}$.

The Kalman algorithm is reported in Table 3.2. The parameters are the initial value of the covariance matrix $\boldsymbol{P}(\ell_1 - 1) = \alpha_3 \cdot \boldsymbol{I}$, where $\boldsymbol{I}$ is the identity matrix and the convergence parameter λ. Settings for TI and FF are the same used for LMS and reported in section 3.4.1.

3.4.3 FIR adaptive filtering by MF

The above FIR algorithms are easily generalized for MF updating, to be used for FF. In this case, at each step a different coefficient set will be considered. For example, considering for subcarrier $z = Q$ we adapt the pattern $c_{q,1}$, i.e. we set $\nu(Q) = 1$. Then for $z = Q + 1$ we adapt $c_{q,2}$, $\nu(Q+1) = 2$, and so on. But, when we reach the step $z = Q + \Delta_B$, we will adapt the coefficient set adapted Δ_B steps before, i.e. $c_{q,1}$, since the surrounding pilots of $z = Q$ and $z = Q + \Delta_B$ have the same reliability distribution. This is true for all the patterns, in other words there is an implicit periodicity on the updating procedure which allows for complexity savings. At each step the algorithm roundly changes the pattern to adapt. Moreover, when another OFDM block is received, i.e. new TI estimates are computed, the initial pattern from which we start the adaptation procedure changes, although the circular pattern order is still the same. The first pattern has to be chosen with respect to the current reliability distribution, i.e. position of TI and LS estimates on the surrounding pilots. In the Kalman filter method, also the matrix $\boldsymbol{P}$ depends by the step, since each $\boldsymbol{P}$ is an element of memory updated by the opportune coefficient pattern, and so it has to be stored and roundly changed.

In Table 3.1 we denote with $\xi_{\nu(i)}$ a binary variable depending by the algorithm step, in order to turn on or off the update of a particular coefficient set. This variable plays the role of weighting factor for the reliabilities of the TI estimates. For example, by selecting $\xi_{\nu(i)} = 0$ for all positions i corresponding to a pilot, while leaving $\xi_{\nu(i)} = 1$ for all positions corresponding to a TI estimate (see (3.18)), we update the filter only when the reference signal is a TI estimate, thus considering unreliable pilot estimates. On the other side, by setting $\xi_{\nu(i)} = 1$ for all $\nu(i)$, we do not introduce different reliability weights for each estimate. In this way, for FF-MF we have Δ_B adaptation stages, one

for each coefficient set, namely $\{\{c_{\ell,1}\},\{c_{\ell,2}\},\ldots,\{c_{\ell,\Delta_B}\}\}$. For each set we have a different configuration of $\xi_{\nu(i)}$. For example, the adaptation stage of $\{c_{\ell,1}\}$ sets $\xi_{\nu(i)}$ to be 1 whenever $\nu(i)=1$, and 0 elsewhere. On the contrary, for $\{c_{\ell,\Delta_B}\}$ we set $\xi_{\nu(i)}$ to be 1 whenever $\nu(i)=\Delta_B$, and 0 elsewhere. In this way the single filter case is obtain just setting as constant $\xi_{\nu(i)}=1$, $\forall i\in\mathcal{I}$.

3.4.4 IIR adaptive filtering

IIR filters have an infinite impulse response and therefore should better exploit the correlation in time and frequency than FIR filters. On the other hand, convergence of adaptive IIR filters is critical. Moreover, an IIR filter may be unstable if its frequency response has poles on the unit circle and this should be avoided in the adaptation.

Let us consider a general IIR filter with z-transform

$$C(z)=\frac{B(z)}{A(z)}=\frac{\sum_{q=1}^{U} b_q z^{-q}}{1+\sum_{q=1}^{Q_R} a_q z^{-q}}\,. \tag{3.41}$$

For the filter coefficients adaptation we consider a lattice structure that allows to express the stability conditions in a simple form and enforce them in the adaptation process [38]. In the lattice form, $A(z)$ is parametrized by the column vector of *reflection coefficients* $\boldsymbol{g}=[\sin\gamma_1,\sin\gamma_2,\ldots,\sin\gamma_{Q_R}]^T$. From these coefficients we can derive a_q by a recursive algorithm [37]. We first set

$$a_\ell^{(\ell)}=\sin\gamma_\ell\,, \tag{3.42}$$

for $\ell=1,2,\ldots,Q_R$, then we compute

$$a_q^{(\ell)}=a_q^{(\ell-1)}+\sin\gamma_q\cdot a_{\ell-q}^{(\ell-1)}\qquad 1\le q\le \ell-1. \tag{3.43}$$

Lastly, we have

$$A(z)=1+\sum_{q=1}^{Q_R} a_q^{(Q_R)} z^{-q}\,. \tag{3.44}$$

Assuming that the angles γ_q belong to the interval $[-\frac{\pi}{2},\frac{\pi}{2})$ for $1\le q\le Q_R$, we have that the roots of $A(z)$ are all within the circle of unitary radius.

Let $\boldsymbol{a}(i)$ and $\boldsymbol{b}(i)$ be the column vectors of the recursive and direct filter coefficients, respectively, at adaptation step i. By defining the column vector $\boldsymbol{Y}(i)=[y_{i-1},\ldots,y_{i-Q_R}]^T$, the error signal at adaptation step i can be written as

$$\epsilon(i)=d_i-\boldsymbol{X}(i)^T\boldsymbol{b}(i-1)-\boldsymbol{Y}(i)^T\boldsymbol{a}(i-1)\,. \tag{3.45}$$

For the adaptation of the IIR filter coefficients we consider the set of the parameters at the ith adaptation step

$$\boldsymbol{\theta}(i)=[\boldsymbol{b}(i)^T,\boldsymbol{g}(i)^T]^T\,, \tag{3.46}$$

The adaptation of the parameters is performed as follows

$$\boldsymbol{\theta}(i+1)=\boldsymbol{\theta}(i)+\mu(i)\boldsymbol{V}(i)\epsilon(i)\,, \tag{3.47}$$

where $\mu(i)$ is the step size and $\boldsymbol{V}(i)$ is the driving vector sequence. For the Steiglitz-McBride [39] algorithm, consider the signal u_i obtained by filtering x_i with the filter

Table 3.1: LMS adaptation for FIR filter

Update for $i \in \mathcal{I}$

$$\boldsymbol{X}(i) = [x_{\ell_1(i)}, x_{\ell_2(i)}, \ldots, x_{\ell_U(i)}]^T$$

$$\epsilon(i) = \xi_{\nu(i)} \left[d_i - \boldsymbol{X}(i)^T \boldsymbol{c}(i-1) \right]$$

$$M_X(i) = \|\boldsymbol{X}(i)\|^2$$

$$\boldsymbol{c}(i) = \boldsymbol{c}(i-1) + \mu(i)\epsilon(i)\boldsymbol{X}^H(i)$$

$$\mu(i+1) = \frac{\alpha_1}{\alpha_2 + M_X(i)}$$

Table 3.2: Kalman filter for FIR filter

Initialization

$$\boldsymbol{P}(\ell_1 - 1) = \alpha_3 \cdot \boldsymbol{I}$$

Update for $i \in \mathcal{I}$

$$\boldsymbol{X}(i) = [x_{\ell_1(i)}, x_{\ell_2(i)}, \ldots, x_{\ell_U(i)}]^T$$

$$\boldsymbol{\pi}^H(i) = \boldsymbol{P}(i-1)\boldsymbol{X}(i)^*$$

$$\epsilon(i) = \xi_{\nu(i)} \left[d_i - \boldsymbol{X}(i)^T \boldsymbol{c}(i-1) \right]$$

$$r(i) = \frac{1}{\lambda + \boldsymbol{X}(i)^T \boldsymbol{\pi}(i)^H}$$

$$\boldsymbol{K}(i)^H = \xi_{\nu(i)} r(i) \boldsymbol{\pi}(i)^H$$

$$\boldsymbol{c}(i) = \boldsymbol{c}(i-1) + \epsilon(i)\boldsymbol{K}(i)^H$$

$$\boldsymbol{P}(i) = \lambda^{-1}[\boldsymbol{P}(i-1) - \boldsymbol{K}(i)^H \boldsymbol{\pi}(i)]$$

Table 3.3: Adaptation algorithm for IIR filter

Update for $i \in \mathcal{I}$

$$\boldsymbol{X}(i) = [x_{\ell_1(i)}, x_{\ell_2(i)}, \ldots, x_{\ell_U(i)}]^T$$

$$\boldsymbol{Y}(i) = [y_{i-1}, y_{i-2}, \ldots, y_{i-Q_R}]^T$$

$$\epsilon(i) = d_i - \boldsymbol{X}(i)^T \boldsymbol{b}(i-1) - \boldsymbol{Y}(i)^T \boldsymbol{a}(i-1)$$

$$\mu(i) = \mu(i-1) + \alpha_4 \epsilon(i) \frac{|d_i|}{\mathrm{E}\left[|x_j|\right]}$$

Obtain $\boldsymbol{a}(i)$ from $\boldsymbol{g}(i)$ as (3.42), (3.43) and (3.44)

$$\boldsymbol{U}(i) = [u_{i-1}, u_{i-2}, \ldots, u_{i-Q_R}]^T$$

$$[\boldsymbol{V}_1(i)]_q = x_{\ell_1(i-q)} - \boldsymbol{U}(i-q)^T \boldsymbol{a}(i-q), \quad \text{for } q = 1, \ldots Q_R$$

$$\boldsymbol{V}_2(i) = [-d_{i-1}, -d_{i-2}, \ldots, -d_{i-Q_R}]^T,$$

$$\boldsymbol{\theta}(i) = [\boldsymbol{b}(i)^T, \boldsymbol{g}(i)^T]^T$$

$$\boldsymbol{\theta}(i+1) = \boldsymbol{\theta}(i) + \mu(i) \boldsymbol{V}(i) \epsilon(i)$$

having z-transform response $1/A(z)$. Let $\boldsymbol{V}_1(i)$ be the Q_R-size column vector having entries $[\boldsymbol{V}_1(i)]_q = u_{i-q}$ and $\boldsymbol{V}_2(i)$ be the Q_R-size column vector having entries $[\boldsymbol{V}_2(i)]_q = -d_{i-q}$, with $q = 1, 2, \ldots, Q_R$. We have

$$\boldsymbol{V}(i) = [\boldsymbol{V}_1(i)^T, \boldsymbol{V}_2(i)^T]^T. \tag{3.48}$$

In order to ensure a better convergence, the updating step is modified with respect to [37] using the following normalization

$$\mu(i) = \mu(i-1) + \alpha_4 \epsilon(i) \frac{|d_i|}{\frac{1}{L_T} \sum_{j=1}^{L_T} |x_{\ell_j(i)}|}. \tag{3.49}$$

For both TI and FF adaptations, the reference, the input and output signals are as for the FIR case. In particular, for TI $Q_R = R$, while for FF $Q_R = Q_2$. Since convergence is critical for IIR, we did not applied IIR to MF, due to the lack of useful samples per filter.

3.5 Complexity analysis

In order to compare our estimation methods with alternative existing techniques, we consider the low complexity *delay-subspace* tracking method proposed in [23]. This technique takes advantage of the slow variability of the delay-subspace on pilots to estimate the channel frequency response. The pilots considered are the TI subcarriers $z \in \mathcal{Z}$, i.e. the subspace tracking (ST) does not consider the TI step, or better, it assumes a pilot estimate at each TI position. This technique can be decomposed in three

Table 3.4: List of computational complexity for several channel estimation methods.

	mac	$\mathcal{O}(\cdot)$
ST & rank adapt. & projection	$4L_T r_{\max}^2 + L_T^2 r_{\max} + 2L_T^2 + r_{\max}^2$	$\max\{\mathcal{O}(L_T r_{\max}^2), \mathcal{O}(L_T^2 r_{\max})\}$
LMS FF	$5L_T Q$	$\mathcal{O}(L_T Q)$
Kalman FF	$3L_T Q^2 + 2L_T Q$	$\mathcal{O}(L_T Q^2)$

parts: ST, rank estimation and projection. It aims at estimate an orthonormal basis of the delay-subspace, and project on it the LS estimates of the channel gains on pilots. The algorithm used in [23] needs an adaptive rank estimation to find the dimension of the orthonormal basis. The maximum rank is found to be the minimum between the channel impulse response (N_h) and the number of pilots used to estimate the channel. Denoting as L_T the number of TI pilots, and $r_{\max}$ the minimum between L_T and the channel length N_h, we draw a comparison between the complexities of the ST method and the techniques proposed in this chapter. We report in Table 3.4 the computational complexity of several methods, measured as number of complex multiplications ('mac') and with $\mathcal{O}(\cdot)$ notations. Besides, a plot of the complexities concerning the FF part of channel estimation is given in Fig. 3.3.

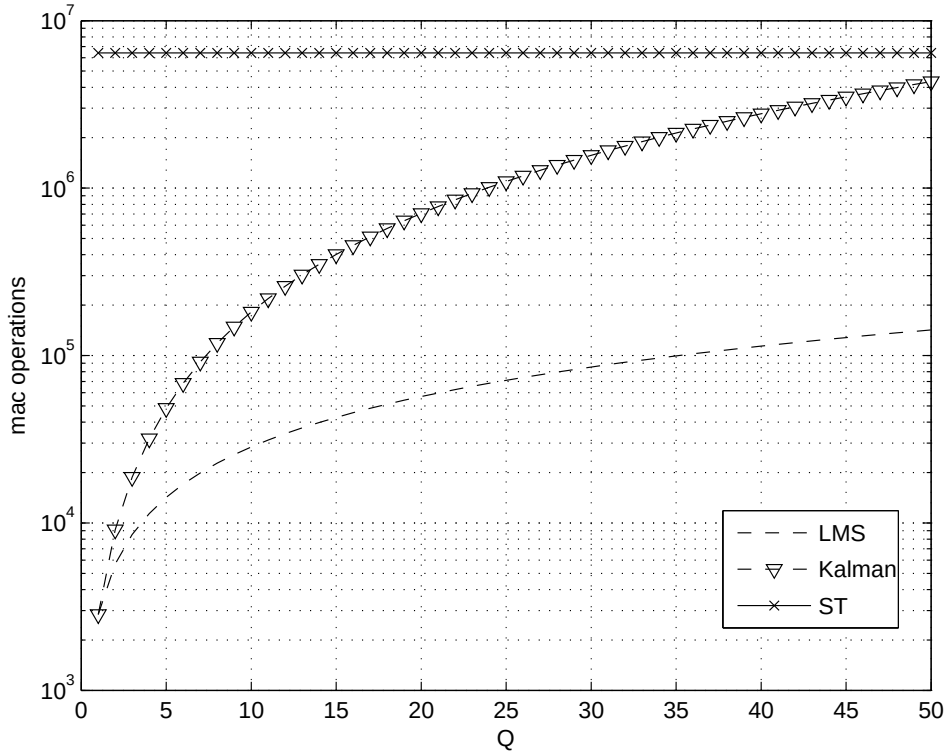

Figure 3.3: Comparison of computational complexity for several channel estimation methods.

Chapter 4

Time and Frequency Synchronization for DVB-T2

The new digital video terrestrial standard DVB-T2 [3] has been recently defined and will substitute DVB-T [4] in the coming years, providing high definition television and new additional services. In upgrading the terrestrial digital video broadcasting (DVB-T) standard to its new version DVB-T2, particular attention has been paid to synchronization and fast channel acquisition. To this end, among the novelties introduced in the new standard, a specific frame structure has been adopted. Each data frame is preceded by a signaling block denoted *P1 symbol* [3], whose main purposes are i) to allow fast DVB-T2 signal discovery, ii) to allow initial time and frequency synchronization and iii) provide some basic signaling for decoding forthcoming data.

P1 symbol is modulated by an inverse fast Fourier transform (IFFT), however, it differs from conventional orthogonal frequency division multiplexing (OFDM) modulation (as it is described in [40]) in two aspects: a) two guard intervals (GIs) are added, before and after the IFFT modulated symbol and b) GIs are frequency-shifted versions of the corresponding portions of the IFFT modulated symbol. This structure avoids to confuse regular OFDM DVB-T symbols with P1 symbols.

Here we focus on the use of this special frame structure for synchronization and signal acquisition. An overview of synchronization techniques for OFDM can be found in [41], however they do not apply immediately to P1 symbol because it is not a conventional OFDM symbol, since it includes two guard intervals with a suitable frequency shift. The implementation guidelines [42] suggest a technique for time and frequency synchronization, exploiting the correlation among the main part of the received P1 symbol and the two guard intervals, similarly to what has been considered for conventional OFDM synchronization (see e.g. [7]). We denote this technique correlation-based synchronization (CBS).

The contribution provided by the following sections of this chapter are listed below. First, we show how CBS is implemented as reported in the implementation guidelines. Second, we provide an analytical formulation showing that CBS has significant limitations even on a very simple two-taps channel that is commonly considered for assessing the performance of DVB-T2. Third, we propose a new detection technique, still based on the correlation approach, which overcomes the limitations of CBS. Finally, we provide an analytical description of the optimal estimator in the Maximum-Likelihood

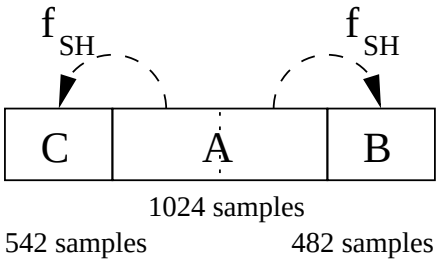

Figure 4.1: Structure of P1 symbol.

(ML) sense.

In particular, in the last section, namely section 4.4, the maximum likelihood (ML) synchronization scheme to track P1 symbol is derived. Similarly to [7], to derive the ML scheme we assume a flat additive white Gaussian noise (AWGN) channel, while performance is evaluated on frequency-selective channels as well. In fact, as P1 symbol synchronization is the first operation of a receiver, to assume channel knowledge for design is not realistic. Moreover, complexity considerations favor schemes where a coarse synchronization is achieved with P1 symbol, while channel estimation is performed in subsequent data symbols, as well as a more refined time and frequency estimation [42]. Anyway we will show that the exact maximization of the likelihood function requires numerical methods, making it difficult to design a practical ML estimator. Therefore, we derive a suboptimal algorithm implementing just ML time synchronization, while using a simplified scheme based on CBS for carrier frequency offset (CFO) estimation. The proposed synchronization schemes are compared with existing solutions in a typical DVB-T2 scenario on both AWGN and frequency selective channels. Simulation results are reported in Chapter 5.

4.1 System model

The DVB-T2 system employs a classical guard interval (GI) based OFDM modulation. OFDM symbols are organized in frames, and each frame includes at the beginning a special preamble, called P1 symbol which allows fast detection of the DVB-T2 signal on the channel bandwidth, and acquisition of initial timing and frequency offset. Furthermore, P1 symbol carries some signaling data providing information about the data-symbol FFT size, use of multiple transmit antennas, and some indication about the GI length.

For all the transmission mode provided by DVB-T2 standard, P1 symbol has always a fixed-length structure including an OFDM symbol with $K = 1024$ sub-carriers, together with a special time-domain repetition scheme, as depicted in Fig. 4.1.

The part named C is a frequency shifted version of the first $N_c = 542$ samples of the OFDM symbol which forms the useful part, A. While the part B is the frequency shifted version of the last $N_b = 482$ samples of A. Within the OFDM symbol, according to the constraints of the emission mask, 853 carriers could be transmitted. However, just 384 out of 853 carry non null symbols, hence we refer to this subset of $M = 384$ carriers as P1 symbol *active* carriers with indexes $k_{P1}(i),\ i = 0, \ldots, M-1$. The active carriers in P1 are differentially BPSK (DBPSK) modulated and used to transmit the

signaling information. Let $d_i,\ i = 0, \ldots, M-1$ be the DBPSK modulated signal to be transmitted on the active carriers. The main part of block A is generated as

$$s_n^{(A)} = \frac{1}{\sqrt{M}} \sum_{i=0}^{M-1} d_i \, e^{j2\pi \frac{k_{P1}(i)-426}{K} n} \tag{4.1}$$

The two guard interval-like portion are appended as depicted in Fig. 4.1. Parts C and B are obtained applying a frequency shift $f_{\mathrm{SH}} = 1 \,/\, KT_s$ to the first N_c samples and the last N_b samples of $s_n^{(A)}$, respectively. This allows us to write the signal transmitted in the DVB-T2 preamble as

$$s_n = \begin{cases} e^{j2\pi f_{\mathrm{SH}} T_s n} s_n^{(A)} & 0 \le n < N_c \text{ (part C)} \\ s_{n-N_c}^{(A)} & N_c \le n < N_c + N_a \text{ (part A)} \\ e^{j2\pi f_{\mathrm{SH}} n T_s} s_{n-N_a}^{(A)} & N_a + N_c \le n < 2N_a \text{ (part B)}, \end{cases} \tag{4.2}$$

where T_s is the sampling period and N_a is the number of complex values of the useful part, i.e. $N_a = K$. Without loss of generality we assume a unitary variance of the signal s_n, which is also assumed to have zero mean.

Similarly to [43], for the derivation of the synchronization scheme we assume a flat additive white Gaussian noise (AWGN) channel affected by a CFO (normalized with respect to the channel bandwidth) Φ_0, and a delay of θ_0. In other words, we are assuming that the receiver does not have any a-priori information on the channel and does not perform any channel estimation before synchronization. This is a reasonable assumption since in practice P1 synchronization is the first operation of the receiver, while channel estimation is performed on the next OFDM symbols.

For the AWGN case, the received signal can be written as

$$r_n = s_{n-\theta_0} e^{j2\pi\Phi_0(n-\theta_0)/N_a} + w_n \tag{4.3}$$

where w_n is the zero-mean Gaussian noise term with power σ_w^2. We also define the $2N_a-$size vector of the received samples. When perfect time synchronization is achieved the vector writes as

$$\boldsymbol{r}_{\theta_0} = [r_{\theta_0}, r_{\theta_0+1}, \ldots, r_{\theta_0+2N_a}]^T. \tag{4.4}$$

Without loss of generality, in the following we assume $\theta_0 = 0$.

4.2 Correlation-Based Synchronization

Even if s_n samples are assumed to be independent and identically distributed, and just AWGN is assumed to corrupt the transmitted signal, the received samples r_n are not uncorrelated. In fact, due to the guard interval-like portions of the P1 symbol structure, some of the received samples with a time separation of N_cT_s or N_bT_s seconds are strong correlated. For example, let correlate together pair of samples, from the received stream, separated by $N_cT_s = 542T_s$ seconds, i.e. multiply r_{n+N_c} with the conjugate of r_n. From (4.3) for the first N_c received samples pertaining to P1 we can write

$$r_n^* r_{n+N_c} = y_n^* y_{n+N_c} e^{j2\pi\Phi_0 N_c/K} + w_n' \tag{4.5}$$

where, noting that $y_n = y_{n+N_c} e^{j2\pi f_{\mathrm{SH}} n T_s}$ for $n = 0, \ldots, N_c - 1$ we get

$$r_n^* r_{n+N_c} = |y_n|^2 e^{-j2\pi f_{\mathrm{SH}} n T_s} e^{j2\pi \Phi_0 N_c / K} + w'_n, \quad n = 0, \ldots, N_c - 1 \tag{4.6}$$

In the last equation the term accounting for CFO, $e^{j2\pi\Phi_0 N_c/K}$, is independent by n. Moreover, f_{SH} is known at the receiver (it is fixed to $1/KT_s$), hence the exponential term accounting for the frequency shift can be corrected multiplying the received samples by $e^{j2\pi f_{\mathrm{SH}} n T_s}$, which yields

$$u_n = r_n^* r_{n+N_c} e^{j2\pi f_{\mathrm{SH}} n T_s} = |y_n|^2 e^{j2\pi \Phi_0 N_c / K} + w'_n, \quad n = 0, \ldots, N_c - 1 \tag{4.7}$$

where w'_n encompasses all the noise terms, which are zero mean random processes. The samples of u_n have the same phase for the time index $n = 0, \ldots, N_c - 1$. The same reasoning can be provided for what concerns the correlation of the part B of P1 symbol, yielding

$$v_n = r_n^* r_{n+N_b} e^{-j2\pi f_{\mathrm{SH}} n T_s} = |y_n|^2 e^{j2\pi \Phi_0 N_b / K} + w''_n, \quad n = 2N_c, \ldots, N_a + N_c - 1 \tag{4.8}$$

where w''_n has the same statistics of w'_n.

A running average filter is used to reduce the degree of noisiness on the samples u_n and v_n. This filter is a rectangular window where each tap has amplitude the reciprocal of the window's width. A filter of duration N_r yields

$$u'_n = \frac{1}{N_r} \sum_{k=0}^{N_r - 1} u_{n-k} \tag{4.9a}$$

$$v'_n = \frac{1}{N_r} \sum_{k=0}^{N_r - 1} v_{n-k} \tag{4.9b}$$

When N_r is large enough to provide the mean of the random variables (i.e. neglecting the noise) and assuming that P1 symbol is uncorrelated with previous and next data transmissions, both $|u'_n|$ and $|v'_n|$ have a trapezoidal shape. The DVB-T2 implementation guidelines [42] assumes N_r to be equal to K, hence for what concerns $|u'_n|$, the resulting trapezoidal has the smaller parallel side of length $(N_r - N_c) = N_b$, while for $|v'_n|$ it has smaller side of length $(N_r - N_b) = N_c$. In formulas, defining the trapezoid function

$$\mathrm{trap}_n(a, b) = \begin{cases} \frac{2}{b-a} n + \frac{b}{b-a} & -b/2 \le n \le -a/2\,, \\ 1 & -a/2 \le n \le a/2\,, \\ \frac{2}{a-b} n - \frac{b}{a-b}\,, & a/2 \le n \le b/2 \\ 0 & \text{otherwise}\,, \end{cases} \tag{4.10}$$

we have

$$u'_n \approx \mathrm{trap}_{n+N_a/2+N_b}(N_b, 2N_c + N_b) e^{j2\pi\Phi_0 N_c / N_a} \tag{4.11a}$$

$$v'_n \approx \mathrm{trap}_n(N_c, 2N_b + N_c) e^{j2\pi\Phi_0 N_b / N_a} \tag{4.11b}$$

where $\approx$ indicates the fact that we neglected the additive noise. Note that u'_n, and v'_n, have respectively N_c, N_b, samples with the same phase proportional to Φ_0.

By time-aligning and multiplying the output of the two correlation outputs we obtain

$$|z_n| = |v'_n \cdot u'_{n-N_a}| \approx \begin{cases} \frac{1}{N_b N_c}(n+\alpha)^2, & -\alpha \le n < -(N_b+N_c) \\ \frac{1}{N_c}(n+\alpha), & -(N_b+N_c) \le n < -\frac{N_b}{2} \\ 1 & -\frac{N_b}{2} \le n < \frac{N_b}{2} \\ \frac{(n-\alpha)}{N_b N_c}(n-\frac{3}{2}N_b), & \frac{N_b}{2} \le n < \alpha, \end{cases} \tag{4.12}$$

where $\alpha = \frac{2N_c+N_b}{2}$. Note that, being the result of the multiplication of two straight lines, $|z_n|$ has sections of two different parabolas as edges. Hence the absolute value of z_n is not symmetrical with respect to $n = 0$. These reasonings provide a way to perform initial estimations of symbol timing and CFO. The resulting correlation-based synchronization (CBS) scheme is shown in Fig. 4.3. It comprises two branches, one for correlating parts A and B and the other for correlating parts A and C. While the result of the correlation signals in CBS scheme are plotted in Fig. 4.2. The synchronization procedures as from the CBS scheme output are described in the following clues.

Threshold based symbol timing

Time synchronization is achieved by taking the maximum of $|z_n|$. In a practical scheme, we look for the first sample above a threshold Z_T, i.e. $|z_{\tau_1}| > Z_T$, and the first sample $\tau_2 > \tau_1$ below the threshold, i.e. $|z_{\tau_2}| < Z_T$. Then, the middle point $m_\tau = \frac{\tau_1+\tau_2}{2}$

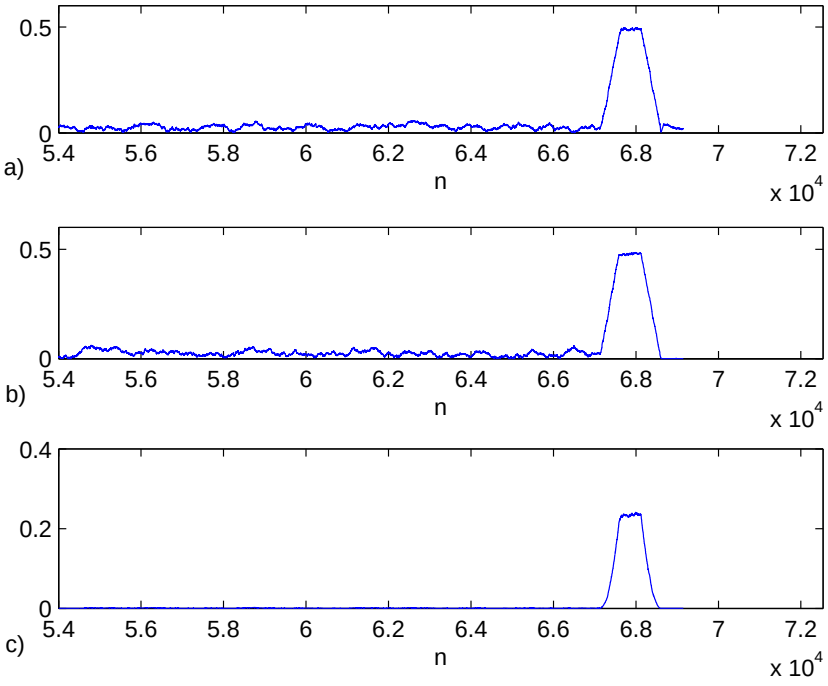

Figure 4.2: Absolute value of the waveforms at the input of the running average filters a)u'_n, b) v'_n, and c) z_n. AWGN channel with SNR of 10dB.

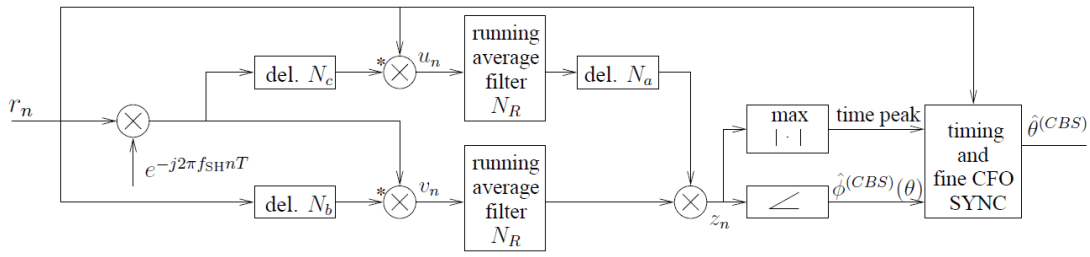

Figure 4.3: Correlation Based Synchronization (CBS) scheme.

provides the delay estimate $\hat{\theta}_{\text{CBS}}$ corresponding to the first sample of the P1 symbol useful part (part A)

$$\hat{\theta}_{\text{CBS}} = (m_\tau)_R - (2N_a + N_b/2) + \tau_0\,, \tag{4.13}$$

where $(x)_R$ denotes the integer nearest to x and τ_0 is a correcting factor accounting for the asymmetry of $|z_n|$ which has to be tuned empirically (our simulations assume $\tau_0 = 18$). Moreover, the delay $(2N_a + N_b/2)$ accounts for the latency accumulated during the correlation operations in the following way: 1) $N_b/2$ accounts for the fact we are taking the middle point of a trapezoid with shorter parallel side of length N_b, 2) a delay N_a is due to the time-alignment of the two branches and 3) an additional delay N_a accounts for the duration of the useful part A.

CFO estimation

CFO can be decomposed in an integer number of subcarrier spacings (F_0), and a fractional part ($0 \leq \phi_0 < 2\pi$), i.e.

$$\Phi_0 = F_0 + \frac{\phi_0}{2\pi}. \tag{4.14}$$

The integer part of CFO can be recovered by exploiting the fact that only a subset of the P1 symbol subcarriers is active, therefore by collecting the power on shifted versions of the active pattern and finding the peak of the collected power we can obtain the integer part of CFO (for details refer to Appendix A). For the fractional part, we can write z_n as

$$z_n = |z_n| e^{j2\pi(F_0 + \frac{\phi_0}{2\pi})N_a/N_a} = |z_n| e^{j\phi_0}\,. \tag{4.15}$$

Hence, an estimate of the fractional CFO is obtained by taking the phase of z_n, after proper time synchronization, i.e. with $n = \theta_{\text{CBS}}$

$$\hat{\phi}_{\text{CBS}}(n) = \angle z_n\,. \tag{4.16}$$

4.2.1 CBS in a two-taps Channel

When a two taps channel is considered in place of a single tap channel, the received signal is constituted by two replicas of the transmitted signal delayed by a significant

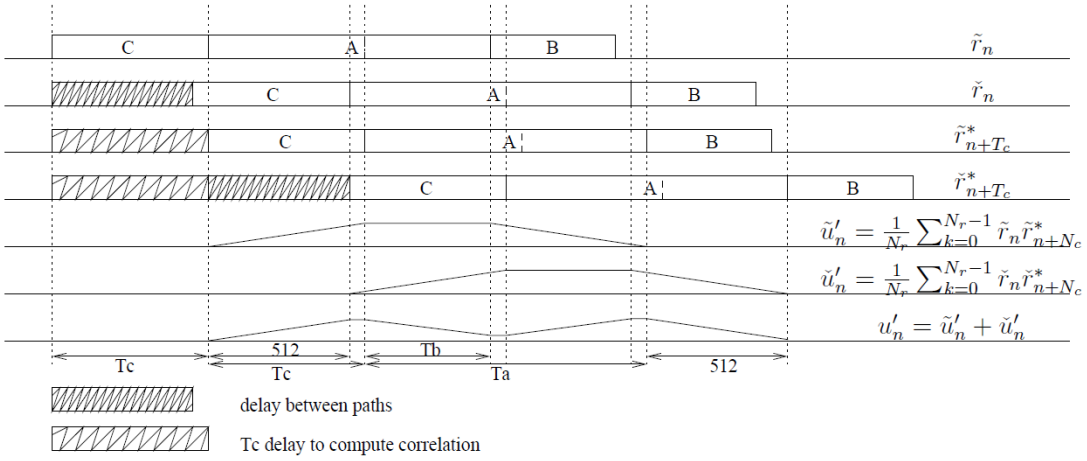

Figure 4.4: Scheme of CBS's upper branch signals.

time. In this case the received sampled signal can be written as

$$r_n = \underbrace{h_0 s_n e^{j2\pi\Phi_0 n/N_a}}_{\tilde{r}_n} + \underbrace{h_1 s_{n-\tau} e^{j2\pi\Phi_0 n/N_a}}_{\check{r}_n} + w_n \,, \tag{4.17}$$

where τ is relative delay of the second path with respect to the first one, while h_0 and h_1 are the amplitudes of the two taps. Without loss of generality we assume $|h_0|^2+|h_1|^2 = 1$ so that the average SNR is still SNR $= 1/\sigma_w^2$. We denote as $\tilde{r}_n$ and $\check{r}_n$ the received signals corresponding to the first and second channel tap, respectively. In the following analysis we neglect the noise term w_n as we are interested in analyzing the shape of the useful signals for synchronization purposes. Moreover, we focus on the case where both taps have unitary gain ($h_0 = h_1 = \sqrt{2}/2$), and the delay between the channel path is $512T_s$ seconds, but the following considerations apply also in more general cases. For the part C branch (i.e. CBS branch correlating part A with part C of P1 symbol) the signal at the input of the running average filter u_n becomes

$$u_n = e^{-j2\pi f_{\mathrm{SH}} n T_s} \left[\check{r}_n \check{r}^*_{n+N_c} + \check{r}_n \tilde{r}^*_{n+N_c} + \tilde{r}_n \check{r}^*_{n+N_c} + \tilde{r}_n \tilde{r}^*_{d,n+N_c}\right]. \tag{4.18}$$

Since $\check{r}_n$, $\tilde{r}_{n+N_c}$, and $\tilde{r}_n$, $\check{r}_{n+N_c}$ are uncorrelated pairs of samples, after the averaging filter their contribution is negligible and we have

$$\begin{aligned} u'_n \approx & e^{j2\pi\Phi_0 N_c/N_a} \Big[\mathrm{trap}_{n+N_a/2+N_b}(N_b, 2\alpha) + \\ & e^{-j2\pi f_{\mathrm{SH}}\tau T_s} \mathrm{trap}_{n+N_a/2+N_b-512}(N_b, 2\alpha)\Big] \,. \end{aligned} \tag{4.19}$$

For $\tau = N_a/2$ we have $e^{-j2\pi f_{\mathrm{SH}}\tau T_s} = -1$ and in the intersection the trapezoids of (4.19) are nulled, letting the waveform go to nearly zero in the middle. A similar derivation can be obtained also for the branch relative to part B, yielding

$$\begin{aligned} v'_n \approx & e^{j2\pi\Phi_0 N_c/N_a} \left[\mathrm{trap}_n(N_c, 2N_b + N_c) + \right. \\ & \left. e^{-j2\pi f_{\mathrm{SH}}\tau T_s} \mathrm{trap}_{n-512}(N_c, 2N_b + N_c)\right] \,. \end{aligned} \tag{4.20}$$

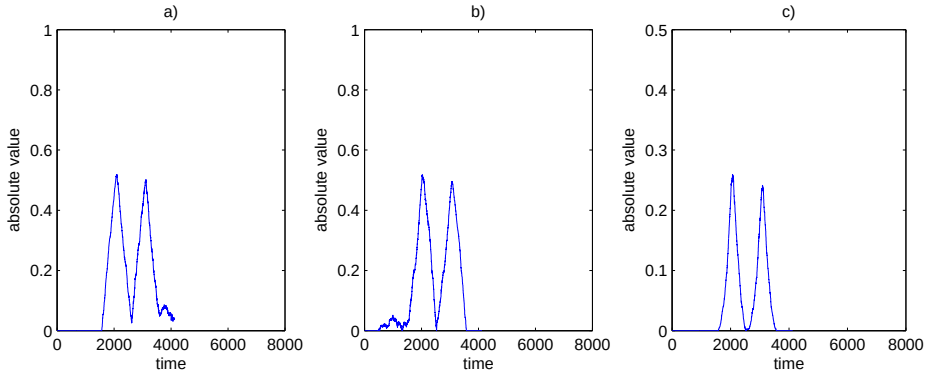

Figure 4.5: Absolute value of the waveforms at the input of the moving average filters a) upper branch, b) lower branch, and after the branches multiplication at the output c), for a 2 taps channel. SNR is 20dB, both taps have the same gain and a mutual delay of 512 samples.

Thus, the time alignment and product of the two-peaks-waveforms of the upper and lower branch results in a waveform with two peaks separated by N_a samples and trapezoidal shapes, as shown in scheme of Fig. 4.4. Moreover, the plot in Fig. 4.5, showing the absolute value of the CBS output, confirms our theoretical reasonings. This argumentation explains why the timing synchronization method described in the previous section (4.13) fails. Note that even when synchronization is implemented by taking the maximum of $|z_n|$ we still miss the correct delay.

4.3 Slope-Based Synchronization

In order to overcome the issue on the two-taps channel we consider here an alternative approach denoted slope-based synchronization (SBS) where we look for the rising and falling edge of the absolute value waveform at the output of the CBS scheme. By detecting the correct edges we will identify the start and the end of the channel impulse response. To this end, the output of CBS is filtered with a derivative filter, which estimates the slope of the ramp. In particular, we compute

$$q'_n = |z_{n+1}| - |z_n| \,. \tag{4.21}$$

For rising edge we have $q_n \geq 0$ while for falling ramps we have $q_n \leq 0$. In order to average out noise and other interferences we then apply an averaging filter of N_q taps to obtain

$$q_n = \frac{1}{N_q} \sum_{n=0}^{N_q-1} q'_n \,. \tag{4.22}$$

Note that the cascade of the derivative and averaging filters turns out to be the difference between two input samples spaced by N_q, i.e.

$$q(n) = |z_{n+N_q}| - |z_n| \,. \tag{4.23}$$

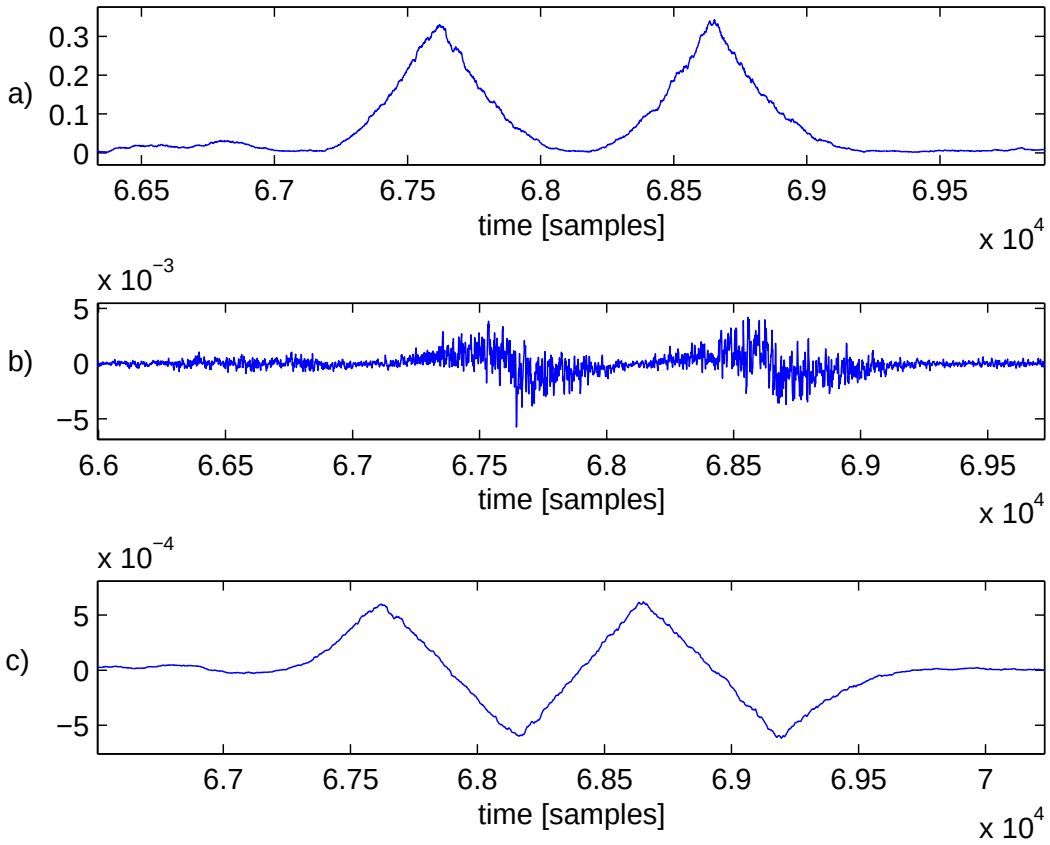

Figure 4.6: Signal at the a) output of the initial synchronizer ($|z_n|$), b) output of the derivative filter (q'_n) and c) output of the averaging filter (q_n) for two-taps channel with echoes at 0 dB. SNR = 0 dB.

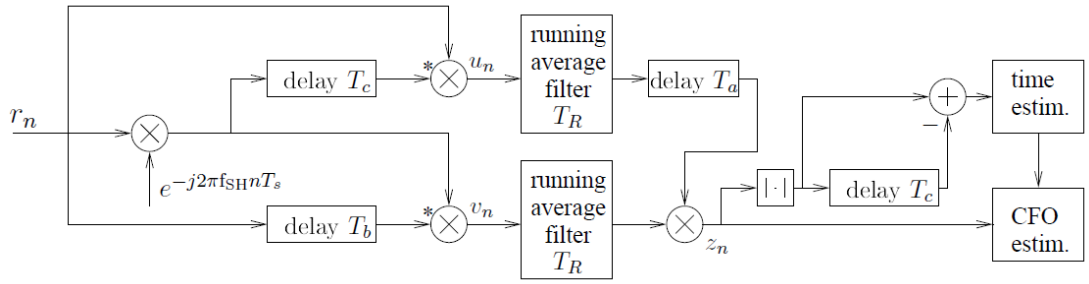

Figure 4.7: Slope Based Synchronization (SBS) scheme.

Fig. 4.6 shows the resulting signals for a two-taps channel assuming $N_q = N_c$. This choice for N_q results from considering that the rising edge due to the first channel tap is N_c samples long.

Once the derivative has been computed, we look for the maximum absolute value of $q(n)$, which corresponds to the sharper variation of the derivative signal. Let $n' = \text{argmax}\{|q(n)|\}$. Now, if $q(n') > 0$ the derivative is positive and we are on the rising edge due to the first channel tap, while if $q(n) < 0$ the derivative is negative and we are on the declining ramp of the second tap. In the first case, the synchronization is computed as in (4.13), while if the derivative is negative we have an additional delay of N_a and

$$\hat{\theta}_{\text{CBS}}|_{q(n')<0} = (m_\tau)_R - (N_a + N_b/2) + \tau_0 \,. \tag{4.24}$$

The SBS scheme implementation is plotted in Fig. 4.7.

4.4 Maximum Likelihood Synchronization

Maximum Likelihood (ML) synchronization aims at estimating both timing and CFO, which maximize the probability of receiving $\{r_n\}$, assuming a-priori equally likely offsets. To this end, we exploit the structure of P1 symbol in the time domain (see Fig. 4.1). For a generic delay θ and CFO Φ, the log-likelihood function (LLF) is defined as

$$\Lambda(\theta, \Phi) = \log f(\boldsymbol{r}_\theta) \,, \tag{4.25}$$

where $f(\cdot)$ denotes the conditional probability density function (PDF) of the variables in its argument *given* $\theta_0 = \theta$ and $\Phi_0 = \Phi$. The ML estimate is obtained by maximizing $\Lambda(\theta, \Phi)$. In particular, the ML synchronization algorithm works as follows. For each value of θ we maximize $\Lambda(\theta, \Phi)$ with respect to Φ, obtaining

$$\hat{\Phi}_{\text{ML}}(\theta) = \text{argmax}_\Phi\{\Lambda(\theta, \Phi)\} \,. \tag{4.26}$$

Then we find the delay that maximizes the LLF, i.e.

$$\hat{\theta}_{\text{ML}} = \text{argmax}_\theta\{\Lambda(\theta, \hat{\Phi}^{(ML)}(\theta))\} \,. \tag{4.27}$$

Note that with the ML estimator we aim at determining both the integer and the fractional part of the CFO. The maximization of (4.27) is achieved by checking when the LLF exceeds a threshold and then selecting the delay that maximizes the LLF within an observation window.

4.4.1 Computation of LLF

Detailed derivation of the LLF is reported in Appendix B. This section just review the most important steps.

We first observe that parts B and C are correlated only with part A and that each sample of part B or C is correlated only with one sample of part A, therefore we can decompose $f(\boldsymbol{r}_\theta)$ into two parts. The conditional PDF can be written as

$$f(\boldsymbol{r}_\theta) = \prod_{n=0}^{N_c-1} f(r_n, r_{n+N_c}) \prod_{n=2N_c}^{2N_c+N_b-1} f(r_n, r_{n+N_b}) \tag{4.28}$$

and the LLF (4.25) becomes

$$\Lambda(\theta, \Phi) = \sum_{n=0}^{N_c-1} \log f(r_n, r_{n+N_c}) + \sum_{n=2N_c}^{2N_c+N_b-1} \log f(r_n, r_{n+N_b}) \,. \tag{4.29}$$

We then approximate the received block $\boldsymbol{r}_\theta$ as Gaussian distributed, as commonly assumed for OFDM transmissions [43]. Hence

$$f(r_n, r_{n+k}) = \frac{1}{\pi^2 \det(\boldsymbol{R})} \exp\left\{-[r_n, r_{n+k}]\boldsymbol{R}^{-1}[r_n, r_{n+k}]^H\right\} , \tag{4.30}$$

where $\boldsymbol{R} = \mathrm{E}\{[r_n, r_{n+k}]^H[r_n, r_{n+k}]\}$. Defining $\rho = \frac{\sigma_s^2}{\sigma_s^2+\sigma_w^2}$, we have

$$\mathrm{E}[r_n r^*_{n+N_c}] = (\sigma_s^2 + \sigma_w^2)\rho\, e^{-j2\pi\Phi N_c/N_a} e^{j2\pi(n-\theta)/N_a} \tag{4.31}$$

$$\mathrm{E}[r_n r^*_{n+N_b}] = (\sigma_s^2 + \sigma_w^2)\rho\, e^{-j2\pi\Phi N_b/N_a} e^{-j2\pi(n-\theta)/N_a} . \tag{4.32}$$

From (4.30) we have

$$\begin{aligned} &\log f(r_n, r_{n+N_c}) = \\ &\quad c_1 + c_2\left[-\frac{\rho}{2}\left(|r_n|^2 + |r_{n+N_c}|^2\right) + \Re\left\{r_n r^*_{n+N_c} e^{j2\pi\Phi N_c/N_a} e^{-j2\pi(n-\theta)/N_a}\right\}\right] \end{aligned} \tag{4.33}$$

$$\begin{aligned} &\log f(r_n, r_{n+N_b}) = \\ &c_1 + c_2\left[-\frac{\rho}{2}\left(|r_n|^2 + |r_{n+N_b}|^2\right) + \Re\left\{r_n r^*_{n+N_b} e^{j2\pi\Phi N_b/N_a} e^{j2\pi(n-\theta-N_c)/N_a}\right\}\right] , \end{aligned} \tag{4.34}$$

where $\Re\{x\}$ denotes the real part of x, and c_1 and c_2 are positive constants which do not depend on θ and Φ, thus can be neglected for the maximization. Let us define the following variables

$$\gamma_c(\theta) = \sum_{n=\theta}^{\theta+N_c-1} r_n r^*_{n+N_c} e^{j2\pi(n-\theta)/N_a} \tag{4.35a}$$

$$\gamma_b(\theta) = \sum_{n=\theta+2N_c}^{\theta+2N_c+N_b-1} r_n r^*_{n+N_b} e^{-j2\pi(n-\theta)/N_a} \tag{4.35b}$$

$$\phi_c(\theta) = \frac{1}{2} \sum_{n=\theta}^{\theta+N_c-1} |r_n|^2 + |r_{n+N_c}|^2 \tag{4.35c}$$

$$\phi_b(\theta) = \frac{1}{2} \sum_{n=\theta+2N_c}^{\theta+2N_c+N_b-1} |r_n|^2 + |r_{n+N_b}|^2 \,. \tag{4.35d}$$

By inserting (4.33) and (4.34) into (4.29) and using (4.35) we obtain

$$\begin{aligned} \Lambda(\theta, \Phi) \simeq & -\rho \left[\phi_c(\theta) + \phi_b(\theta)\right] + |\gamma_c(\theta)| \cos\left(2\pi\Phi\frac{N_c}{N_a} + \angle\gamma_c(\theta)\right) + \\ & |\gamma_b(\theta)| \cos\left(2\pi\Phi\frac{N_b}{N_a} + \angle\gamma_b(\theta)\right), \end{aligned} \tag{4.36}$$

where $\simeq$ means that both the left and right side of the equation attain the maxima for the same values of θ and Φ. A scheme for the computation of the required variables from the received signal is shown in Fig. 4.8.

Although time synchronization can be obtained by evaluating the values of $\Lambda(\theta, \Phi)$ for each time instant, estimating the CFO requires numerical methods for the maximization of $\Lambda(\theta, \Phi)$ with respect to Φ.

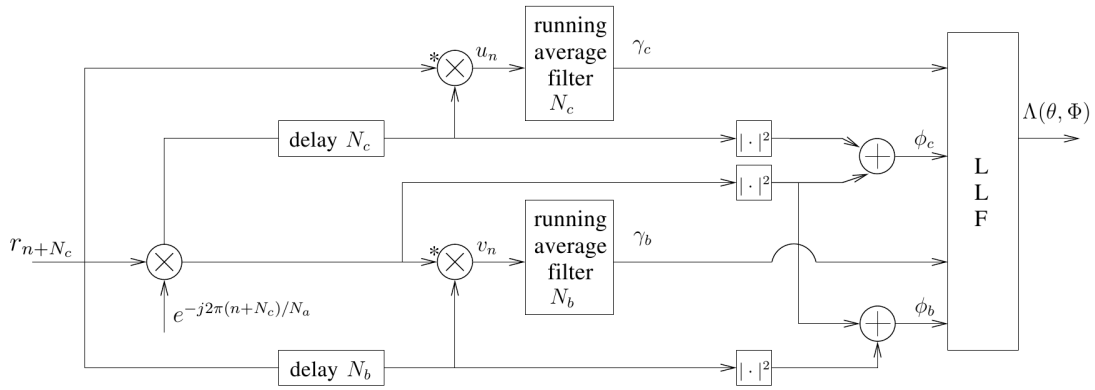

Figure 4.8: ML estimator scheme.

4.4.2 ML Timing estimation

In order to avoid complex numerical methods to estimate the CFO, we propose to merge the correlation-based approach (for CFO estimation) and the ML approach (for timing estimation) in what we denote as ML time (MLT) estimator.

First note that when time and frequency synchronization is achieved, by inserting (4.3) into (4.35a) and (4.35b) we have

$$2\pi\Phi\frac{N_c}{N_a} + \angle\gamma_c(\theta) \approx 2\pi\Phi\frac{N_b}{N_a} + \angle\gamma_b(\theta) \approx 0 \tag{4.37}$$

and therefore the cosine terms in (4.36) can be approximated with ones. Then, we observe that $\phi_c(\theta) + \phi_b(\theta)$ is almost constant with respect to θ since the P1 symbol is found within the data stream and P1 samples have also the same statistical power of data samples. Therefore, we can consider the alternative LLF function

$$\Lambda(\theta) \approx |\gamma_c(\theta)| + |\gamma_b(\theta)| \,. \tag{4.38}$$

Table 4.1: MLT estimator.

1. Use the scheme of Fig. 4.8 to compute $\gamma_b(\theta)$ and $\gamma_c(\theta)$
2. Use (4.38) to compute $\Lambda(\theta)$
3. **If** $\Lambda(\theta_1) > \Lambda_T$ and $\Lambda(\theta_2) < \Lambda_T$ with $\theta_2 > \theta_1$
4. Find the maximum of $\Lambda(\theta)$ among all $\theta \in [\theta_1, \theta_2]$

$$\hat{\theta}_{\text{MLT}} = \underset{\theta \in [\theta_1, \theta_2]}{\text{argmax}} \{\Lambda(\theta)\}$$

5. Use (4.16) to compute $\hat{\phi}_{\text{CBS}}(\hat{\theta}_{\text{MLT}})$

$$\hat{\phi}_{\text{CBS}}(\hat{\theta}_{\text{MLT}}) = \angle z_{\hat{\theta}_{\text{MLT}}}$$

6. Correct the time delay $\hat{\theta}_{\text{MLT}}$ and the CFO $\hat{\phi}_{\text{CBS}}(\hat{\theta}_{\text{MLT}})$
7. Compute the FFT of part A of the received P1 symbol
8. Use the P1 active subcarriers to estimate the integer part of CFO F_0, as described in [42] and detailed in Appendix A
9. **End If**

The MLT synchronization looks for the maximum of (4.38) with respect to time offset θ. This is obtained first by finding when $\Lambda(\theta) > \Lambda_T$, where Λ_T is a threshold value, and then finding the maximum of $\Lambda(\theta)$, namely $\Lambda(\hat{\theta_{\text{MLT}}})$, before it goes below Λ_T again. Lastly, the CFO is estimated using the CBS scheme fixing the time index with the ML estimated timing $\hat{\theta}_{\text{MLT}}$. The MLT estimation algorithm is summarized in Table 4.1.

Chapter 5

Simulation Results and Conclusions

5.1 Chapter 2 - Simulation results

This section reports and discuss the performance of the OFDM receiver, covered in chapter 2, which exploits the entire GI in order to improve data detection. Simulations have been performed as to assess the performance of the proposed receiver in a particular DVB-T2 configuration scenario involving a demodulation technique called CD3, and LDPC coding. In the following we will denote our proposed receiver as FR (Full Recovery), and the receiver proposed in [12] as PR (Partial Recovery). Before presenting the results, we calculate the expected performance of the system without coding. For example, we consider a conventional OFDM system with FFT size of $N = 2048$ symbols, with GI length ratio of $\frac{1}{4}$, then G is equal to $\frac{1}{4}$ (G/N) of the FFT size (N), i.e. $G = 512$ symbols. The performance is measured with respect to the Signal-to-Noise Ratio (SNR). For a given value of Bit Error Rate (BER), in presence of white Gaussian noise, we suppose that the standard SNR is ρ. Assuming perfect IBI cancellation and perfect reconstruction of the useful ISI components, the improvement on the conventional performance is easily calculated. With a transmitted power uniformly distributed over all carriers (P_{Tx}), taking the average of the GI samples we decrease the variance of the noise (N_0) by half, so we have a portion of the received signal with power of noise halved. Taking as reference the above example, the increased SNR is

$$\rho_{new} = \frac{P_{Tx}}{\frac{N-G}{N}N_0 + \frac{G}{N}N_0/2} = \frac{P_{Tx}/N_0}{1-\frac{G}{2N}} = \frac{\rho}{1-\frac{1}{8}} = \frac{8}{7}\rho \tag{5.1}$$

The extent of the improvement without coding, in ideal conditions and assuming perfect recovering of the GI, is therefore only function of GI ratio G/N, namely $\left(1-\frac{G}{2N}\right)$. With our example parameters $G/N = \frac{1}{4}$ the improvement factor is $\frac{8}{7}$, or equivalently 0.58 dB. So we expect that the curve BER versus SNR, for the proposed receiver, will be shifted to the left with respect to the conventional performance curve of about 0.58 dB. In our simulations we use the CD3 channel estimation [14], that is an OFDM system organizing the transmission stream dividing the information bits in several frames, each containing an equal number of OFDM blocks. To reduce the pilot symbols overhead, channel estimation is computed only by the first OFDM block of the frame, used as training sequence at the receiver, and then the channel estimation for each following OFDM symbols is obtained refining the previous channel estimation with the received data signal.

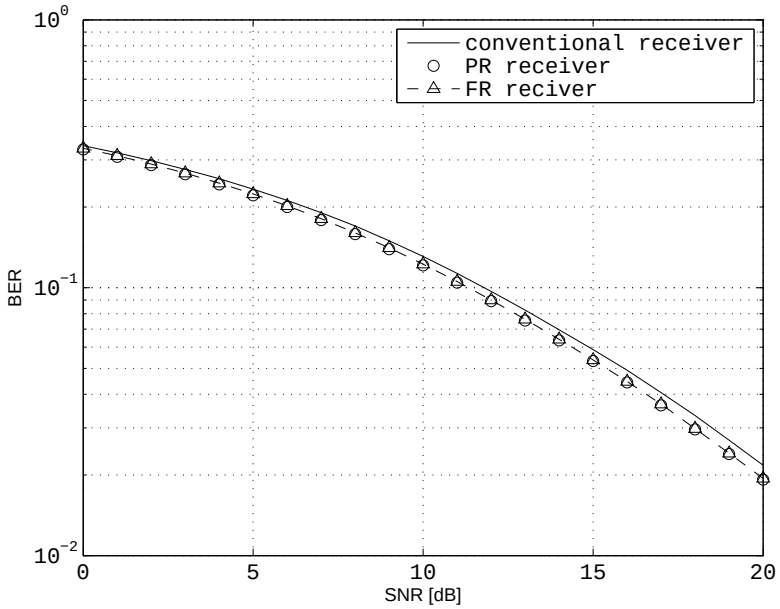

Figure 5.1: BER vs SNR for the three different receivers for a Rayleigh channel with 20 taps.

In Fig. 5.1 the performance of FR receiver with respect to a conventional and PR is shown in a Rayleigh fading channel in the following scenario. No coding is used, the total OFDM symbol duration is $T_S \sim 0.11\mu$s, the FFT size considered is $N = 16384$, GI of length $G = 4096$, and channel impulse response with $L = 20$ taps. Note that this scenario either assumes $G/N = \frac{1}{4}$. The performance improvement of FR equals the expected one calculated in (5.1), moreover the curve of BER vs SNR for PR is superimposed to the curve for FR. This is due to the high number of symbols free from IBI. In fact PR receiver exploits $G - L = 4076$ GI samples, that is almost equivalent to use the whole GI. In Fig. 5.2 the results of the simulations are plotted for the three receivers with a channel which has the same Rayleigh statistic, but longer. In particular we have used a channel which cause a leakage of the whole GI. For this type of channel, which we called "Long Raileigh", all the samples of GI are corrupted by IBI, hence the PR receiver can not exploit any GI symbol ($G - L = 0$) as well as the conventional receiver. On the contrary, FR still exploits all the GI symbols, with the only drawback of an increased recovering interference due to improper channel estimation. With the channel having so many taps, the performance improvement of our receiver is decreased to 0.2 dB, but still better than the other two receivers.

Both Fig.s 5.3 and 5.4 show that introducing LDPC coding with rate 8/9, the performance improvements of the non-conventional receivers are not influenced: an improvement of about 0.5 dB and 0.2 dB respectively is maintained. This is not to be taken for granted as other types of non conventional data detection, which initially appear to be promising in absence of coding, when even weak coding is used, the performance improvement decreases with respect to the conventional.

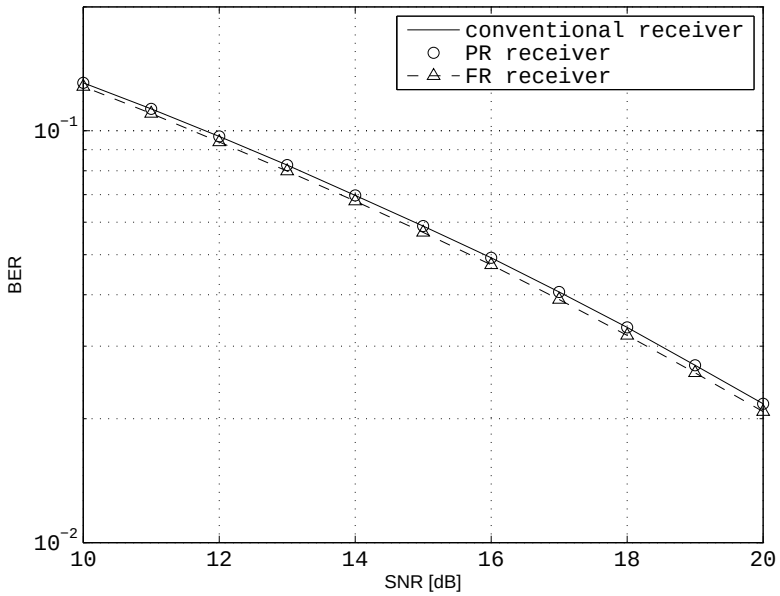

Figure 5.2: BER vs SNR for the three different receivers for a Rayleigh channel with 4096 taps.

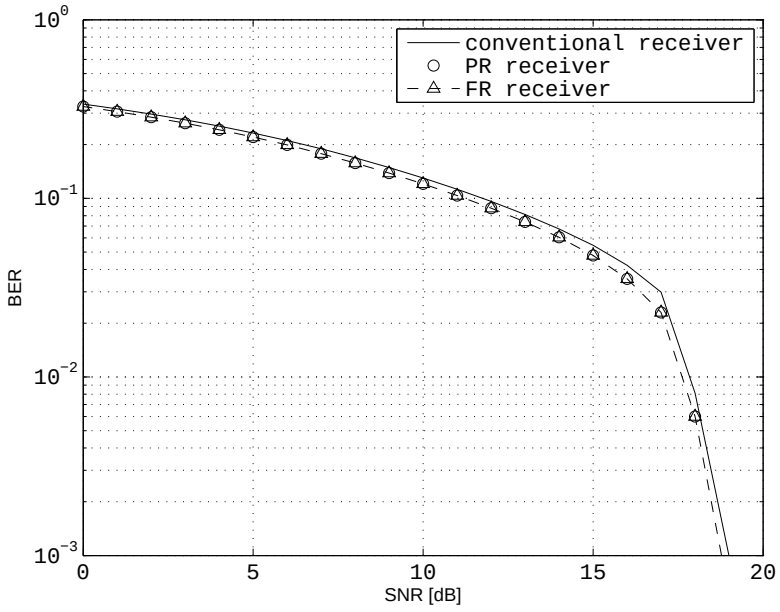

Figure 5.3: BER vs SNR for the three different receivers for a Rayleigh channel with 20 taps with a LDPC coding of rate 8/9.

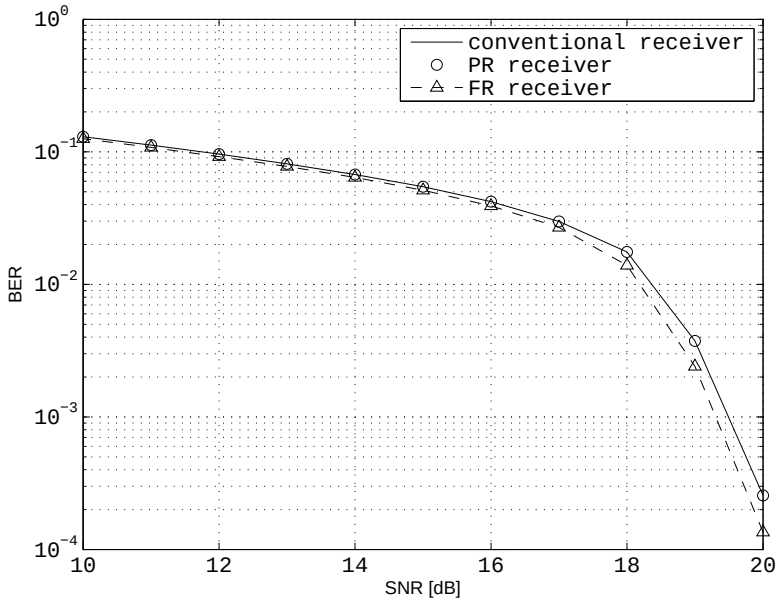

Figure 5.4: BER vs SNR for the three different receivers for a Rayleigh channel with 4096 taps with a LDPC coding of rate 8/9.

5.1.1 Conclusions

We have proposed a new receiver architecture which fully exploits the redundancy introduced by GI symbols. We have compared our solution with the conventional OFDM receiver and with the scheme proposed in [12]. Although the interference cancellation, and ISI reconstruction, strongly depend on the quality of the channel estimation, which in the particular scenario selected does not use any scattered pilot [14], we have shown that our detection method keeps a performance improvement even with severe channel conditions, where the leakage is extended to the whole GI. Using iterative interference cancellation, our educated guess is that performance can be improved further on.

5.2 Chapter 3 - Simulation results

In this section we evaluate the performance of the channel estimation techniques in terms of MSE of the channel estimate

$$MSE = \mathrm{E}\left[\frac{1}{L_T}\sum_{z\in\mathcal{Z}}\left|\tilde{H}_z(n) - H_z(n)\right|^2\right], \tag{5.2}$$

where $\tilde{H}_k(n)$ is the generic channel estimate on subcarrier k.

We compare our estimation methods with the low complexity delay-subspace tracking (ST) method, proposed in [23], which takes advantage of the slow variability of the *delay-subspace* on pilots to estimate the channel frequency response, but does not consider the different reliabilities of the estimates.

As described in section 3.1, the channel is characterized with $N_J = 30$ random frequencies per tap, $f_0 = 626\,\mathrm{MHz}$ as central carrier frequency, and multipath channel with zero-mean Gaussian taps. Each channel tap has an exponentially decaying power delay profile, with root mean square delay spread $\tau_{\mathrm{rms}} = 2\mu\mathrm{s}$ corresponding to a typical urban channel with six taps (TU6) [44]. System parameters are obtained from the DVB-T standard [4] and are summarized in Table 5.1. In the following, results are presented just for DVB-T transmissions with 8 MHz channel bandwidth. Although the considered parameter settings are just a part of the possible configurations of DVB-T2, we stress that similar results can be obtained even for other DVB-T2 transmission modes. For the position of continual and scattered pilots we refer to [4], or equivalently PP1 pilot pattern of [3].

Table 5.1: DVB-T parameters

Parameter	**8K mode**	**2K mode**
FFT size N	8192	2048
Number of carriers K_{tot}	6817	1705
Duration of the useful part of the OFDM block T_U	896 μs	224 μs
Duration of the GI T_G,	224 μs	56 μs
$G = 1/4\cdot$ FFT size	2048	512
OFDM block duration,	1120 μs	280 μs
$T_S = T_U + T_G$	10240 T_s	2560 T_s
Elementary period T_s	7/64 μs	
Spacing between scattered pilots on a single OFDM symbol	12	
Spacing between scattered pilots on the same frequency Δ_B	4	

For the parameter settings considered, after at most 4 OFDM blocks each continual pilot frequency is used by a scattered pilot, hence the number of pilot symbols per OFDM block is $L_{init} = 569$ for the 8K mode, and 143 for the 2K mode. As we focus on channel estimation, we do not consider any specific constellation for data symbols. Anyway, we recall that pilot subcarriers are BPSK modulated, so that the power of noise in the LS estimate (3.13) is the same for all subcarriers.

TI results.

We first show the results of TI. Since the minimum number of OFDM blocks between two blocks having the same position of pilot carriers is $\Delta_B = 4$, the number of TI filters to design is $\Delta_B - 1 = 3$. Using three times the algorithms of section 3.4 we can obtain the pattern of coefficients we need in order to interpolate the LS estimate. Taking into account memory limitations which affect practical systems, we consider filters with two coefficients, i.e $N_B = N_F = Q = 1$. A critical issue in the design of TI filters is the setting of the parameters to ensure stability and fast convergence. Regarding the FIR filters, the fundamental parameters are the updating step $\mu(i)$ for the LMS algorithm, and the initialization of the covariance matrix $\boldsymbol{P}(i)$ for the Kalman filter. The best performance has been obtained with the following choices: $\alpha_1 = 0.008$, $\alpha_2 = 0.2$, $\alpha_3 = 0.025$, $\alpha_4 = 10^{-4}$ and $\lambda = 1$.

In order to compare the proposed techniques with existing solutions, we considered fixed TI, where the TI filter coefficients are $\boldsymbol{c}(1) = [0.25,\ 0.75]$, $\boldsymbol{c}(2) = [0.50,\ 0.50]$ and $\boldsymbol{c}(3) = [0.75,\ 0.25]$.

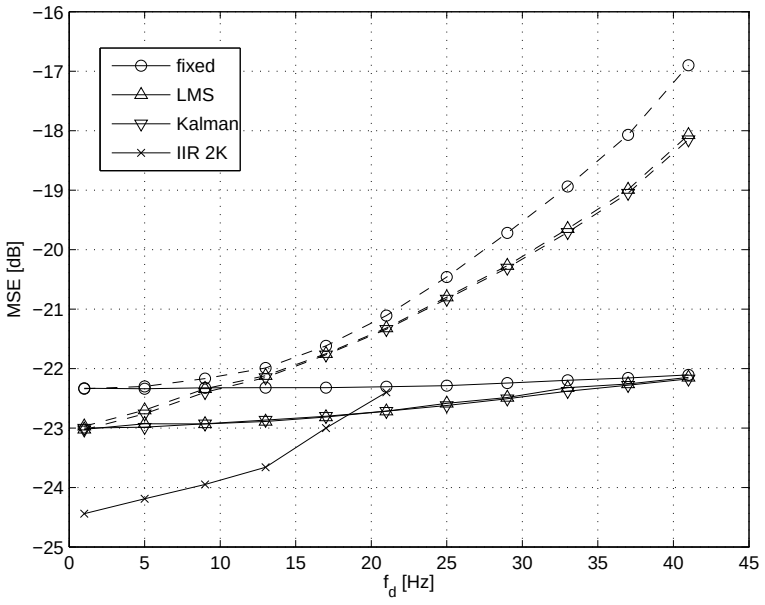

Figure 5.5: MSE as function of f_d for TI. 2K mode (solid lines) and 8K mode (dashed lines). SNR = 20 dB. $N_F = N_B = 1$.

Fig. 5.5 shows the MSE of TI pilots estimates, obtained from (5.2) with $\tilde{H}_z(n) = \tilde{H}_z^{(T)}(n)$ as a function of the maximum Doppler frequency f_d. We note that for the

system operating in the 2K mode, and using FIR filters for TI, the performance of both LMS and Kalman filter is equivalent and independent from f_d. On the other hand, the performance of both filters shows a strong dependence from f_d in the 8K mode. This is due to the duration of the OFDM block, as even at a high Doppler frequency the channel is slowly changing from block to block in the 2K mode, whereas in the 8K mode the channel changes are four times faster. Note that the reliability of the estimation on the TI pilots is higher than the LS estimate. In fact, for the considered scenario the MSE of the LS channel estimate is equal to -20 dB. Fig. 5.5 reports also the comparison between the MSE of TI with FIR filters and the MSE of TI using IIR filters. The comparison is limited to $f_d = 21$ Hz because the IIR filter exhibits convergence and stability issues at Doppler frequencies above 21 Hz. In fact, even the recursive design approach by [37] does not guarantee convergence to a stable solution in all cases. Moreover, note that IIR filters require additional memory as their state is defined by three elements (two for the direct and one for the recursive part), instead of two.

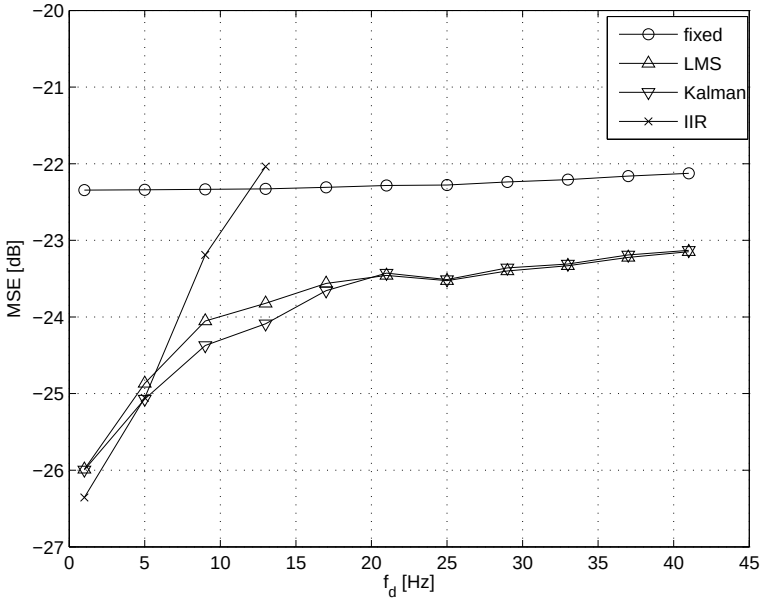

Figure 5.6: MSE as function of f_d for TI. 2K mode, SNR = 20 dB, $N_F = 1$, and $N_B = 3$.

Fig. 5.6 and Fig. 5.7 show results with longer interpolating filters. Two approaches are considered: the first method considers asymmetric filters, i.e. using $N_B = 3$ past OFDM blocks and one future OFDM block $N_F = 1$; the second approach uses an equal number of past and future OFDM blocks, i.e. $N_F = N_B = 2$. The first approach requires to store two sets of pilot symbols and two entire OFDM blocks, i.e. the current and the future block. The second approach instead requires to store one set of pilot symbols and three entire OFDM blocks, the current and two in the future. Therefore, the second approach requires a much higher memory then the first approach. However, the best performance in terms of MSE is achieved for symmetric patterns of coefficients, as shown in Fig. 5.6 and Fig. 5.7. This is due to the fact that OFDM blocks closer to the current block have a higher correlation than those further in the past. We further

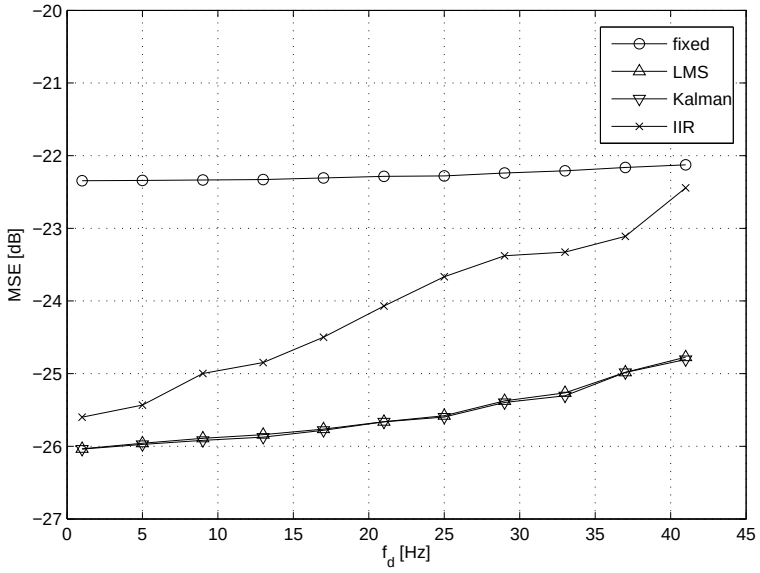

Figure 5.7: MSE as function of f_d for TI with symmetrical FIR filters, 2K mode, SNR = 20 dB. $N_F = N_B = 2$.

observe that in the symmetric approach the IIR is more robust to Doppler phenomena. Anyway, we remark that an increase of the TI filters dimension immediately brings additional latency in transmission. In practical systems we suggest to never use filters with more than 2 taps.

FF results.

The overall numerical results of FF and ST applied on TI estimates are reported in Fig. 5.8 for several values of the filter size $2Q$, where MSE (5.2) is computed with $\tilde{H}_z(n) = \tilde{H}_z^{(F)}(n)$. We note that since ST is not designed to work on estimates with different reliabilities, when filter dimensions are increased, for instance setting $Q = 2$ or $Q = 3$, the proposed MF technique slightly outperforms ST method. In any case we observe that the proposed MF technique has a much lower complexity than ST. This makes FF affordable for practical systems. Moreover, in Fig. 5.8 we have plotted the performance obtained using the minimum MSE solution (3.28) for the computation of the combining coefficients. In absence of a suitable estimator for σ_w^2 and $\sigma_{\mathrm{P}}^2(\nu(z))$ our combination technique shows a performance loss of about 1 dB. Last, we considered the use of a single filter with different reliabilities. In particular, we set $\xi_{\nu(i)} = 1$ only when the reference signal d_i collects only TI estimates, while the two filtered signals are one a pilot, the other a TI. In all other configurations we set $\xi_{\nu(i)} = 0$. Results are reported in Table 5.2 showing that SF with reliability (SF-R) can actually improve MF design using the suboptimal adaptation of the combining coefficients. Indeed, in other configurations in which d_i is a pilot the update is very noisy and the resulting filter performs worse than those having TI estimates as reference. In any case, performance are very close to the optimum solution, while implementation complexity is considerably reduced, since a single filter is used. For comparison purposes we show also the MSE

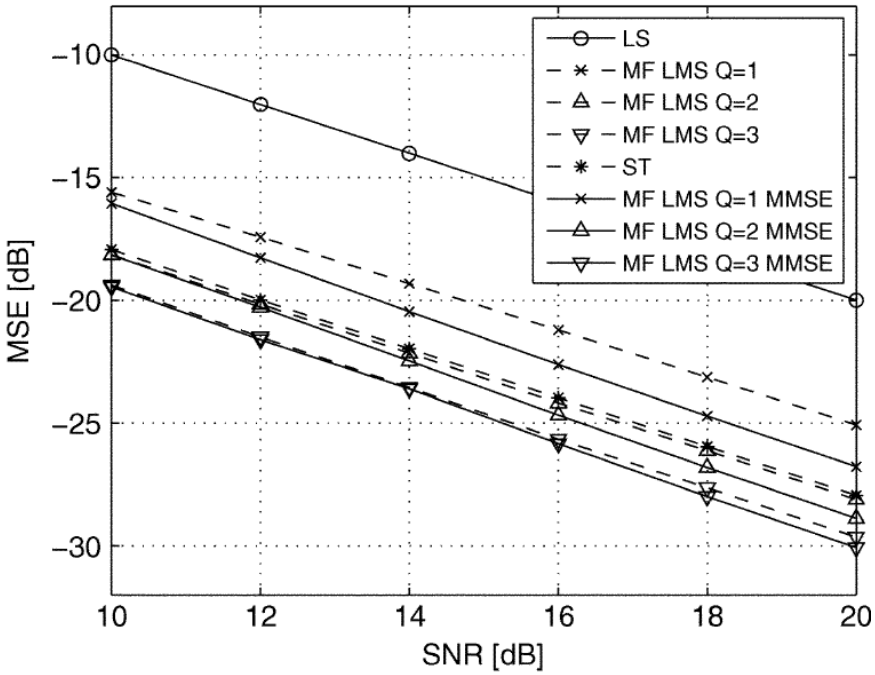

Figure 5.8: MSE as function of the SNR for Kalman TI and comparing LMS FF by means of MF with ST technique. 2K mode, $f_d = 2$Hz, $r_{\max} = 16$.

Table 5.2: MSE comparison among MF, SF and SF with reliability (SF-R)

	MF	SF	SF-R
SNR (dB)	MSE (dB)		
10	-15.51	-12.71	-15.67
12	-17.36	-14.76	-17.48
14	-19.25	-16.77	-19.33
16	-21.17	-18.72	-21.23
18	-23.12	-20.61	-23.15
20	-25.08	-22.43	-25.10

of SF with all unitary reliabilities, i.e. $\xi_{\nu(i)} = 1$ for all symbols. In this case, the MSE is higher than MF as SF adaptation is significantly affected by noise. Lastly, note that reliability coefficients $\xi_{\nu(i)}$ may be optimized in order to minimize MSE, but we leave this topic for future study.

5.2.1 Conclusions

Chapter 3 has considered various adaptive techniques for channel estimation in OFDM systems with pilot signals. By using adaptive filters along both the frequency and time axis, the channel estimate can be refined exploiting the time and frequency correlation of the channel. The criteria for the design of the filters have been the mean square error of the channel estimate and the complexity of the resulting algorithms, with reference to the terrestrial digital TV standards. Combinations of frequency filtering and time interpolation have been considered to identify the best performing technique. In particular a new frequency domain technique for smoothing the channel estimation on time interpolated estimates has been proposed. This technique uses multiple filters for refining the time-interpolated estimate obtained from the pilots. Each filter used for FF-MF is adapted using the LMS method. The proposed technique has been applied in receivers for the DVB-T and DVB-T2 standards, and numerical results show that the proposed technique performs close to other approaches found in literature, with a reduction of two or three orders of complexity.

5.3 Chapter 4 - Simulation results

In this section we consider a DVB-T2 scenario [3] and we compare SBS and ML schemes performance against CBS. P1 symbol comprises two groups of bits (S1 and S2) which carry different signaling information. Performance is assessed in terms of decoding probability P[D] of the S1 and S2 bits, false alarm probability P[FA] and miss detection probability P[MD]. However, we are interested in computing the decoding probability only when the system is synchronized, i.e. P[D|S]. Then, we have to consider false alarms, which occur when no P1 symbol is received, but still $|z_n| > Z_T$ or $\Lambda(\theta) > \Lambda_T$, and a false synchronization is obtained. Moreover, we have also to account for miss detections, when a valid P1 symbol, evaluated as output of the correlator, is not recognized. Hence, we have

$$\mathrm{P[D]} \;=\; \mathrm{P[D|S]}\;\mathrm{P[S]} \;+\; \mathrm{P[D|FA]}\;\mathrm{P[FA]}\,, \tag{5.3}$$

where P[S] is the probability of being synchronized, i.e.

$$\mathrm{P[S]} \;=\; 1 \;-\; \mathrm{P[MD]} \;-\; \mathrm{P[FA]}\,. \tag{5.4}$$

From simulations we have that P[FA] = 0 for all the proposed schemes, hence the probability of detection given the synchronization is simply given by

$$\mathrm{P[D|S]} \;=\; \frac{\mathrm{P[D]}}{1 \;-\; \mathrm{P[MD]}}\,. \tag{5.5}$$

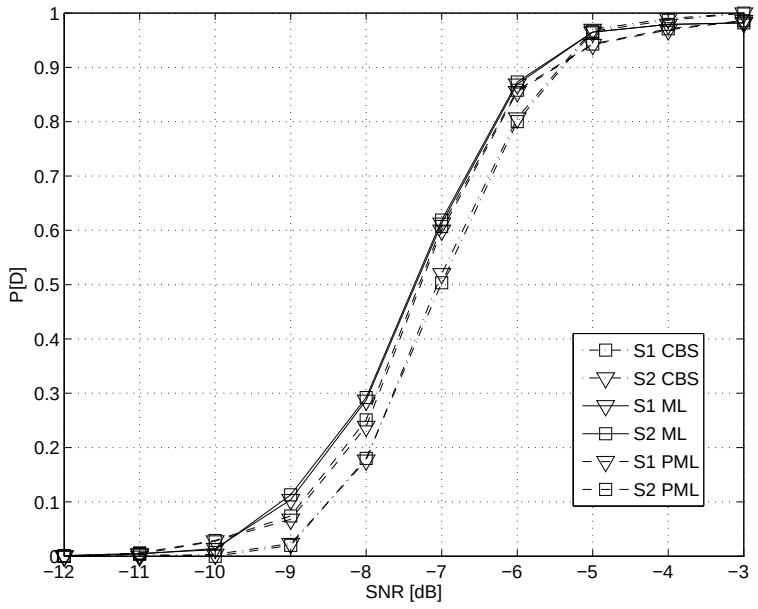

Figure 5.9: Detection probability for S1 and S2 and various synchronization schemes as a function of the SNR in an AWGN scenario.

Fig. 5.9 shows the probability of detection for S1 and S2 bits considering an AWGN channel for CBS, ML and MLT schemes. Probability is plotted as a function of the

SNR. SBS scheme performs very similar to CBS, hence for the sake of making the plot clearer we omitted its curve. We observe that ML always outperforms CBS. Moreover, the MLT scheme performs very closely to ML.

The SNR range of Fig. 5.9 is very low because synchronization on an AWGN channel is very robust due to the length of the P1 symbol. More challenging channels are usually experienced in a DVB-T2 transmission. In particular, similarly to the implementation guidelines for DVB-T2 [42], a transmit channel having two taps is considered. The relative delay τ, and the ratio between the second and the first tap amplitudes $(G)_{\mathrm{dB}}$ are chosen in the following, while phases of the two taps are uniformly random in $(0, 2\pi]$ for each simulation run. The signal to noise ratio (SNR) σ_s^2/σ_w^2 is set at 0 dB, corresponding to a very noisy scenario. Both transmitted data signals, before and after P1 symbol, have power σ_s^2 and generate interference due to the dispersive nature of the channel.

We first consider two taps having the same amplitude, i.e. $(G)_{\mathrm{dB}} = 0$ dB, while the delay τ is varied in the range $[0, 1024]$. From results shown in Fig. 5.10 note that both ML and MLT achieve P[MD] = 0 for the entire delay range, while CBS scheme exhibits poor performance (P[MD] $\simeq 1\%$) for long echoes with $\tau > 400$ samples, as previously shown in section 4.2.1.We now focus on delay $\tau = 512$, which is the most critical for CBS. Fig. 5.11 shows P[D], P[MD] and P[D|S] for CBS and SBS schemes as a function of the ratio of the gains of the two taps $|h_0|^2/|h_1|^2$. We note that SBS scheme outperforms CBS on the entire range of tap gains. This happens because the filter we have introduced in SBS exploits the edges of the correlator response to a P1 symbol. Although SBS scheme shows a slight performance decrease when the two taps have the same gain, SBS greatly outperforms CBS scheme, with a negligible additional complexity. In fact SBS only needs to store N_q values of $|z_n|$ in order to compute (4.23), which just requires an additional sum-between-reals operation.

Besides, Fig. 5.12 shows the detection and synchronization probabilities of CBS, ML, and MLT schemes, again as a function of $(G)_{\mathrm{dB}}$. We note that both ML and MLT significantly outperform CBS when the amplitudes of the two taps are comparable. When the absolute value of one tap is significantly larger than the other one, CBS gets synchronous with the stronger tap and decoding is correct. On the other hand, for the ML scheme we have P[D] $\simeq 1$ for the entire range of $(G)_{\mathrm{dB}}$. Since MLT has a significant lower complexity than ML, we conclude that MLT scheme is a good alternative to ML, as it retains the same low error probability.

Finally, if we compare the performance of SBS and MLT schemes we can easily choose MLT, since it gives a better performance still guaranteeing the computational complexity of CBS.

5.3.1 Conclusions

In chapter 4 we derived the ML synchronization scheme for the P1 symbol used by DVB-T2 standard. Performance results have shown that this scheme significantly outperforms the scheme proposed in [42], here called Correlation-Based Synchronization (CBS) scheme. However, ML is significantly more complex, due to the need of heuristic techniques to find the optimal CFO. Therefore, we considered a Slope-Based Synchronization (SBS) scheme, and a hybrid scheme, that both use the CFO estimate of CBS. They differs in the timing estimation, since the first applies a derivation block to the output of CBS scheme, while the other still use the LLF to determine the optimum

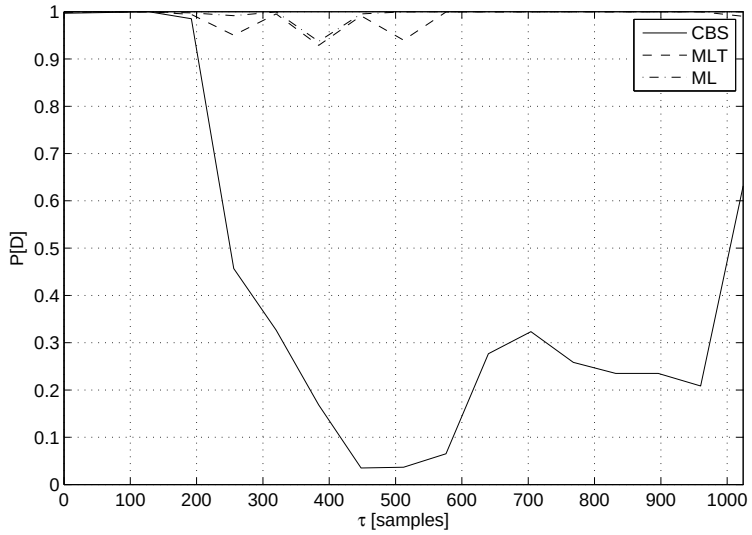

Figure 5.10: P[D] for the CBS scheme (dash-dot lines), ML (dashed lines) and MLT (solid lines) schemes as a function of the delay τ between the taps of the two-taps channel.

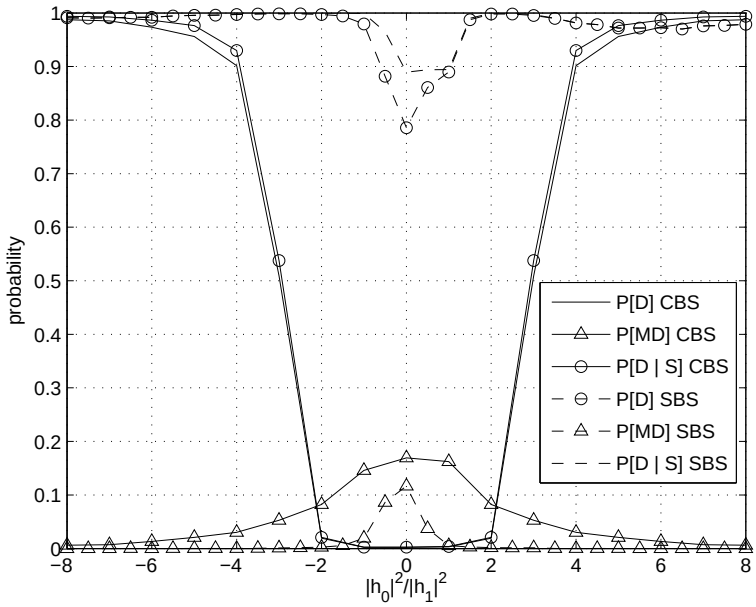

Figure 5.11: P[D], P[MD] and P$[D/S]$ as function of $(G)_{\mathrm{dB}}$.

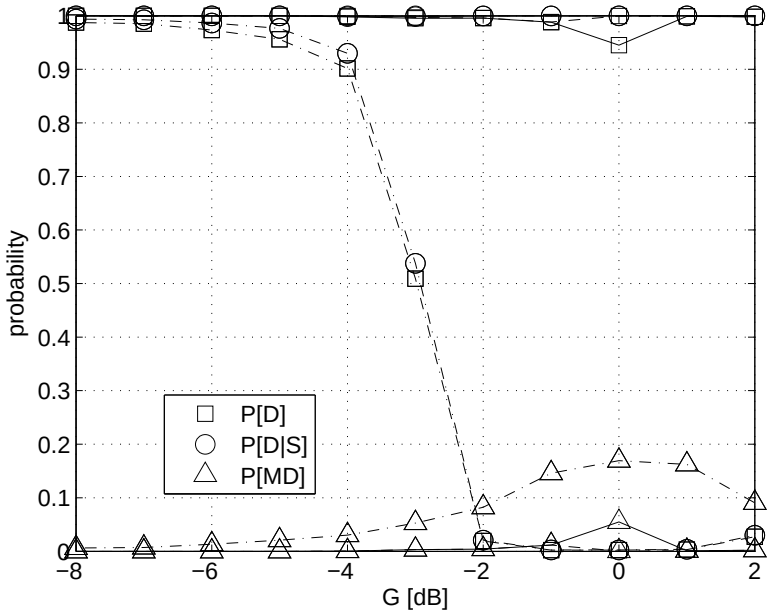

Figure 5.12: P[D], P[MD] and P[D|S] for the CBS scheme (dash-dot lines), ML (dashed lines) and MLT (solid lines) schemes as a function of the amplitude ratio $(G)_{\mathrm{dB}}$. Tap delay is set at $\tau = 512$.

timing. The last solution has almost optimal performance while having a much lower complexity than the ML approach.

Appendix A

P1 Symbol Demodulation Chain

In order to explain the full demodulation chain we first need to review in more detail the structure of P1, starting from the main features and its generation at the transmitting side.

We already have discussed the particular structure of the P1 symbol (Fig. 4.1), also called $C - A - B$ due to the time-domain repetition of two guard interval-like portions of the useful part A of $N_a = K$ samples. These GIs are respectively, the first $N_c = 542$, and the last $N_b = 482$ frequency shifted samples of A. The frequency shift is equal to the sub-carrier spacing of a $1K$ OFDM symbol. The fixed P1 structure, together with the limited and highly protected signaling part, enables a fast scanning of the broadcast frequencies. The receiver can recognize the presence of a DVB-T2 transmission and store the key parameters, e.g. the FFT size or the presence of a FEF frame.

The main characteristics of P1 symbol are:

- 1K OFDM symbol with two 1/2 guard interval-like portions added. See Fig. 4.1, where $f_{\mathrm{SH}} = 1/(KT_s)$, and for 8 MHz bandwidth $T_s = 7/64\mu$s.

- With reference to Fig. A.1, 766 carriers out of 853 from the middle are considered, but just $M = 384$ carry pilots; the others are set to zero. The active carriers are identified by three concatenated Complementary Sequences (CS) of 128, 512 and 128 bits, respectively. The last two bits of the third sequence (CS3) are zero, so the last carrier used is 809.

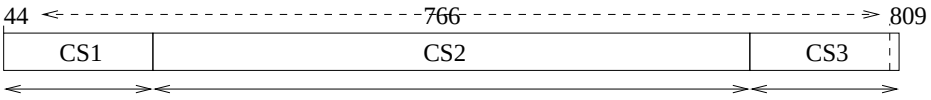

Figure A.1: Active Carriers.

- P1 contains two signaling fields, S1 and S2, respectively modulated by the concatenation of 8 CS of length 8, and 16 CS of length 16. The sum of the autocorrelation (SoAC) of all the sequences of each set is equal to a Kronecker δ, whilst the cross correlations sum to zero. To take advantage of this property the sequences alphabet must be the set {-1, +1}.

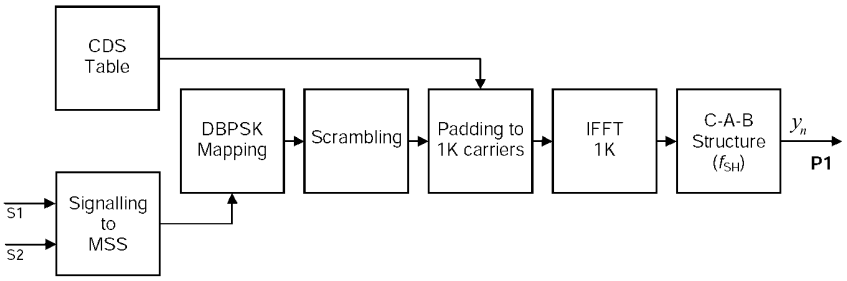

Figure A.2: P1 modulator.

A.1 Modulation steps

The modulator of P1 symbol is shown in Fig. A.2. It comprises the following steps:

1. Create the Modulating sequence (MSS_SEQ), select the S1 and S2 signaling patterns, $\mathrm{CS}_{\mathrm{S1}}$ and $\mathrm{CS}_{\mathrm{S2}}$, arranging them as follows:

$$\{\mathrm{MSS\_SEQ}_0..\mathrm{MSS\_SEQ}_{383}\} = \{\mathrm{CS}_{\mathrm{S1}},\ \mathrm{CS}_{\mathrm{S2}},\ \mathrm{CS}_{\mathrm{S1}}\};$$

2. DBPSK modulate MSS_SEQ, setting the dummy value $\mathrm{MSS\_DIFF}_{-1} = +1$. Note that DBPSK modulation convert the alphabet, i.e. $\{0, 1\}$ –> $\{-1, +1\}$;

3. Apply Scrambling on MSS_DIFF:

$$\mathrm{MSS\_SCR}_i = \mathrm{MSS\_DIFF}_i \times 2\{1/2 - \mathrm{PRBS}_i\};$$

4. Apply MSS_SCR on the active carriers, as in Fig. A.1;

5. Generate the main part A with (4.1) where $d_i = \mathrm{MSS\_SCR}_i$ and $k_{\mathrm{P1}}(i)$ for $i = 0, \ldots, M-1$ are the indexes of the active carriers, in increasing order, as defined in Fig. A.1;

6. The two guard interval-like portions are appended as depicted in Fig. 4.1. Parts C and B are obtained applying a frequency shift (f_{SH}) to the first N_c samples and the last N_b samples of $s_n^{(A)}$, respectively. This provides the transmitted signal in (4.2).

A.2 P1 receiver architecture

The block diagram of the receiver is given in Fig. A.3. In the following we will explain the task of each block and how it is performed.

Synchronization block

The synchronization block has the twofold purpose of providing a) DVB-T2 signal identification and b) timing and carrier frequency offset (CFO) estimation. We already dedicated chapter 4 to describe this block in detail.

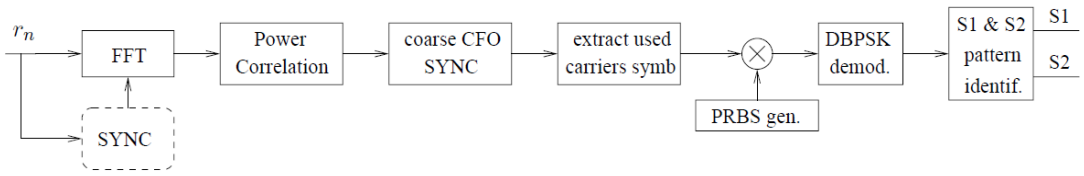

Figure A.3: Complete P1 symbol receiver.

FFT and power CDS correlation

When the synchronization block triggers the second part of the P1 receiver, i.e. a correlation peak has been found, fine CFO is first corrected. Then, using the symbol timing, a 1K samples window is set to compute the 1K FFT from the output of the correlator. If perfect timing has been achieved, and the channel is just a single tap, FFT demodulation block yields the sequence MSS_SCR on P1 pilots, superimposed to AWGN noise, cyclically shifted by $(426 - F_0)$ subcarriers to the left. F_0 is the integer component of the CFO, whilst 426 is a factor introduced at the transmitter in order to center the active carriers in the middle of the channel bandwidth. After the FFT block, we correlate the square absolute values of the frequency domain signal with the subcarrier pattern tabulated in the Carrier Distribution Sequence (CDS) table [3]. The power correlation gives a peak delayed by $(426 - F_0)$ to the left of the zero position. From this peak we can immediately correct the integer part of CFO, cyclically delaying the signal after FFT by $(426 - F_0)$ to the right, thus obtaining the correct MSS_SCR. Two reasons may lead to lack of a power correlation peak. The first one is that we could have not achieved a sufficiently reliable symbol timing, hence the FFT window is not correctly placed. The second case happens when SNR is too low, and the noise on the correlation output hides the peak. In both cases we choose to discard the symbol because we are not able to provide a correct demodulation.

The correlation is implemented in the following way. We load the CDS table, and prepare a 1K array carrying ones for the positions listed within the CDS table and zeros elsewhere. Then we compute the correlation between the absolute values of the signal and this vector. The detection operates as follows. We select the maximum of the correlation output (`max_CDS_corr`), and then the second maximum value (`max_CDS_out_of_peak`), i.e. the maximum value of the correlation except `max_CDS_corr`. Finally, we compute the ratio

$$\texttt{CDSpeak\_ratio} = \texttt{max\_CDS\_out\_of\_peak}/\texttt{max\_CDS\_corr} \tag{A.1}$$

If $\texttt{CDSpeak\_ratio} < 0.92$, the peak of the correlation is far enough from the noise level, hence we can validate the symbol, correct the coarse CFO, and move forward to the next block. Otherwise the symbol is discarded, leading again to a miss detection. In this case the following blocks of Fig. A.3 are not executed saving computation time.

Extract used carriers – PRBS generator

Hereinafter, blocks are executed only when the signal is validated, i.e. when the system has identified a DVB-T2 signal and it is properly synchronized. After symbol validation, we have to identify which signaling pattern has been sent. To identify the right pattern

we first extract the used carriers (given by CDS table), obtaining a sequence of M complex values. These values refer to MSS_SCR, i.e. the scrambled DBPSK modulated version of MSS_SEQ, which is the signaling sequence embedding S1 and S2 fields. To invert the scramble applied at the transmitter, it is enough to multiply the estimated sequence of M symbols with the same sequence used to scramble MSS_DIFF. We remark that the initial status of the Pseudo-Random Bit Sequence (PRBS) generator is known at the receiver ('100111001000110'), so there is no ambiguity on the scrambling sequence to use (see clause 5.2.4 of [3] for details).

Before descrambling we have to convert the output bits of the PRBS from the binary alphabet $\{0, 1\}$ to $\{+1, -1\}$, i.e. 0 –> +1, 1 –> -1, as it was done at the transmitter.

DBPSK demodulation

DBPSK demodulation computes an hard decision on the received sequence, symbol by symbol. Starting from the dummy value 0, we compare the phase of adjacent symbols, if the absolute value of the phase difference is grater than $\pi/2$ than we decode 1, otherwise we decode 0. The binary sequence of {0,1} is the estimation of MSS_SEQ.

Identification of S1 and S2

The possible transmitted patterns for MSS_SEQ are $8 \times 16 = 128$ (8 signaling patterns for S1 and 16 for S2). However, only one bit out of 3 are used for S1, leaving the others for future uses (FEF). For S2 only 12 patterns are used, then we have only $2 \times 12 = 24$ different MSS_SEQ. Signaling patterns are orthogonal to each other, hence scalar products are used to identify the correct patterns, as shown in Fig. A.4.

We takes into consideration all possible patterns, including the FEF patterns, thus the detector comprises 8 + 16 devices which compute the scalar product of the input sequence with one of the signaling patterns. The pattern which gives the maximum is identified as the transmitted pattern.

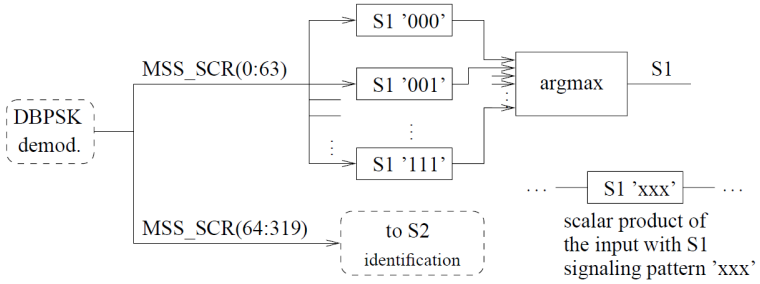

Figure A.4: Scalar products used for S1 identification. S2 is analogous with the appropriate scalar products.

The S1 signaling pattern is repeated twice in MSS_SEQ. Denoting with m the index of the symbols of MSS_SEQ, at $m = 0, ..., 63$ and $m = 320, ..., 383$ we find the S1 signaling pattern, whilst at $m = 64, ..., 319$ we find S2.

The identification of S2 is performed in an analogous way to the one depicted in Fig. A.4, whilst to decode S1 we can do something better. Since the same field (S1)

is repeated twice, in order to improve the identification accuracy we could duplicate the architecture of Fig. A.4. Though, this would lead to an increase of complexity. Equivalently, we can simply sum the subsequences of MSS_SEQ for $m = 0, ..., 63$ and $m = 320, ..., 383$. Then we use this signal as input of the structure of Fig. A.4.

Appendix B

LLF Detailed Computation

Assume that we observe $4N_a$ consecutive samples of r_n, and these samples contains one complete $(2N_a)$-samples P1 symbol. Define the index sets

$$\begin{aligned}
\mathcal{I}_c &= \{\theta, \ldots, \theta + N_c - 1\} \\
\mathcal{I}'_c &= \{\theta + N_c, \ldots, \theta + 2N_c - 1\} \\
\mathcal{I}_b &= \{\theta + 2N_c, \ldots, \theta + 2N_c + N_b - 1\} \\
\mathcal{I}'_b &= \{\theta + 2N_c + N_b, \ldots, \theta + 2N_c + 2N_b - 1\}
\end{aligned}$$

The set $\mathcal{I}'_c$ contains the indexes of the samples of the first portion of part A, whilst $\mathcal{I}'_b$ contains the indexes of the samples of part B, which in turn are repeated from the second portion of A. Collect the observed samples in the $4N_a$-column vector $\mathbf{r}_\theta = [r_0,\ \ldots,\ r_{4N_a-1}]^T$. Notice that the samples with indexes in the set $\mathcal{I}_c \cup \mathcal{I}'_c$ are pairwise correlated, as for samples with indexes in $\mathcal{I}_b \cup \mathcal{I}'_b$. In fact by denoting $\mathrm{E}[\cdot]$ the expectation operator we have

$$\forall n \in \mathcal{I}_c: \quad \mathrm{E}\left[r_n r^*_{n+m}\right] = \begin{cases} \sigma_s^2 + \sigma_w^2 & m = 0 \\ \sigma_s^2\, e^{-j2\pi\Phi N_c/N_a}\ e^{j2\pi(n-\theta)/N_a} & m = N_c \\ 0 & \text{otherwise} \end{cases} \tag{B.1}$$

$$\forall n \in \mathcal{I}_b: \quad \mathrm{E}\left[r_n r^*_{n+m}\right] = \begin{cases} \sigma_s^2 + \sigma_w^2 & m = 0 \\ \sigma_s^2\, e^{-j2\pi\Phi N_b/N_a}\ e^{-j2\pi(n-\theta-N_c)/N_a} & m = N_b \\ 0 & \text{otherwise} \end{cases} \tag{B.2}$$

while the remaining samples r_n for $n \notin \mathcal{I}_c \cup \mathcal{I}'_c \cup \mathcal{I}_b \cup \mathcal{I}'_b$, are mutually uncorrelated.

Using the correlation properties of the observations $\mathbf{r}_\theta$, the log-likelihood function (4.25) can be written as

$$\begin{aligned}
\Lambda(\theta, \Phi) &= \log\left(\prod_{n\in\mathcal{I}_c} f(r_n, r_{n+N_c}) \prod_{n\in\mathcal{I}_b} f(r_n, r_{n+N_b}) \prod_{n\notin\mathcal{I}_{tot}} f(r_n)\right) \\
&= \log\left(\prod_{n\in\mathcal{I}_c} \frac{f(r_n, r_{n+N_c})}{f(r_n) f(r_{n+N_c})} \prod_{n\in\mathcal{I}_b} \frac{f(r_n, r_{n+N_b})}{f(r_n) f(r_{n+N_b})} \prod_n f(r_n)\right)
\end{aligned} \tag{B.3}$$

where $f(\cdot)$ denotes the probability density function of the variables in its argument given θ and Φ, omitted for notation clarity. The product $\Pi_n f(r_n)$ in (B.3) is independent of θ and Φ, hence we can omit this factor for the maximization. An equivalent expression of (B.3) can thus be written as

$$\Lambda(\theta,\Phi)=\sum_{n=\theta}^{\theta+N_c-1}\log\left(\frac{f(r_n,r_{n+N_c})}{f(r_n)f(r_{n+N_c})}\right)+\sum_{n=\theta+2N_c}^{\theta+2N_c+N_b-1}\log\left(\frac{f(r_n,r_{n+N_b})}{f(r_n)f(r_{n+N_b})}\right) \tag{B.4}$$

Under the assumption that $\boldsymbol{r}_\theta$ is a jointly Gaussian vector, $f(r_n)$ is given by

$$f(r_n)=\frac{\exp\left(-\frac{|r_n|^2}{(\sigma_s^2+\sigma_w^2)}\right)}{\pi(\sigma_s^2+\sigma_w^2)}. \tag{B.5}$$

The numerators of (B.4) are 2-D zero-mean complex-valued Gaussian distributions. Hence, defining $\mathbf{Z}_i=[r_n,r_{n+N_i}]^H$, where N_i can be N_c or N_b, $f(r_n,r_{n+N_i})$ is the following joint probability density function

$$f_{\mathbf{Z}_i}(\mathbf{z}_i)=\frac{1}{\pi^2\det(\boldsymbol{R}_i)}\exp\left\{-\mathbf{z}_i^*\boldsymbol{R}_i^{-1}\mathbf{z}_i\right\} \tag{B.6}$$

where $\boldsymbol{R}_i$ is the complex covariance matrix $\boldsymbol{R}_i=\mathrm{E}\left[\mathbf{Z}_i\,\mathbf{Z}_i^H\right]$. Using the correlation properties of (B.1) and (B.2), we obtain the following correlation matrices

$$\boldsymbol{R}_c=(\sigma_s^2+\sigma_w^2)\begin{bmatrix}1 & \rho\,e^{-2\pi\Phi N_c/N_a}e^{j2\pi(n-\theta)/N_a}\\ \rho\,e^{2\pi\Phi N_c/N_a}e^{-j2\pi(n-\theta)/N_a} & 1\end{bmatrix} \tag{B.7}$$

$$\boldsymbol{R}_b=(\sigma_s^2+\sigma_w^2)\begin{bmatrix}1 & \rho\,e^{-2\pi\Phi N_b/N_a}e^{-j2\pi(n-\theta-N_c)/N_a}\\ \rho\,e^{2\pi\Phi N_b/N_a}e^{j2\pi(n-\theta-N_c)/N_a} & 1\end{bmatrix} \tag{B.8}$$

Since $\det(\boldsymbol{R}_c)=\det(\boldsymbol{R}_b)=(\sigma_s^2+\sigma_w^2)^2(1-\rho^2)$, putting (B.7) into (B.6) we get

$$f(r_n,r_{n+N_c})=\frac{\exp\left\{-\dfrac{|r_n|^2+|r_{n+N_c}|^2-2\rho\,\Re\left\{r_n r_{n+N_c}^* e^{2\pi\Phi N_c/N_a}e^{-j2\pi(n-\theta)/N_a}\right\}}{(\sigma_s^2+\sigma_w^2)(1-\rho^2)}\right\}}{\pi^2(\sigma_s^2+\sigma_w^2)^2(1-\rho^2)}. \tag{B.9}$$

Hence, using (B.5), the first log-ratio of (B.4) is given by

$$\begin{aligned}
&\log\left(\frac{f(r_n,r_{n+N_c})}{f(r_n)f(r_{n+N_c})}\right)=\\
&c_1+\left\{-\frac{|r_n|^2+|r_{n+N_c}|^2-2\rho\,\Re\left\{r_n r_{n+N_c}^* e^{2\pi\Phi N_c/N_a}e^{-j2\pi(n-\theta)/N_a}\right\}}{(\sigma_s^2+\sigma_w^2)(1-\rho^2)}+\frac{|r_n|^2+|r_{n+N_c}|^2}{(\sigma_s^2+\sigma_w^2)}\right\}\\
=&c_1+\left\{\frac{-\rho^2\left(|r_n|^2+|r_{n+N_c}|^2\right)+2\rho\,\Re\left\{r_n r_{n+N_c}^* e^{2\pi\Phi N_c/N_a}e^{-j2\pi(n-\theta)/N_a}\right\}}{(\sigma_s^2+\sigma_w^2)(1-\rho^2)}\right\}\\
=&c_1+c_2\left(-\frac{\rho}{2}\left(|r_n|^2+|r_{n+N_c}|^2\right)+\Re\left\{r_n r_{n+N_c}^* e^{2\pi\Phi N_c/N_a}e^{-j2\pi(n-\theta)/N_a}\right\}\right).
\end{aligned} \tag{B.10}$$

Analogously, for N_b we get

$$\begin{aligned} &\log\left(\frac{f(r_n, r_{n+N_b})}{f(r_n)f(r_{n+N_b})}\right) = \\ &c_1 + c_2\left(-\frac{\rho}{2}\left(|r_n|^2 + |r_{n+N_b}|^2\right) + \Re\left\{r_n r^*_{n+N_b} e^{2\pi\Phi N_b/N_a} e^{j2\pi(n-\theta-N_c)/N_a}, \right\}\right) \end{aligned} \tag{B.11}$$

where c_1 and c_2 are positive constants which can be neglected during maximization. Note that (B.10) and (B.11) match exactly (4.33) and (4.34).

Bibliography

[1] L. Vangelista, N. Benvenuto, S. Tomasin, C. Nokes, J. Stott, A. Filippi, M. Vlot, V. Mignone, and A. Morello, "Key technologies for next-generation terrestrial digital television standard DVB-T2," *IEEE Commun. Mag.*, vol. 31, pp. 146–153, Oct. 2009.

[2] *Digital Video Broadcasting (DVB); Second Generation Framing Structure, Channel Coding and Modulation Systems for Broadcasting, Interactive Services, News Gathering and Other Broadband Satellite Applications*, European Telecomm. Standards Inst. (ETSI) EN 302 307 V1.2.1, Aug. 2009.

[3] *Digital Video Broadcasting (DVB); Frame structure channel coding and modulation for a second generation digital terrestrial television broadcasting system (DVB-T2)*, European Telecomm. Standards Inst. (ETSI) EN 302 755, Sep. 2009.

[4] *Digital Video Broadcasting (DVB); Framing structure, channel coding and modulation for digital terrestrial television*, European Telecomm. Standards Inst. (ETSI) EN 300 744, Jun. 2004.

[5] T. Pollet, M. van Bladen, and M. Moeneclaey, "BER sensitivity of OFDM systems to carrier frequency offset and wiener phase noise," *IEEE Trans. Commun.*, vol. 43, pp. 191–193, 1995.

[6] B. L. Floch, M. Alard, and C. Berrou, "Coded orthogonal frequency division multiplex," vol. 83, no. 6, pp. 982–996, Jun. 1995.

[7] T. Schmidl and D. Cox, "Robust frequency and timing synchronization for OFDM," *IEEE Trans. Commun.*, vol. 45, pp. 1613–1621, Jul. 1997.

[8] V. Mignone and A. Morello, "CD3-OFDM: a novel demodulation scheme for fixed and mobile receivers," *IEEE Trans. Commun.*, vol. 44, pp. 1144–1151, Sep. 1996.

[9] S. M. Alamouti, "A simple transmit diversity technique for wireless communications," *IEEE J. Sel. Areas Commun.*, vol. 16, no. 8, pp. 1451–1458, Oct. 1998.

[10] *Digital Audio Broadcasting (DAB); DAB to mobile, portable and fixed receiver*, European Telecomm. Standards Inst. (ETSI) EN 300 401, Feb. 1995.

[11] (2007, Apr.) DVB-T2 call for technologies and list of commercial requirements. sb1644r1.01.T2_CfT.pdf. [Online]. Available: http://www.dvb.org/technology/dvbt2/

[12] A. Tarighat and A. Sayed, "An optimum ofdm receiver exploiting cyclic prefix for improved data estimation," in *Proc. IEEE ICASSP 2003*, vol. 4, Hong Kong, China, Apr. 2003, pp. 217–220.

[13] D. Bertrand, J. Louveaux, and L. Vanderdorpe, "Exploiting cyclic prefix for performance improvement in single carrier systems," in *7-th IEEE Workshop on SPAWC 2006*, Cannes, France, Jul. 2006, pp. 1–5.

[14] M. V. V. Mignone, A. Morello, "CD3-OFDM: a new channel estimation method to improve the spectrum efficiency in digital terrestrial television systems," in *Broadcasting Convention, 1995 IBC 95., International*, Sep. 14–18, 1995, pp. 122–128.

[15] S. M. Kay, Ed., *Fundamentals of Statistical Signal Processing, vol. I: Estimation Theory*. River, NJ: Prentice-Hall, 1993.

[16] *IEEE 802.11b - Part 11: Wireless LAN Medium Access Control (MAC) and Physical Layer (PHY) Specifications*, IEEE Standard Specifications Std., 1999.

[17] *IEEE 802.16 - Part 16: Air interface for fixed broadband wireless access systems*, IEEE Standard Specification Std., 2004.

[18] D. Schafhuber and G. Matz, "MMSE and adaptive prediction of time-varying channels for OFDM systems," *IEEE Trans. Wireless Commun.*, vol. 4, pp. 593–602, Mar. 2005.

[19] K. J. Kim, J. Yue, R. A. Iltis, and J. D. Gibson, "A QRD-M/kalman filter-based detection and channel estimation algorithm for MIMO-OFDM systems," *IEEE Trans. Wireless Commun.*, vol. 4, pp. 710–721, Mar. 2005.

[20] P. Hoher, S. Kaiser, and P. Robertson, "Pilot-symbol-aided channel estimation in time and frequency," in *Proc. 6th Commun. Theory Miniconf. at GLOBECOM 1997*, Phoenix (AZ), Nov. 1997, pp. 90–96.

[21] O. Edfors, M. Sandell, J. van de Beek, S. K. Wilson, and P. O. Borjesson, "OFDM channel estimation by singular value decomposition," *IEEE Trans. Commun.*, vol. 46, pp. 931–939, Jul. 1998.

[22] J. Ye Li, L. J. Cimini and N. R. Sollenberger, "Robust channel estimation for ofdm systems with rapid dispersive fading channels," *IEEE Trans. Commun.*, vol. 46, pp. 902–915, Jul. 1998.

[23] O. Simeone, Y. Bar-Ness, and U. Spagnolini, "Pilot-based channel estimation for OFDM systems by tracking the delay-subspace," *IEEE Trans. Wireless Commun.*, vol. 3, pp. 315–325, Jan. 2004.

[24] M. Sandell, "Design and analysis of estimators for multicarrier modulation and ultrasonic imaging," Ph.D. dissertation, Lulea University of Technology, Sweden, Sep. 1996.

[25] M. Necker, F. Sanzi, and J. Speidel, "An adaptive wiener-filter for improved channel estimation in mobile OFDM-systems," in *Proc. Int. Simp. on Signal Proc. and Inform. Technology (ISSPIT)*, Dec. 2001, pp. 213–216.

[26] F. Sanzi and J. Speidel, "An adaptive two-dimensional channel estimator for wireless OFDM with application to mobile DVB-T," *IEEE Trans. Broadcast.*, vol. 46, pp. 128–133, Jun. 2000.

[27] D. Schafhuber, G. Matz, and F. Hlawatsch, "Adaptive wiener filters for time-varying channel estimation in wireless OFDM systems," in *Proc Int. Conf. on Acoustics, Speech, and Signal Proc. (ICASSP)*, vol. 4, Apr. 2003, pp. 688–691.

[28] T. Cui, C. Tellambura, and Y. Wu, "Low-complexity pilot-aided channel estimation for OFDM systems over doubly-selective channels," in *Proc. Int. Conf. on Commun. (ICC)*, vol. 3, May 2005, pp. 1980–1984.

[29] P.-Y. Tsai and T.-D. Chiueh, "Frequency-domain interpolation-based channel estimation in pilot-aided OFDM systems," in *Proc. Vehic. Techn. Conf. 2004-Spring*, vol. 1, May 2004, pp. 420–424.

[30] X. Dong, W.-S. Lu, and A. Soong, "Linear interpolation in pilot symbol assisted channel estimation for OFDM," *IEEE Trans. Commun.*, vol. 6, pp. 1910–1920, May 2007.

[31] X. Hou, S. Li, D. Liu, C. Yin, and G. Yue, "On two-dimensional adaptive channel estimation in OFDM systems," in *Proc. Vehic. Tech. Conf. (VTC)*, Nov. 2004, pp. 498–502.

[32] H. M. Park and J. H. Lee, "Estimation of time-variant channels for OFDM systems using kalman and wiener filters," in *Proc. Vehic. Tech. Conf. (VTC)*, Sep. 2006, pp. 1–5.

[33] S. Tomasin, A. Gorokhov, H. Yang, and J.-P. Linnartz, "Iterative interference cancellation and channel estimation for mobile ofdm," *IEEE Trans. Wireless Commun.*, vol. 4, pp. 238–245, Jan. 2005.

[34] W.-G. Song and J.-T. Lim, "Pilot-symbol aided channel estimation for OFDM with fast fading channels," *IEEE Trans. Broadcast.*, vol. 49, pp. 398–402, Dec. 2003.

[35] N. Benvenuto and G. Cherubini, *Algorithms for Communications Systems and Their Applications.* Chichester, UK: Wiley, 2002.

[36] C. Jakes, *Microwave Mobile Communications.* J. Wiley and Sons Inc., 1974.

[37] R. Lopez-Valcarce and F. Perez-Gonzalez, "Adaptive IIR lattice filtering revisited: convergence issues and new algorithms with improved stability properties," *IEEE Trans. Signal Process.*, vol. 49, pp. 811–821, Apr. 2001.

[38] P. A. Regalia, *Adaptive IIR Filtering in Signal Processing and Control.* New York, NY: Marcel Dekker, 1995.

[39] H. Fan and W. K. Jenkins, "A new adaptive IIR filter," *IEEE Trans. Circuits Syst.*, vol. 33, pp. 939–947, Oct. 1986.

[40] J. A. C. Bingham, "Multicarrier modulation for data transmission: an idea whose time has come," *IEEE Commun. Mag.*, vol. 28, pp. 5–14, May 1990.

[41] M. Morelli, C. C. J. Kuo, and M.-O. Pun, "Synchronization techniques for orthogonal frequency division multiple access (OFDMA): a tutorial review," in *Proc. of the IEEE*, vol. 95, no. 7, Jul. 2007, pp. 1394–1427.

[42] *Implementation guidelines for a second generation digital terrestrial television broadcasting system(DVB-T2)*, European Telecomm. Standards Inst. (ETSI) Std. DVB Document A133.

[43] J. van de Beek, M. Sandell, and P. Borjesson, "ML estimation of time and frequency offset in OFDM systems," *IEEE Trans. Signal Process.*, vol. 45, pp. 1800–1805, Jul. 1997.

[44] "Digital land mobile radio communications," COST 207, Commission of the European Communities, Luxembourg, 1989.